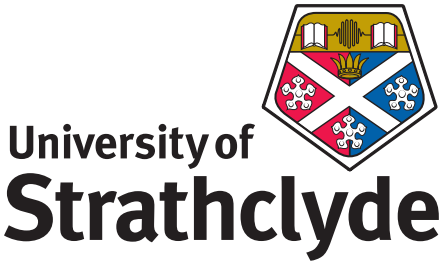

Theoretical modelling of the collapse of a shelled Ultrasound Contrast Agent used in the treatment of cancer

James Francis Cowley

Department of Mathematics and Statistics
University of Strathclyde, Glasgow

Acknowledgements

I am extremely grateful to my supervisor Prof Anthony J. Mulholland for his guidance, support and valuable time. I also want to thank my second supervisor Prof Tony Gachagan and CUE for their financial support and encouragement. My special thanks goes to my mother, brother and sister-in-law for their love and support. Finally, I would like to dedicate this thesis to my late father, Joseph Cowley.

Abstract

Premanufactured shelled microbubbles composed of a protein shell are currently licensed in the UK as ultrasound imaging contrast agents. Current research is focussing on using the shelled microbubbles as transportation mechanisms for localised drug delivery particularly in the treatment of various types of cancer. The aim of this PhD study is to identify how the shell's material parameters influence the collapse and relaxation times of the shelled microbubbles. A theoretical model is proposed which utilises an analytical approach to predict the dynamics of a stressed, compressible shelled microbubble. This model can be used to identify the optimal material parameters for the shells. A neo-Hookean, compressible strain energy density function is used to model the potential energy per unit volume of the shell. A stress is applied to the inner surface of the spherical shell whilst setting the outer surface's stress to zero. The collapse phase of the stressed shelled microbubble is then considered. Applying the momentum balance law, a dynamical model is used to predict the dynamics of the collapsing shelled microbubble. An analytical approach is adopted using an asymptotic expansion. A second model is then constructed to model the deformation of an open, shelled microbubble. This is achieved by considering a reference configuration (stress free) consisting of a shelled microbubble with a spherical cap removed. This is then deformed angularly and radially by applying a stress load to the free edge of the shell. This forms a deformed open sphere possessing a stress. This is used to represent the change in geometry of a shelled microbubble. The third and final model focusses on developing a Rayleigh-Plesset equation for an incompressible, thin shelled, gas loaded shelled microbubble with a shell that is composed of a

liquid-crystalline material. The technique of linearisation is used to predict the shelled microbubble's natural frequency and relaxation time. The influence of the material properties of the shell on the natural frequency and relaxation time are discussed.

Contents

Chapter 1

Introduction

1.1 Ultrasound Contrast Agents (UCAs) as drug carriers

Premanufactured shelled microbubbles are currently licensed in the UK as ultrasound imaging contrast agents. Current research is focussing on using the microbubbles as a transportation mechanism for localised drug delivery specifically in the treatment of various cancers [1–9]. Ultrasound contrast agents (UCAs) are shelled microbubbles typically composed of a layer or several layers of a protein shell encapsulating a perfluoro gas that helps to stabilise the microbubble when it is injected into the bloodstream [10–12]. The shelled microbubbles have a typical radius of between 1 and 4 μm allowing them to propagate through the capillaries in the human body and a shell thickness that varies between 4 and 100 nm depending on whether the UCA is a monolipid or polymer variant [13]. A typical shear modulus value for a monolipid UCA is 20MPa with a Poisson ratio of $\nu = 0.48$ [14,15]. UCAs create a contrast with the surrounding tissue primarily due to an impedance mismatch and the production of higher harmonics. Microbubbles resonate with

typical frequencies in the range of 1 to 10 MHz producing nonlinear, multiple harmonic signals that enhance the quality of the medical imaging process [16]. There has been research momentum growing in recent years to use the UCAs as localised drug delivery agents [17]. Much progress has been made but much remains to be done before this can be deployed routinely in patients [18]. Hence there is a need to develop virtual simulation tools to better understand the challenges. This thesis contributes to this effort by identifying how the material parameters of the shell influence the dynamics and collapse time of the shell where the collapse time is defined as the time taken for a stressed shelled microbubble to collapse back to its stress free state. The outer shell of the shelled microbubbles will be coated with chemical receptors which act as a targeting mechanism for cancerous tumours and encapsulated within the shell will be cancer treating drugs [19]. The practitioners have laid out a vision wherein microbubbles will be injected into the bloodstream and the blood flow will pump them around the body [20]. The region of the body which possesses the tumour is then subjected to ultrasound chirps typically in the range of 3 - 7 MHz [13]. Acoustic microstreaming generated by shelled microbubbles near the cellular walls will result in the formation of cavitation bubbles that collapse rapidly to produce shock waves that create pores in the capillary walls. This enhancement of the porosity of the capillaries is known as sonoporation [21–27]. The pores provide a doorway to the surface of the tumour where the chemical receptors will guide the shelled microbubbles onto the surface of the tumour where they will be burst by a further high power ultrasound pulse in a controlled and highly localised manner. This procedure aims to minimise the pernicious side effects associated with current conventional chemotherapy treatments. It is worth emphasising that there are competitor technologies being proposed and, for example, some studies have focussed on exploiting the photothermal properties

of gold and silver coated shelled microbubbles (and nanorods) to kill the cancer cells [28–30].

1.2 Sonoporation and material identification

At present the mathematical modelling behind sonoporation is still in its infancy with only a handful of articles attempting to quantify the physical mechanisms behind sonoporation [31,32]. In vitro experiments performed on phantoms have shown that high frequency chirps significantly enhance the sonoporation procedure when used along with shelled microbubbles [4,13,21,33–35]. This is because the microbubble populations have a spread of radii and therefore a distribution of resonant frequencies. Since maximum sonoporation will occur when each microbubble shears against the capillary wall at its resonant frequency, it is no surprise that the chirp containing a range of frequencies performs better. Fundamental to the sonoporation efficiency are the material parameters of the shell which can include the thickness of the shell, its stiffness (shear modulus) and its Poisson ratio. The fundamental goal of the work presented here is therefore to identify the most suitable material parameters for the shelled microbubbles. As a possible experimental mechanism for testing the efficiency of the shells is in the bursting phase of the microbubble, this PhD will focus on developing mathematical models for evaluating the material parameters' influence on the collapse and relaxation times for shelled microbubbles. The relaxation time is defined as the time taken for the amplitude of an oscillating shelled microbubble to decrease to $1/e$ of its original amplitude.

1.3 Rayleigh-Plesset model

Most current shelled microbubble models are based on the Rayleigh-Plesset equation for a free gas bubble, which is derived by balancing the pressures acting on the inner surface of the shelled microbubble with those acting on the outside of the shelled microbubble's surface and the surrounding liquid. This gives [36–38]

$$R\ddot{R} + \frac{3}{2}\dot{R}^2 = \frac{1}{\rho_L}\left(P_g\left(\frac{R_o}{R}\right)^{3\kappa} - \frac{2\sigma}{R} - 4\mu_L\frac{\dot{R}}{R} - P_o - P_{ac}(t)\right) \tag{1.1}$$

where $R(t)$ is the instantaneous radius of the microbubble, $\dot{R} = dR/dt$, $\ddot{R} = d^2R/dt^2$, κ is the polytropic index, $P_g = P_o + 2\sigma/R_o$ is the equilibrium pressure inside the microbubble, R_o is the radius of the microbubble at rest, μ_L is the viscosity of the liquid, P_o is the ambient pressure in the surrounding liquid, σ is the surface tension at the liquid-gas interface and $P_{ac}(t)$ is the acoustic pressure applied by the ultrasound. The Rayleigh-Plesset equation assumes that the microbubble oscillations are purely radial and that the surrounding liquid is incompressible. The gas in the shelled microbubble is assumed to behave adiabatically despite its polytropic index being relatively close to one which is associated with isothermal behaviour [39]. The damping contributors are the viscosity of the liquid that surrounds the microbubble, thermal damping between the gas and the surrounding liquid, and damping associated with liquid compressibility via the external acoustic energy. The thermal damping can be accounted for by selecting the appropriate value for the polytropic index, κ [39]. The Rayleigh-Plesset equation can be modified to take account of the compressible nature of the surrounding liquid, implying that the Mach number for the microbubble wall given by $\dot{R}/c$, where c is the speed of sound in the liquid, is no longer negligible when compared to unity [39]. Two examples of Rayleigh-Plesset models which allow for compressibility are the Herring

and Trilling equation [40,41] and the Keller-Miksis model [42,43].

1.4 Shelled microbubble modelling

Marmottant et al. [44] modelled lipid shelled microbubbles using the following version of the Rayleigh-Plesset equation

$$R\ddot{R}+\frac{3}{2}\dot{R}^2 = \frac{1}{\rho_L}\left(P_g\left(\frac{R_o}{R}\right)^{3\kappa}\left(1-\frac{3\kappa\dot{R}}{c}\right)-\frac{4\mu_L\dot{R}}{R}-P_o-P_{ac}(t)-4\frac{\kappa_s\dot{R}}{R^2}-\frac{2\sigma(R)}{R}\right) \tag{1.2}$$

where the term $\sigma(R)$ is defined as the effective surface tension and κ_s is the surface dilatational viscosity. This model assumes that when the shelled microbubble oscillates, the elastic region holds only for a small range of radii. However, the model is capable of describing nonlinear effects particularly the compression only behaviour observed in the analysis of certain monolipid shelled microbubbles. This was the first model wherein the surface tension of the shell varies during various stages of its oscillatory motion. This was achieved by expressing the surface tension as a piecewise function dependent on the shell's area density with the shell experiencing a smaller surface tension when the shell itself is smaller. This is due to the area per molecule decreasing during contraction resulting in a smaller number of molecular interactions and therefore a smaller surface tension. Paul et al. [45] developed a Rayleigh-Plesset model using an effective surface tension that incorporated a dilatational elasticity term which was a function of the surface area change. The dilatational elasticity term was modelled using both quadratic and exponential terms with each approach giving similar results and predicting the subharmonic response with a reasonable level of accuracy [45]. Both of these models rely heavily on experimental observations for one particular type of UCA. Several other models also adopt an empirical approach which involves incorporating additional terms

into the Rayleigh-Plesset equation based on physical observations of experimental data. One such model has been developed by de Jong et al. [46–49].

1.5 Encapsulated interfacial shelled microbubble models

Church [50] developed a model for an encapsulated shelled microbubble incorporating both the inner and outer radii and the interfacial surface tension. This approach was developed using rigorous mathematical arguments rather than relying on an empirical method. Church assumed that the incompressible spherical encapsulated gas shelled microbubble was surrounded by an unbounded incompressible liquid and experienced radial oscillations when it was subjected to an external acoustic pressure. The model uses two surface tension expressions: a surface tension for the outer shell/liquid interface and an interfacial surface tension between the shell's inner radius and the gas layer. Church exploited the Rayleigh-Plesset equation and assumed that the shell material behaved as a viscoelastic solid obeying the Kelvin-Voigt constitutive equation

$$\tau_{rr}^{(s)} = 2\mu_s \frac{\partial u}{\partial r} + 2\eta_s \frac{\partial v}{\partial r}, \tag{1.3}$$

where μ_s and η_s are the shear modulus and the shear viscosity of the material, $u(r,t)$ is the radial displacement inside the shell and $v(r,t)$ is the radial component of the velocity inside the shell. Experimental evidence indicates that this model is more suited to albumin shelled bubbles with shell thicknesses of the order of 15 to 20 nm [39]. Note that the Kelvin-Voigt model is analogous to an elastic spring in parallel with a dashpot (damper).

Doinikov and Dayton [51] suggested a model for lipid encapsulated microbubbles where the shell is treated as a viscoelastic fluid that obeys the Maxwell constitutive equation

$$\tau_{rr}^{(s)} + \lambda_s \frac{\partial \tau_{rr}^{(s)}}{\partial t} = 2\eta_s \frac{\partial v}{\partial r}, \tag{1.4}$$

where λ_s is the relaxation time and η_s is the shear viscosity of the shell. This approach models the shell as an intermediate material between an elastic solid and a viscous fluid. Incorporating a Maxwell viscoelastic behaviour into the model helps to explain some of the experimental data that contradicted previous assumptions that the lipid shell behaved like a viscoelastic solid. The model predicts that a shelled microbubble possessing a viscoelastic fluid shell can have both higher and lower resonance frequencies than a free bubble. This depends on the choice of the shell parameters μ_s and η_s [39,51]. The Maxwell viscoelastic fluid model involves modelling an elastic spring in series with a dashpot (damper).

Doinikov et al. [52] proposed a modification to this model where the shell's viscous constant, κ_s, was replaced by a function of the shell's shear rate. Despite numerous Rayleigh-Plesset models existing for UCAs, experimental observations have been made that challenge the current, existing models [39]. The experimental observations of compression only behaviour for monolipid coated UCAs is highlighted by the asymmetrical oscillation curves that are experimentally observed and that were subsequently modelled empirically by Marmottant et al. [44] who separated the shell elastic behaviour into three different regions. According to current models, the shell's material parameters such as viscosity and elasticity, display a dependency on the initial radius of the shelled microbubble. However, large shelled microbubbles possess a greater mass and surface area yet should still

have the same viscosity and elasticity for the same type of material. This highlights a current flaw in the modelling of the rheological properties of monolipid UCAs which clearly requires a more fundamental and mathematically rigorous treatment [39].

1.6 Shelled microbubble collapse

The literature pertaining to the mathematical modelling of shelled microbubble collapse is very limited. Bogoyavlenskiy's paper [53] on the differential criterion of microbubble collapse is an analytical approach that exploits the Rayleigh-Plesset equation specifically for a viscous, Newtonian liquid. This work derives a general collapse condition relating to the viscosity of the surrounding fluid but it deals only with a gas microbubble and not a shelled, viscoelastic microbubble [53]. Rayleigh's [36] original work from 1917 contains an analytical solution for the collapse time of a ruptured microbubble but it is valid only for a gas microbubble (not shelled) in an inviscid liquid.

1.7 Collapse of shelled microbubbles and nonlinear elasticity

There currently exists very little literature pertaining specifically to UCA modelling using nonlinear elasticity, which is the standard approach for modelling large deformations of elastic materials and in particular soft materials such as in biological settings [54–59]. There are however, numerous publications relating to the dynamics of spherical bodies using nonlinear elasticity [60]. Tsiglifis and Pelekasis [61] used constitutive laws from nonlinear elasticity alongside the Kelvin-Voigt vis-

coelastic model to study the physical behaviour of various UCA types ranging from monolipids to polymer UCAs. They reported that the polymer based UCAs were consistent with the neo-Hookean model whereas monolipid UCAs were consistent with the Mooney-Rivlin constitutive law due to the presence of strain softening behaviour. Strain softening behaviour occurs due to the area density of the monolipid decreasing as the material stretches radially outwards. This behaviour has been observed in monolipids typically used in UCA shells such as Sonovue [39,61,62]. Gaudron et al. [63] have developed Rayleigh-Plesset models describing cavitation bubbles in soft tissue. They achieved this using nonlinear elasticity in conjunction with the Kelvin-Voigt viscoelastic model. They utilised both the neo-Hookean and the Mooney-Rivlin models to develop their Rayleigh-Plesset equations. Despite this work being directly relevant to cavitation, a similar analytical approach could be adopted to consider the nonlinear behaviour of UCAs.

1.8 Outline of Thesis

The aim of this PhD thesis is to understand and identify how various material parameters such as the shear modulus (stiffness), Poisson ratio and thickness of the shell influence the collapse and relaxation times and natural frequency of shelled microbubbles.

Chapter 2 proposes an analytical model developed using an asymptotic expansion for a stressed, compressible shelled microbubble that oscillates about its equilibrium position and considers how varying the shear modulus, Poisson ratio and shell thickness influences the shell's collapse time.

Chapter 3 discusses the physical model for the deformation of an open microbubble shell. An opening angle approach is used with the original stress free configuration being represented by an open, deformed and incomplete shelled microbubble which is stressed via a hoop stress in order to subject the shell's surface to both a radial and an angular deformation. Future work will focus on modelling both the forward (inflationary) stage and the collapse phase of the shell and the influence of the material parameters on the collapse time.

Chapter 4 develops a Rayleigh-Plesset equation describing an incompressible, thin shelled, gas loaded microbubble with a shell composed of a liquid-crystalline material. Time-dependent perturbation theory is used to linearise the physical model and the relaxation time and natural frequency of the shelled microbubble and their dependency on the material parameters (Leslie viscosities [64]) of the shell are considered.

The original work in this thesis is:

Chapter 2 proposes an analytical model for a stressed oscillating shelled microbubble and identifies how the key material parameters influence the dynamic behaviour of the shelled microbubble. No previous study has isolated and identified the influence of these physical parameters nor has any previous study developed a model for a compressible shell.

Chapter 3 proposes for the first time an analytical model for an angularly and radially deformed, open shelled microbubble by exploiting an opening angle approach for a shelled microbubble. There is no spherical model in the literature that has used an opening angle approach to model a stressed shelled bubble nor is there any model that has attempted to model the shell's surface unfolding.

Chapter 4 develops a model for a shelled liquid-crystal microbubble. Despite there being numerous Rayleigh-Plesset models for shelled microbubbles there is no existing model that views the shell as a mesophase. This is the first serious attempt at modelling a shelled microbubble which exhibits both solid and liquid characteristics by utilising liquid-crystal theory [65–67]. The model is linearised and expressions are determined for the relaxation time and the natural frequency of the shell. The influence of the material parameters of the shell on the relaxation time and the natural frequency are discussed.

Chapter 2

The analysis of the collapse of a shelled microbubble

2.1 Introduction

In this chapter a theoretical model is proposed to predict the dynamics of an oscillating shelled microbubble. A compressible, neo-Hookean [54] strain energy density function is used to model the potential energy per unit volume of the shell. Previous studies by Tsiglifis and Pelekasis [61] and Efthymiouhas et al. [62] show that thick shelled ultrasound contrast agents (thicknesses of the order of 15nm and above) can be modelled by using a neo-Hookean strain energy density function whereas monolipid shells (thicknesses of the order of 4nm) are consistent with a Mooney-Rivlin strain energy density function. This study will focus on microbubble shells with thicknesses between 20-50nm whose shell can be be described via a compressible, neo-Hookean strain energy density function. A neo-Hookean strain energy density function has the added advantage of being among the simplest of nonlinear models to study. Nonlinear elasticity can account for large scale defor-

mations and has been used in numerous studies pertaining to modelling rubber mediums and soft tissue [54,68]. Experimental studies [14,15] have shown that the Poisson ratio of a typical ultrasound contrast agent is between 0.48 and 0.49 which is similar to rubber. The standard approach to modelling rubber is to utilise nonlinear strain energy density functions which are either neo-Hookean or Mooney-Rivlin [69]. The third invariant describes the compressibility of the material and requires the use of Poisson's ratio. Including Poisson's ratio in the modelling process allows us to identify how this parameter influences the collapse time of the shell whereas a neo-Hookean or Mooney-Rivlin strain energy density function only uses the shear modulus [69]. In the approach adopted here, a stress is applied to the shell by applying a series of radially directed small stress steps to the inner surface of the shell and setting the outer surface's stress normal to the surface to zero. This stressing process is quasistatic and is thus independent of time. The spatial profiles of the Cauchy radial and angular (hoop) stresses that are created within the shell during this process are evaluated using an asymptotic expansion. The nonlinear model is linearised primarily to give some analytical insight into how the material parameters influence both the inflationary phase of the shell and its subsequent collapse time. The derived nonlinear model displays a level of complexity that does not lend itself to being easily solved analytically or numerically. Linearising circumvents the necessity of large scale numerical schemes since solving the nonlinear model computationally is a formidable task due to the complexity of the model, the stiffness of the equations and the required convergence of the numerical scheme. The stress applied to inflate the shell (commensurate with typical values used in sonoporation) works out to be around 1% of the shear modulus of the shell [15,21]. This small stress load makes the asymptotic expansion possible. Once a certain radial deformation is reached, the stress load at the inner radius is

switched off causing the shell to collapse and oscillate about its equilibrium (stress free) position. The inflated shell configuration is used as an initial condition to model the time evolving collapse phase of the shell. The collapse phase is modelled by applying the momentum balance law and mass conservation. The model is then used to show the influence of the shell's thickness, its Poisson ratio and the shear modulus on the collapse times of the shelled microbubble.

2.2 Stressing a shelled microbubble

2.2.1 Defining the coordinate frames

Consider the reference configuration of a stress free, fully formed spherical shell with inner and outer radii of R_I and R_O respectively ([70],p246). A configuration of a body is defined as a one-to-one correspondence that maps the particles of the body onto their locations in Euclidean space ([70],p77). Figure 2.1 illustrates such a scenario.

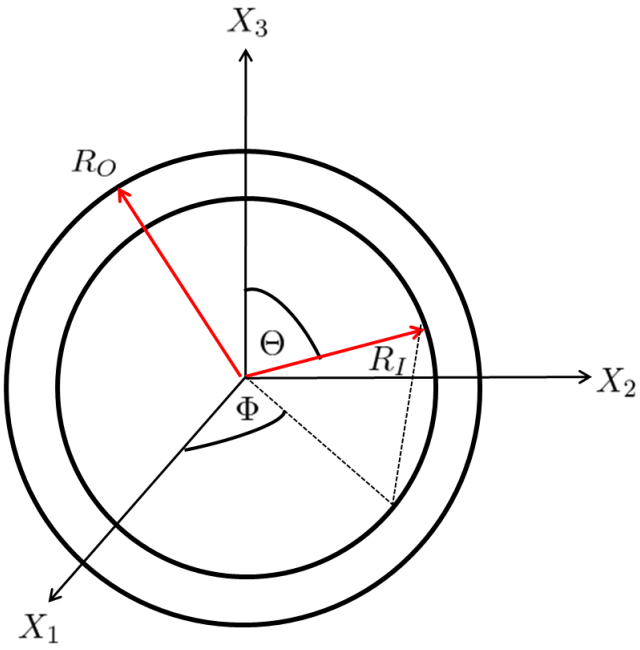

Figure 2.1: Reference configuration for a stress free spherical shell.

The reference configuration of the system is a spherical shell possessing no stress. A spherical polar coordinate system with coordinates $(X^1, X^2, X^3) = (R, \Theta, \Phi)$ has the coordinate transformation (Cartesian coordinates) $(X_1, X_2, X_3) = (R\sin\Theta\cos\Phi, R\sin\Theta\sin\Phi, R\cos\Theta)$. The reference configuration basis vectors e_R, e_Θ and e_Φ can be written in terms of the Cartesian basis vectors e_1, e_2, e_3 to give

$$e_R = \sin\Theta\cos\Phi e_1 + \sin\Theta\sin\Phi e_2 + \cos\Theta e_3, \tag{2.1}$$

$$e_\Theta = \cos\Theta\cos\Phi e_1 + \cos\Theta\sin\Phi e_2 - \sin\Theta e_3, \tag{2.2}$$

and

$$e_\Phi = -\sin\Phi e_1 + \cos\Phi e_2. \tag{2.3}$$

The following relationships for the basis vectors hold

$$\frac{\partial e_R}{\partial \Theta} = \cos\Theta\cos\Phi e_1 + \cos\Theta\sin\Phi e_2 - \sin\Theta e_3 = e_\Theta, \tag{2.4}$$

$$\frac{\partial e_R}{\partial \Phi} = -\sin\Theta\sin\Phi e_1 + \sin\Theta\cos\Phi e_2 = \sin\Theta e_\Phi, \tag{2.5}$$

$$\frac{\partial e_\Theta}{\partial \Theta} = -\sin\Theta\cos\Phi e_1 - \sin\Theta\sin\Phi e_2 - \cos\Theta e_3 = -e_R, \tag{2.6}$$

$$\frac{\partial e_\Theta}{\partial \Phi} = -\cos\Theta\sin\Phi e_1 + \cos\Theta\cos\Phi e_2 = \cos\Theta e_\Phi, \tag{2.7}$$

$$\frac{\partial e_\Phi}{\partial \Theta} = 0, \tag{2.8}$$

and

$$\frac{\partial e_\Phi}{\partial \Phi} = -\cos\Phi e_1 - \sin\Phi e_2 = -\sin\Theta e_R - \cos\Theta e_\Theta. \tag{2.9}$$

The current configuration is an inflated spherical shell possessing a stress. Let the current configuration basis vectors be represented by e_r, e_θ and e_ϕ where e_1, e_2 and e_3 are the standard Cartesian basis vectors, and so

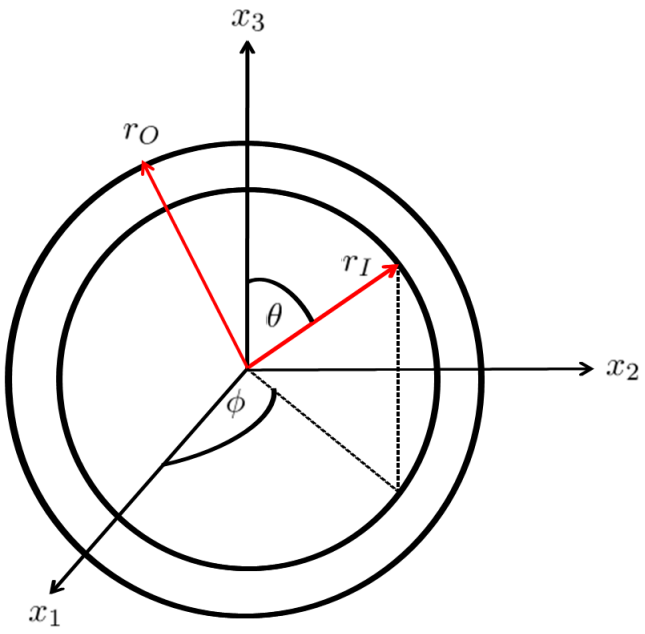

Figure 2.2: Current configuration for a stressed spherical shell.

$$e_r = \sin\theta\cos\phi e_1 + \sin\theta\sin\phi e_2 + \cos\theta e_3, \tag{2.10}$$

$$e_\theta = \cos\theta\cos\phi e_1 + \cos\theta\sin\phi e_2 - \sin\theta e_3, \tag{2.11}$$

and

$$e_\phi = -\sin\phi e_1 + \cos\phi e_2. \tag{2.12}$$

2.2.2 Tensor theory and vector fields

Consider the following discussion from Ogden ([70], p55) regarding curvilinear coordinates. Let $\psi : \mathscr{D} \to \mathbb{R}^3$ represent a one-to-one continuous mapping whose inverse ψ^{-1} is also continuous. If $x \in \mathscr{D}$ then

$$\psi(x) = (x^1, x^2, x^3), \text{ and } x = \psi^{-1}(x^1, x^2, x^3). \tag{2.13}$$

Assuming that ψ and ψ^{-1} have continuous derivatives up to infinity, given ψ and $\mathscr{D}$, there are three scalar fields $\psi^i : \mathscr{D} \to \mathbb{R}$, such that

$$\psi(x) = (\psi^1(x), \psi^2(x), \psi^3(x)), \quad x \in \mathscr{D}. \tag{2.14}$$

The fields ψ^i are the coordinate functions of ψ on $\mathscr{D}$, ψ is a coordinate system on $\mathscr{D}$ which is a coordinate neighbourhood. The coordinates x^i of the point x in the coordinate system ψ are given by

$$x^i = \psi^i(x). \tag{2.15}$$

They are called the curvilinear coordinates covering $\mathscr{D}$ where x^i represents the curvilinear coordinates and x_i denote the Cartesian coordinates [70]. Equation (2.15) can be used to define a subset of $\mathscr{D}$ called an x^i-coordinate surface of ψ in $\mathscr{D}$ such that

$$x^i \equiv \psi^i(x) = \text{constant}. \tag{2.16}$$

The natural basis of ψ at x is written as

$$g_i(x) = \frac{\partial x_j}{\partial x^i} e_j, \tag{2.17}$$

where g_i is a vector field on $\mathscr{D}$ and g_i is a tangent to the x^i-coordinate curve of ψ. A reciprocal basis g^i of g_i at each point x of $\mathscr{D}$ may be defined such that

$$g^i(x) \cdot g_j(x) = \delta^i_j \tag{2.18}$$

where δ^i_j is the Kronecker delta and $\{g_i\}_{i\in\{1,2,3\}}$ represents a fixed set of general basis vectors whose elements are assumed to be non-zero and non-parallel to each other. The general basis vectors are linearly independent [58]. The reciprocal general basis vectors are defined as

$$g^i\,(x) = \frac{\partial x^i}{\partial x_j} e_j. \tag{2.19}$$

From equation (2.18), let I denote the identity matrix, such that

$$\mathrm{I} = g^i(x) \otimes g_i(x) = g_i(x) \otimes g^i(x), \tag{2.20}$$

for each x in $\mathscr{D}$. The contravariant and covariant components of I are denoted by $g^{ij}(x)$ and $g_{ij}(x)$ respectively, where

$$g^{ij}(x) = g^i(x) \cdot g^j(x), \quad g_{ij}(x) = g_i(x) \cdot g_j(x),$$

$$g^i(x) = g^{ij}(x) g_j(x), \quad g_i(x) = g_{ij}(x) g^j(x), \tag{2.21}$$

and the mixed components are δ^i_j. To distinguish between the reference and current vector fields, we employ an uppercase (G) for the reference configuration and a lowercase (g) for the current configuration. Using equations (2.17) and (2.18), the vector fields for the reference configuration are

$$G_1 = e_R, \tag{2.22}$$

$$G^1 = e_R, \tag{2.23}$$

$$G_2 = R\cos\Theta\cos\Phi e_1 + R\cos\Theta\sin\Phi e_2 - R\sin\Theta e_3 = R e_\Theta, \tag{2.24}$$

$$G^2 = \frac{1}{R} e_\Theta, \tag{2.25}$$

$$G_3 = -R\sin\Theta\sin\Phi e_1 + R\sin\Theta\cos\Phi e_2 = R\sin\Theta e_\Phi, \tag{2.26}$$

and

$$G^3 = \frac{1}{R\sin\Theta} e_\Phi. \tag{2.27}$$

Similarly, for the current configuration

$$g_1 = e_r, \tag{2.28}$$

$$g^1 = e_r, \tag{2.29}$$

$$g_2 = r\cos\theta\cos\phi e_1 + r\cos\theta\sin\phi e_2 - r\sin\theta e_3 = re_\theta, \tag{2.30}$$

$$g^2 = \frac{1}{r}e_\theta, \tag{2.31}$$

$$g_3 = -r\sin\theta\sin\phi e_1 + r\sin\theta\cos\phi e_2 = r\sin\theta e_\phi, \tag{2.32}$$

and

$$g^3 = \frac{1}{r\sin\theta}e_\phi. \tag{2.33}$$

Using the identities from equation (2.21) the reference and current configurations can be written as

$$G_{ij} = \begin{pmatrix} 1 & 0 & 0 \\ 0 & R^2 & 0 \\ 0 & 0 & R^2\sin^2\Theta \end{pmatrix},$$

and

$$g_{ij} = \begin{pmatrix} 1 & 0 & 0 \\ 0 & r^2 & 0 \\ 0 & 0 & r^2\sin^2\theta \end{pmatrix}.$$

The g_{ij} and g^{ij} are commonly referred to as the metric coefficients and determine the geometrical characteristics of a given basis [58].

2.2.3 The gradient and divergence of a tensor

For a tensor field T of order n, grad T is written as $\nabla \otimes T$ and represents a tensor field of order $n+1$. If v is a vector field, the scalar field $\nabla \cdot v$ (the divergence of v), is defined as

$$\text{div } v \equiv \nabla \cdot v = \text{tr}\left(\nabla \otimes v\right), \tag{2.34}$$

where tr represents the trace which is defined as the sum $(\nabla \otimes v)_{ii}$. The divergence operation is the contraction of the second order tensor field $\nabla \otimes v$. Consider the vector field v, then

$$\text{grad } v(x) \equiv \nabla \otimes v(x) = \frac{\partial v(x)}{\partial x_j} \otimes e_j, \tag{2.35}$$

where $v = v_i e_i$. Contraction of equation (2.35) gives the component expression for div v. Hence

$$\nabla \cdot v(x) = \frac{\partial v_i(x)}{\partial x_i}. \tag{2.36}$$

For a vector field v where $v = v_k g^k$ then it follows that ([70], p65)

$$\nabla \otimes v = \left(\frac{\partial v_k}{\partial x^j} - \Gamma^i_{kj} v_i\right) g^k \otimes g^j, \tag{2.37}$$

(note that $\Gamma^i_{kj} = \Gamma^i_{jk}$) where the Christoffel symbols are ([70], p58)

$$\Gamma^i_{kj} = -g_k \cdot \frac{\partial g^i}{\partial x^j}. \tag{2.38}$$

For a tensor field T of order n, equation (2.35) generalises to

$$\nabla \otimes T = \frac{\partial T}{\partial x_i} \otimes e_i,$$

$$\nabla \otimes T = \frac{\partial T_{i_1 i_2 \ldots i_n}}{\partial x_i} \otimes e_{i_1} \otimes e_{i_2} \otimes \ldots \otimes e_{i_n} \otimes e_i, \tag{2.39}$$

where the components $T_{i_1 i_2 \ldots i_n}$ are scalar fields. For a second order tensor ([70], p65)

$$T = T_{ij} g^i \otimes g^j. \tag{2.40}$$

2.2.4 Calculating the gradient of the deformation

The applied stress is due to a stress load that is applied to the interior surface of the microbubble's shell. The formal derivation of the deformation gradient of an inflated sphere will be included to prepare the reader for the novel derivation that will be performed in Chapter 3. The deformation gradient F is a two point tensor (mixed tensorial basis) with a deformation, $\chi = \chi_i g^i$, where the gradient of the deformation is defined as $F = \nabla \otimes \chi$. From equations (2.37) and (2.38) we get

$$\begin{aligned} \nabla \otimes \chi = \frac{\partial}{\partial X^j}\left(\chi_i g^i\right) \otimes G^j &= \left(\frac{\partial \chi_i}{\partial X^j} g^i + \chi_i \frac{\partial g^i}{\partial X^j}\right) \otimes G^j, \\ &= \left(\frac{\partial \chi_i}{\partial X^j} g^i + \chi_i \frac{\partial g^i}{\partial X^j} \cdot g_i g^i\right) \otimes G^j, \\ &= \left(\frac{\partial \chi_i}{\partial X^j} + \chi_i \frac{\partial g^i}{\partial X^j} \cdot g_i\right) g^i \otimes G^j. \end{aligned} \tag{2.41}$$

The magnitude of the change in the basis vectors via the Cauchy stress is readily evaluated using the Christoffel symbols. Note that the Cauchy stress is not based on a mixed tensorial basis and is described by the area and the force in the current configuration. In spherical polar coordinates the current configuration can be transformed into physical components ([70],p64) to give $\chi_1 g^1 = \chi_1 e_r = \chi_r e_r$ resulting in $\chi_1 = \chi_r$. The χ_θ term is $\chi_2 g^2 = \chi_2 e_\theta / r = \chi_\theta e_\theta$ resulting in $\chi_2 = r\chi_\theta$. The χ_ϕ term is $\chi_3 g^3 = \chi_3 e_\phi / (r \sin\theta) = \chi_\phi e_\phi$ where $\chi_3 = r \sin\theta \chi_\phi$. Using equation

(2.41) we can determine the gradient of the deformation where the deformation is defined by $\chi_1 = r(R)$, and $\chi_2 = \chi_3 = 0$. Assuming $\theta(\Theta) = \Theta$ and $\phi(\Phi) = \Phi$, the terms for equation (2.41) are

$$(\nabla \otimes \chi)_{rR}\, e_r \otimes e_R = \left(\frac{\partial \chi_1}{\partial X^1} + \chi_1 \frac{\partial g^1}{\partial X^1} \cdot g_1\right) g^1 \otimes G^1 = \left(\frac{\partial r}{\partial R} + r\frac{\partial e_r}{\partial R} \cdot e_r\right) e_r \otimes e_R = r' e_r \otimes e_R, \tag{2.42}$$

$$(\nabla \otimes \chi)_{r\Theta}\, e_r \otimes e_\Theta = \left(\frac{\partial \chi_1}{\partial X^2} + \chi_1 \frac{\partial g^1}{\partial X^2} \cdot g_1\right) g^1 \otimes G^2 = (r e_\theta \theta' \cdot e_r)\, \frac{e_r \otimes e_\Theta}{R} = 0, \tag{2.43}$$

$$(\nabla \otimes \chi)_{r\Phi}\, e_r \otimes e_\Phi = \left(\frac{\partial \chi_1}{\partial X^3} + \chi_1 \frac{\partial g^1}{\partial X^3} \cdot g_1\right) g^1 \otimes G^3 = \left(r\frac{\partial e_r}{\partial \Phi} \cdot e_r\right) \frac{e_r \otimes e_\Phi}{R \sin \Phi} = (r \sin\theta e_\phi \phi' \cdot e_r)\, \frac{e_r \otimes e_\Phi}{R \sin \Theta} = 0, \tag{2.44}$$

$$(\nabla \otimes \chi)_{\theta R}\, e_\theta \otimes e_R = \left(\frac{\partial \chi_2}{\partial X^1} + \chi_1 \frac{\partial g^1}{\partial X^1} \cdot g_2\right) g^2 \otimes G^1 = \left(r\frac{\partial e_r}{\partial R} \cdot r e_\theta\right) \frac{e_\theta \otimes e_R}{r} = 0, \tag{2.45}$$

$$\begin{aligned}(\nabla \otimes \chi)_{\theta\Theta}\, e_\theta \otimes e_\Theta &= \left(\frac{\partial \chi_2}{\partial X^2} + \chi_1 \frac{\partial g^1}{\partial X^2} \cdot g_2\right) g^2 \otimes G^2 = \left(\chi_1 \frac{\partial g^1}{\partial X^2} \cdot g_2\right) \frac{e_\theta \otimes e_\Theta}{rR} \\ &= \left(r\frac{\partial e_r}{\partial \Theta} \cdot r e_\theta\right) \frac{e_\theta \otimes e_\Theta}{rR} = \left(\frac{r}{R}\theta'\right) e_\theta \otimes e_\Theta,\end{aligned} \tag{2.46}$$

$$(\nabla \otimes \chi)_{\theta\Phi}\, e_\theta \otimes e_\Phi = \left(\frac{\partial \chi_2}{\partial X^3} + \chi_1 \frac{\partial g^1}{\partial X^3} \cdot g_2\right) g^2 \otimes G^3 = \left(r\frac{\partial e_r}{\partial \Phi} \cdot r e_\theta\right) \frac{e_\theta \otimes e_\Phi}{rR \sin \Theta}$$

$$= \left(r \sin\theta e_\phi \phi' \cdot r e_\theta\right) \frac{e_\theta \otimes e_\Phi}{rR \sin\Theta} = 0, \tag{2.47}$$

$$(\nabla \otimes \chi)_{\phi R}\, e_\phi \otimes e_R = \left(\frac{\partial \chi_3}{\partial X^1} + \chi_1 \frac{\partial g^1}{\partial X^1} \cdot g_3\right) g^3 \otimes G^1 = \left(r \frac{\partial e_r}{\partial R} \cdot r \sin\theta e_\phi\right) \frac{e_\phi \otimes e_R}{r \sin\theta} = 0, \tag{2.48}$$

$$(\nabla \otimes \chi)_{\phi\Theta}\, e_\phi \otimes e_\Theta = \left(\frac{\partial \chi_3}{\partial X^2} + \chi_1 \frac{\partial g^1}{\partial X^2} \cdot g_3\right) g^3 \otimes G^2 = \left(r e_\theta \frac{\partial \theta}{\partial \Theta} \cdot r \sin\theta e_\phi\right) \frac{e_\phi \otimes e_\Theta}{rR \sin\theta} = 0, \tag{2.49}$$

and

$$\begin{aligned}(\nabla \otimes \chi)_{\phi\Phi}\, e_\phi \otimes e_\Phi = \left(\frac{\partial \chi_3}{\partial X^3} + \chi_1 \frac{\partial g^1}{\partial X^3} \cdot g_3\right) g^3 \otimes G^3 &= \left(r \frac{\partial e_r}{\partial \Phi} \cdot r \sin\theta e_\phi\right) \frac{e_\phi \otimes e_\Phi}{rR \sin\theta \sin\Theta} \\ &= \left(\frac{r \sin\theta}{R \sin\Theta} \phi'\right) e_\phi \otimes e_\Phi. \end{aligned} \tag{2.50}$$

The gradient of this deformation is a two point tensor, given by $F = \nabla \otimes \chi$, i.e.

$$F = \begin{pmatrix} r' & 0 & 0 \\ 0 & \frac{r\theta'}{R} & 0 \\ 0 & 0 & \frac{r \sin\theta}{R \sin\Theta} \phi' \end{pmatrix}. \tag{2.51}$$

If $\theta = \Theta$ and $\phi = \Phi$, then

$$F = \begin{pmatrix} r' & 0 & 0 \\ 0 & \frac{r}{R} & 0 \\ 0 & 0 & \frac{r}{R} \end{pmatrix}. \tag{2.52}$$

2.2.5 Defining the appropriate strain energy density function

If we assume that the shell material is hyperelastic then there exists a strain energy density function expressing the potential energy per unit volume. The strain energy density function that will be used here to model the microbubble shell is a neo-Hookean strain energy density function [54,58,71], $W(F)$, which includes a compressible term that is used to model the change in volume of the shell of the microbubble as it is inflated. The strain energy term associated with the compressibility of the shell was developed by Blatz ([72], p23-45). The determinant of F (denoted by J) gives a measure of how the volume of the spherical shell changes as it maps from the stress free, reference configuration to the stressed, current configuration. The determinant is given by

$$J = \frac{r'r^2}{R^2}. \tag{2.53}$$

The neo-Hookean strain energy density function is ([54], equation (5))

$$W(F) = \frac{\mu}{2}\left(\mathrm{tr}(FF^T) - 3\right) + \frac{\mu}{2\beta}\left(J^{-2\beta} - 1\right), \tag{2.54}$$

where FF^T is defined as the left Cauchy-Green deformation tensor ([58],p81), μ is the shear modulus, ν is Poisson's ratio and $\beta = \nu/(1-2\nu)$. Consider the following

trace properties

$$\begin{aligned}
\frac{\partial}{\partial F_{mn}}\left(\det F\right) &= \frac{\partial}{\partial F_{mn}}\left(\frac{1}{6}\epsilon_{ijk}\epsilon_{pqr}F_{ip}F_{jq}F_{kr}\right), \\
&= \frac{1}{6}\epsilon_{ijk}\epsilon_{pqr}\left(\delta_{im}\delta_{pn}F_{jq}F_{kr} + F_{ip}\delta_{jm}\delta_{qn}F_{kr} + F_{ip}F_{jq}\delta_{km}\delta_{rn}\right), \\
&= \frac{1}{6}\left(\epsilon_{mjk}\epsilon_{nqr}F_{jq}F_{kr} + \epsilon_{imk}\epsilon_{pnr}F_{ip}F_{kr} + \epsilon_{ijm}\epsilon_{pqn}F_{ip}F_{jq}\right), \\
&= \frac{1}{6}\left(\epsilon_{mjk}\epsilon_{nqr}F_{jq}F_{kr} + \epsilon_{mik}\epsilon_{npr}F_{ip}F_{kr} + \epsilon_{mij}\epsilon_{npq}F_{ip}F_{jq}\right), \\
&= \frac{1}{2}\epsilon_{mjk}\epsilon_{nqr}F_{jq}F_{kr}, \qquad (2.55)
\end{aligned}$$

and premultiplying equation (2.55) by F_{pn} leads to

$$\begin{aligned}
F_{pn}\frac{\partial}{\partial F_{mn}}\left(\det F\right) &= \frac{1}{2}\epsilon_{mjk}\epsilon_{nqr}F_{pn}F_{jq}F_{kr}, \\
&= \frac{1}{2}\epsilon_{mjk}\left(\det F\right)\epsilon_{pjk}, \\
&= \frac{1}{2}\epsilon_{mjk}\epsilon_{pjk}\left(\det F\right), \\
&= \frac{1}{2}\left(2\delta_{mp}\right)\left(\det F\right), \\
&= \left(\det F\right)\delta_{mp}. \qquad (2.56)
\end{aligned}$$

Multiplying equation (2.56) through by $\left(F^{-1}\right)_{qp}$ results in

$$\frac{\partial}{\partial F_{mq}}\left(\det F\right) = \left(\det F\right)\left(F^{-1}\right)_{qm}, \qquad (2.57)$$

which can be written as

$$\frac{\partial J}{\partial F} = |F|(F^{-1})^T = JF^{-T}. \qquad (2.58)$$

Similarly for the trace, where $\mathrm{tr}\left(FF^T\right) = \left(FF^T\right)_{ii} = F_{ij}F_{ij}$, the derivative with respect to F gives

$$\frac{\partial}{\partial F_{pq}}\left(F_{ij}F_{ij}\right) = 2F_{pq}, \tag{2.59}$$

or

$$\frac{\partial(\mathrm{tr}(FF^T))}{\partial F} = 2F. \tag{2.60}$$

The stresses can be described using the first Piola-Kirchhoff stress tensor which is the transpose of the nominal stress tensor, relating the force in the current configuration to the area in the reference configuration [54]. Recall that the Cauchy stresses relate the force in the current configuration to the area in the current configuration. The first Piola-Kirchhoff stress tensor, $S(F)$, is given using equation (2.58) and equation (2.60) along with equation (2.54), to give ([54], equation (5)),

$$\begin{aligned} S(F) = \frac{\partial W}{\partial F} &= \frac{\mu}{2}(2F) + \frac{\mu}{2\beta}\left(-2\beta J^{-2\beta-1}\frac{\partial J}{\partial F}\right) \\ &= \mu\left(-J^{-2\beta}F^{-T} + F\right). \end{aligned} \tag{2.61}$$

Substituting equation (2.52) into equation (2.61) gives

$$\begin{aligned} S = \mu\left(-J^{-2\beta}\frac{1}{r'} + r'\right)e_r \otimes e_R + \mu\left(-J^{-2\beta}\frac{R}{r} + \frac{r}{R}\right)e_\theta \otimes e_\Theta \\ + \mu\left(-J^{-2\beta}\frac{R}{r} + \frac{r}{R}\right)e_\phi \otimes e_\Phi. \end{aligned} \tag{2.62}$$

2.2.6 Calculating the divergence of the first Piola-Kirchoff stress tensor

This subsection will formally derive the divergence of the first Piola-Kirchoff stress tensor for an inflated, shelled microbubble. This task will be performed to prepare

the reader for the novel derivation of the divergence of the first Piola-Kirchoff stress tensor for an open shelled microbubble in Chapter 3. For the static solution of a stressed shelled microbubble, the divergence of the first Piola-Kirchhoff stress tensor will be equal to zero. To determine $\nabla \cdot S$, we need to be able to relate the physical coordinates for the mixed tensorial basis to the general basis vectors represented by the components g_i and G_i where $i \in \{1, 2, 3\}$. The first Piola-Kirchhoff stress tensor is represented by ([70], p34), $S = S_i^{\ j} g^i \otimes G_j$ where $S_i^{\ j}$ are the left-covariant components of S. Converting physical coordinates into generalised coordinates using equations (2.4) to (2.27) and equations (2.28) to (2.33)

$$S_1^{\ 1} g^1 \otimes G_1 = S_1^{\ 1} e_r \otimes e_R = S_{rR} e_r \otimes e_R,$$

where

$$S_{rR} = \mu \left(-J^{-2\beta} \frac{1}{r'} + r' \right), \tag{2.63}$$

$$S_2^{\ 2} g^2 \otimes G_2 = S_2^{\ 2} \frac{R}{r} e_\theta \otimes e_\Theta = S_{\theta\Theta} e_\theta \otimes e_\Theta,$$

where

$$\frac{r}{R} S_{\theta\Theta} = \mu \left(-J^{-2\beta} + \frac{r^2}{R^2} \right), \tag{2.64}$$

and

$$S_3^{\ 3} g^3 \otimes G_3 = S_3^{\ 3} \frac{e_\phi}{r \sin\theta} \otimes R \sin\Theta e_\Phi = S_{\phi\Phi} e_\phi \otimes e_\Phi,$$

where $\theta = \Theta$, results in

$$\frac{r}{R} S_{\phi\Phi} = \mu \left(-J^{-2\beta} + \frac{r^2}{R^2} \right). \tag{2.65}$$

Calculating the divergence of S using equations (2.37), (2.38) and (2.40) results in

$$\nabla \cdot S = \frac{\partial}{\partial X^k}\left(S_i^{\ j} g^i \otimes G_j\right) \cdot G^k. \tag{2.66}$$

Only $S_1^{\ 1}, S_2^{\ 2}$ and $S_3^{\ 3}$ need to be evaluated because the off-diagonal elements are all equal to zero. Calculating each of the terms in $\nabla \cdot S$ using equation (2.66) and equations (2.22) to (2.33), gives

$$\frac{\partial}{\partial X^1}\left(S_1^{\ 1} g^1 \otimes G_1\right) \cdot G^1 = \frac{\partial S_1^{\ 1}}{\partial R}\left(e_r \otimes e_R\right) \cdot e_R = \frac{\partial S_1^{\ 1}}{\partial R} e_r. \tag{2.67}$$

Similarly we get

$$\begin{aligned}\frac{\partial}{\partial X^1}\left(S_2^{\ 2} g^2 \otimes G_2\right) \cdot G^1 &= \frac{\partial}{\partial R}\left(S_2^{\ 2}\frac{e_\theta}{r} \otimes R e_\Theta\right) \cdot e_R \\ &= \frac{\partial}{\partial R}\left(S_2^{\ 2}\frac{R}{r}\right)\left(e_\theta \otimes e_\Theta\right) \cdot e_R = 0,\end{aligned} \tag{2.68}$$

since $(e_\theta \otimes e_\Theta) \cdot e_R = 0$. Similarly

$$\begin{aligned}\frac{\partial}{\partial X^1}\left(S_3^{\ 3} g^3 \otimes G_3\right) \cdot G^1 &= \frac{\partial}{\partial R}\left(S_3^{\ 3}\frac{e_\phi}{r\sin\theta} \otimes R\sin\Theta e_\Phi\right) \cdot e_R \\ &= \frac{\partial}{\partial R}\left(S_3^{\ 3}\frac{R\sin\Theta}{r\sin\theta}\right)\left(e_\phi \otimes e_\Phi\right) \cdot e_R = 0,\end{aligned} \tag{2.69}$$

since $(e_\phi \otimes e_\Phi) \cdot e_R = 0$. Additionally

$$\frac{\partial}{\partial X^2}\left(S_2^{\ 2} g^2 \otimes G_2\right) \cdot G^2 = \frac{\partial}{\partial \Theta}\left(S_2^{\ 2}\frac{e_\theta}{r} \otimes R e_\Theta\right) \cdot \frac{e_\Theta}{R} = \frac{S_2^{\ 2}}{r}\frac{\partial}{\partial \Theta}\left(e_\theta \otimes e_\Theta\right) \cdot e_\Theta$$

$$= \frac{S_2^{\ 2}}{r}\left(\frac{\partial e_\theta}{\partial \Theta} \otimes e_\Theta + e_\theta \otimes \frac{\partial e_\Theta}{\partial \Theta}\right) \cdot e_\Theta = \frac{S_2^{\ 2}}{r}\left(\frac{\partial e_\theta}{\partial \theta}\theta' \otimes e_\Theta\right) \cdot e_\Theta = -\frac{S_2^{\ 2}}{r} e_r, \tag{2.70}$$

since $\theta' = 1$ and S_2^2 depends solely on r, r' and R. Similarly

$$\frac{\partial}{\partial X^2}\left(S_1{}^1 g^1 \otimes G_1\right)\cdot G^2 = \frac{\partial}{\partial \Theta}\left(S_1{}^1 e_r \otimes e_R\right)\cdot\frac{e_\Theta}{R}$$

$$= \frac{S_1{}^1}{R}\left(\theta' e_\theta \otimes e_R + e_r \otimes e_\Theta\right)\cdot e_\Theta = \frac{S_1{}^1}{R}\left(e_r \otimes e_\Theta\right)\cdot e_\Theta = \frac{S_1{}^1}{R}e_r, \tag{2.71}$$

since $(e_\theta \otimes e_R)\cdot e_\Theta = 0$. Continuing

$$\frac{\partial}{\partial X^2}\left(S_3{}^3 g^3 \otimes G_3\right)\cdot G^2 = \frac{\partial}{\partial \Theta}\left(S_3{}^3 e_\phi \otimes e_\Phi \frac{R\sin\Theta}{r\sin\theta}\right)\cdot\frac{e_\Theta}{R}$$

$$= \frac{S_3{}^3}{R}\left(\frac{e_\phi}{\partial\Theta}\otimes e_\Phi\frac{\sin\Theta}{\sin\theta} + e_\phi \otimes \frac{\partial e_\Phi}{\partial\Theta}\left(\frac{\sin\Theta}{\sin\theta}\right) + e_\phi\otimes e_\Phi\frac{\partial}{\partial\Theta}\left(\frac{\sin\Theta}{\sin\theta}\right)\right)\cdot e_\Theta = 0, \tag{2.72}$$

and similarly

$$\frac{\partial}{\partial X^3}\left(S_1{}^1 g^1 \otimes G_1\right)\cdot G^3 = \frac{\partial}{\partial\Phi}\left(S_1{}^1 e_r \otimes e_R\right)\cdot\frac{e_\Phi}{R\sin\Theta} = \frac{S_1{}^1}{R\sin\Theta}\left(\frac{\partial e_r}{\partial\Phi}\otimes e_R + e_r\otimes\frac{\partial e_R}{\partial\Phi}\right)\cdot e_\Phi$$

$$= \frac{S_1{}^1}{R\sin\Theta}\left(\sin\theta\phi' e_\phi \otimes e_R + e_r\otimes\sin\Theta e_\Phi\right)\cdot e_\Phi = \frac{S_1{}^1}{R}\left(e_r\otimes e_\Phi\right)\cdot e_\Phi = \frac{S_1{}^1 e_r}{R}. \tag{2.73}$$

Other terms are

$$\frac{\partial}{\partial X^3}\left(S_2{}^2 g^2 \otimes G_2\right)\cdot G^3 = \frac{\partial}{\partial\Phi}\left(S_2{}^2\frac{R}{r}e_\theta\otimes e_\Theta\right)\cdot\frac{e_\Phi}{R\sin\Theta} = \frac{S_2{}^2}{r\sin\Theta}\frac{\partial}{\partial\Phi}\left(e_\theta\otimes e_\Theta\right)\cdot e_\Phi$$

$$= \frac{S_2{}^2}{r\sin\Theta}\left(\frac{\partial e_\theta}{\partial\Phi}\otimes e_\Theta + e_\theta\otimes\frac{\partial e_\Theta}{\partial\Phi}\right)\cdot e_\Phi = \frac{S_2{}^2}{r\sin\Theta}\left(\phi'\cos\phi e_\phi\otimes e_\Theta + e_\theta\otimes e_\Phi\cos\Theta\right)\cdot e_\Phi$$

$$= \frac{S_2{}^2\cot\Theta}{r}e_\theta, \tag{2.74}$$

and

$$\frac{\partial}{\partial X^3}\left(S_3{}^3 g^3\otimes G_3\right)\cdot G^3 = \frac{\partial}{\partial\Phi}\left(S_3{}^3\frac{R\sin\Theta}{r\sin\theta}e_\phi\otimes e_\Phi\right)\cdot\frac{e_\Phi}{R\sin\Theta} = \frac{S_3{}^3}{r\sin\theta}\frac{\partial}{\partial\Phi}\left(e_\phi\otimes e_\Phi\right)\cdot e_\Phi$$

$$= \frac{S_3^{\,3}}{r\sin\theta}\left(\frac{\partial e_\phi}{\partial \Phi}\otimes e_\Phi + e_\phi \otimes \frac{\partial e_\Phi}{\partial \Phi}\right)\cdot e_\Phi = \frac{S_3^{\,3}}{r\sin\theta}\left(-\phi'\sin\theta e_r \otimes e_\Phi - \phi'\cos\theta e_\theta \otimes e_\Phi\right)\cdot e_\Phi$$

$$= -\frac{S_3^{\,3}\phi'}{r}e_r - \frac{S_3^{\,3}\phi'\cot\theta}{r}e_\theta = -\frac{S_3^{\,3}}{r}e_r - \frac{S_3^{\,3}\cot\theta}{r}e_\theta. \tag{2.75}$$

Gathering together equations (2.67) to (2.75) and substituting into $\nabla \cdot S = 0$ gives the following radial and angular equations

$$\frac{\partial S_1^{\,1}}{\partial R} + \frac{2S_1^{\,1}}{R} - \frac{1}{r}\left(S_2^{\,2} + S_3^{\,3}\right) = 0, \tag{2.76}$$

$$\frac{S_2^{\,2}\cot\Theta}{r} - \frac{S_3^{\,3}\cot\theta}{r} = 0, \tag{2.77}$$

since $S_2^{\,2} = S_3^{\,3}$ due to $\theta = \Theta$. This results in the polar and azimuthal stresses having the same dependency on the radial deformation. Equation (2.76) is equivalent to the first Piola-Kirchoff stress in Daniel et al. [68].

2.2.7 Formulating the Cauchy stresses for the radial equation

To formulate the Cauchy stresses the radial differential equation (2.76) has to be rewritten in terms of the physical coordinates. Calculating the various terms in equation (2.76) using equations (2.63),(2.64) and (2.65) gives, from equation (2.53),

$$\frac{\partial J}{\partial R} = \frac{r''r^2}{R^2} + \frac{2(r')^2 r}{R^2} - \frac{2r'r^2}{R^3} = J\left(\frac{r''}{r'} + \frac{2r'}{r} - \frac{2}{R}\right), \tag{2.78}$$

$$\frac{\partial S_1^{\,1}}{\partial R} = \frac{\partial}{\partial R}\left(\mu\left(-J^{-2\beta}\frac{1}{r'} + r'\right)\right) = \mu\left(2\beta J^{-2\beta-1}\frac{\partial J}{\partial R}\frac{1}{r'} + J^{-2\beta}\left(\frac{1}{r'}\right)^2 r'' + r''\right)$$
$$= \mu\left(r''\left(1 + \frac{(2\beta+1)J^{-2\beta}}{(r')^2}\right) + J^{-2\beta}\left(\frac{4\beta}{r} - \frac{4\beta}{Rr'}\right)\right), \quad (2.79)$$

$$\frac{2S_1^{\,1}}{R} = \mu\left(\frac{-2J^{-2\beta}}{r'R} + \frac{2r'}{R}\right), \quad (2.80)$$

$$\frac{-S_2^{\,2}}{r} = \mu\left(\frac{J^{-2\beta}}{r} - \frac{r}{R^2}\right), \quad (2.81)$$

and (2.82)

$$\frac{-S_3^{\,3}}{r} = \mu\left(\frac{J^{-2\beta}}{r} - \frac{r}{R^2}\right). \quad (2.83)$$

Substituting equations (2.79) to (2.83) into equation (2.76) and dividing throughout by μ and multiplying by $J^{-2\beta}$ gives

$$r''\left(1 + \frac{(2\beta+1)J^{-2\beta}}{(r')^2}\right) + J^{-2\beta}\left(\frac{4\beta}{r} - \frac{4\beta}{Rr'} - \frac{2}{r'R} + \frac{2}{r}\right) + \frac{2r'}{R} - \frac{2r}{R^2} = 0,$$

and rearranging,

$$r''\left((r')^2 J^{2\beta} + 1 + 2\beta\right) = \left(\frac{4\beta r'}{R} - \frac{4\beta(r')^2}{r} + \frac{2r'}{R} - \frac{2(r')^2}{r}\right) + J^{2\beta}\left(\frac{2r(r')^2}{R^2} - \frac{2(r')^3}{R}\right). \quad (2.84)$$

To determine the Cauchy stresses in the radial and angular directions, equation (2.84) is solved for the inner surface of the shell being subjected to a load stress and the outer shell's surface being stress free. Using equation (2.63), at $R = R_I$ (the inner radius), this inner boundary condition is

$$S_{rR} = -pJF_{rR}^{-T}. \tag{2.85}$$

Hence from equations (2.151) and (2.53)

$$S_{rR}(R_I) = \frac{-pr^2(R_I)}{R_I^2}, \tag{2.86}$$

where p represents the stress load on the inner shell. From equation (2.63)

$$\mu \left(-J^{-2\beta} \frac{1}{r'(R)\Big|_{R=R_I}} + r'(R)\Big|_{R=R_I} \right) = \frac{-pr^2(R_I)}{R_I^2}.$$

Hence

$$\mu \left(\frac{r^2(R_I)r'(R)\Big|_{R=R_I}}{R_I^2} \right)^{-2\beta} - \frac{pr^2(R_I)r'(R)\Big|_{R=R_I}}{R_I^2} - \mu(r'(R)\Big|_{R=R_I})^2 = 0. \tag{2.87}$$

Calculating the boundary condition for the outer shell's radius $R = R_O$ gives

$$S_{rR} = 0.$$

Hence

$$-J^{-2\beta} \frac{1}{r'(R)\Big|_{R=R_O}} + r'(R)\Big|_{R=R_O} = 0,$$

and so

$$\left(\frac{r^2(R_O)r'(R)\Big|_{R=R_O}}{R_O^2} \right)^{2\beta} = \left(\frac{1}{r'(R)\Big|_{R=R_O}} \right)^2.$$

Rearranging gives the following boundary condition for $R = R_O$,

$$r'(R)\Big|_{R=R_O} = \left(\frac{R_O}{r(R_O)}\right)^{2\beta/(\beta+1)}. \tag{2.88}$$

Equation (2.84) can now be solved subject to the boundary conditions given by equations (2.87) and (2.88). The Cauchy stresses represented by τ ([58], p111) are then obtained from the first Piola-Kirchhoff stress tensor given by equation (2.61)

$$S = \frac{\partial W}{\partial F} = J\tau F^{-T}. \tag{2.89}$$

and rearranging gives

$$\tau = \frac{1}{J} S F^T. \tag{2.90}$$

The radial and angular stresses are evaluated using equations (2.52), (2.90) and (2.62)

$$\tau_{rr} = \frac{\mu}{J}\left(-J^{-2\beta} + (r')^2\right), \tag{2.91}$$

$$\tau_{\theta\theta} = \tau_{\phi\phi} = \frac{\mu}{J}\left(-J^{-2\beta} + \left(\frac{r}{R}\right)^2\right). \tag{2.92}$$

2.3 Nondimensionalising the quasistatic and collapse phases

Nondimensionalisation is used to assist in solving the quasistatic and collapse phases of the shelled microbubble. This is achieved by using the reference configuration's inner radius, R_I. Let

$$Y = \frac{R}{R_I}, \tag{2.93}$$

and

$$y(Y) = \frac{r(R)}{R_I}, \tag{2.94}$$

so $Y_I = 1$ and $Y_O = R_O/R_I$. This results in

$$\frac{\partial r}{\partial R} = \frac{\partial y}{\partial Y}, \tag{2.95}$$

and

$$\frac{\partial^2 r}{\partial R^2} = \frac{1}{R_I}\left(\frac{\partial^2 y}{\partial Y^2}\right). \tag{2.96}$$

The Jacobian given by equation (2.53) is then

$$J = \frac{y'y^2}{Y^2}, \tag{2.97}$$

which on substituting into equation (2.84) leads to

$$y''\left((y')^2\left(\frac{y'y^2}{Y^2}\right)^{2\beta} + 1 + 2\beta\right) = \left(\frac{4\beta y'}{Y} - \frac{4\beta(y')^2}{y} + \frac{2y'}{Y} - \frac{2(y')^2}{y}\right) + \left(\frac{y'y^2}{Y^2}\right)^{2\beta}\left(\frac{2y(y')^2}{Y^2} - \frac{2(y')^3}{Y}\right). \tag{2.98}$$

Nondimensionalising the boundary condition at the inner radius given by equation (2.87) and rearranging gives

$$\left(y^2(1)y'(Y)\Big|_{Y=1}\right)^{-2\beta} - \hat{p}\left(y^2(1)y'(Y)\Big|_{Y=1}\right) - (y'(Y)\Big|_{Y=1})^2 = 0, \tag{2.99}$$

where $\hat{p} = p/\mu$. Similarly, nondimensionalising the boundary condition at the outer radius represented by equation (2.88) leads to

$$y'(Y)\Big|_{Y=Y_O} = \left(\frac{Y_O}{y(Y_O)}\right)^{2\beta/(\beta+1)}. \tag{2.100}$$

2.4 Linearisation of the inflationary process

The inflationary process, which is purely radially dependent, applies a small stress to the inner radius, with a stress of the order of 1% of the shear modulus of the shell. Applying such a small stress allows us to linearise the model for the inflationary process by assuming that the stress is a small perturbation where $0 < \hat{p} \ll 1$. Assuming that the shell will be deformed by a small amount denoted by $\hat{p}f(Y)$ gives

$$y(Y) = Y + \hat{p}f(Y), \tag{2.101}$$

The Jacobian is linearised, resulting in

$$J \approx 1 + \hat{p}\left(f' + \frac{2f}{Y}\right). \tag{2.102}$$

Determining $J^{2\beta}$ using equation (2.102)

$$J^{2\beta} \approx 1 + 2\beta\hat{p}f' + \frac{4\beta\hat{p}f}{Y}. \tag{2.103}$$

Using equations (2.101), (2.102) and (2.103) and substituting into the first term in equation (2.84) leads to

$$y''\left((y')^2 J^{2\beta} + 1 + 2\beta\right) \approx \hat{p}f''\left(2\beta + 2\right). \tag{2.104}$$

Considering the linearisation process for various terms in equation (2.84) leads to

$$J^{2\beta}\left(\frac{2y(y')^2}{Y^2} - \frac{2(y')^3}{Y}\right) \approx \frac{2\hat{p}f}{Y^2} - \frac{2\hat{p}f'}{Y}, \tag{2.105}$$

and substituting into equation (2.84) and rearranging results in

$$Y^2 f'' + 2Y f' - 2f = 0. \tag{2.106}$$

The second order differential equation (2.106) is solved by using the algebraic substitution $f(Y) = Yq(Y)$ leading to

$$Y^3 q'' + 4Y^2 q' = 0. \tag{2.107}$$

Equation (2.107) is solved using separation of variables to give

$$q(Y) = \frac{A}{Y^3} + B, \tag{2.108}$$

where A and B are parameters determined using the boundary conditions of the physical system. Substituting equation (2.108) into $f(Y) = Yq(Y)$ and combining this with equation (2.101) yields

$$y(Y) = Y + \hat{p}\left(\frac{A}{Y^2} + BY\right). \tag{2.109}$$

Linearising and nondimensionalising the Cauchy radial stress given by equation (2.91) results in

$$\begin{aligned} \hat{\tau}_{yy} = \frac{\tau_{yy}}{\mu} &= \frac{1}{J}\left(-J^{-2\beta} + (y')^2\right) \\ &\approx \hat{p}\left(\frac{4\beta f}{Y} + (2\beta + 2)\, f'\right). \end{aligned} \tag{2.110}$$

Linearising the Cauchy hoop stresses represented by $\tau_{\theta\theta}$ and $\tau_{\phi\phi}$ given by equation (2.92) where $\hat{\tau}_{\theta\theta} = \tau_{\theta\theta}/\mu$ leads to

$$\begin{aligned}\hat{\tau}_{\theta\theta} = \hat{\tau}_{\phi\phi} &= \frac{1}{J}\left(-J^{-2\beta} + \left(\frac{y}{Y}\right)^2\right) \\ &\approx \hat{p}\left(\frac{(4\beta+2)f}{Y} + 2\beta f'\right). \end{aligned} \tag{2.111}$$

The boundary condition at the inner radius is

$$\hat{\tau}_{yy}(1) = -\hat{p}.$$

Linearising using equation (2.91) gives

$$(2\beta+2)\, f'(Y)\Big|_{Y=1} + 4\beta f(1) + 1 = 0. \tag{2.112}$$

Linearising the boundary condition at the outer radius using equation (2.110) and the boundary condition given by equation (2.100) yields

$$f'(Y)\Big|_{Y=Y_O} = \frac{-2\beta}{(\beta+1)}\left(\frac{f(Y_O)}{Y_O}\right). \tag{2.113}$$

Substituting $f(Y)$ from equation (2.109) into the boundary condition given by equation (2.113) leads to the relationship

$$A = \frac{Y_O^3}{2}(3\beta+1)\, B. \tag{2.114}$$

Using equation (2.114) along with the linearised boundary condition for the inner radius given by equation (2.112) and $f(Y)$ gives the following expressions for the

parameters A and B

$$A = \frac{Y_O^3}{4Y_O^3 - 4}, \tag{2.115}$$

and

$$B = \frac{1}{(6\beta + 2)Y_O^3 - (6\beta + 2)}. \tag{2.116}$$

The radial deformation $y(Y)$ is from equations (2.109), (2.115) and (2.116) where

$$y(Y) = Y + \hat{p}\left(\frac{Y_O^3}{Y^2\left(4Y_O^3 - 4\right)} + \frac{Y}{(6\beta + 2)Y_O^3 - (6\beta + 2)}\right). \tag{2.117}$$

Substituting equations (2.115) and (2.116) into equations (2.110) and (2.111) for the Cauchy radial and hoop stresses where $\hat{\tau}_{\theta\theta} = \hat{\tau}_{\phi\phi}$, respectively gives

$$\hat{\tau}_{yy} = \hat{p}\left(\frac{Y^3 - Y_O^3}{Y^3\left(Y_O^3 - 1\right)}\right), \tag{2.118}$$

and

$$\hat{\tau}_{\theta\theta} = \hat{p}\left(\frac{Y_O^3}{Y^3\left(2Y_O^3 - 2\right)} + \frac{1}{Y_O^3 - 1}\right). \tag{2.119}$$

2.5 Linearisation of the time evolving collapse phase of the shell

Applying the momentum balance law where ρ_o denotes the density in the reference configuration, v represents the velocity and t denotes the time, gives

$$\rho_o \frac{Dv}{Dt} = \nabla_R \cdot S, \tag{2.120}$$

where the radial component of the material derivative is given by $Dv_r/Dt = \partial v_r/\partial t + (v \cdot \nabla)v_r - v_\theta^2/r - v_\phi^2/r$ ([70],p143-p145). Writing equation (2.120) in terms of the Cauchy stress leads to

$$\rho \frac{Dv}{Dt} = \nabla_r \cdot \tau \tag{2.121}$$

where $v = v_r e_r,\ v_\phi = 0$ and $v_\theta = 0$ (radial dependency only) ([73], p354-p355). To collapse the shell a change in the boundary conditions has to be applied at the inner radius of the shell. In the inflationary picture there is a stress applied at the inner radius, directed radially outwards, but to collapse the shell the stress at the inner radius is set to zero. The right hand side of equation (2.121) is given by

$$\nabla_r \cdot \tau = \left(\frac{\partial \tau_{rr}}{\partial r} + \frac{2}{r}\left(\tau_{rr} - \tau_{\theta\theta}\right) \right) e_r, \tag{2.122}$$

where τ_{rr} and $\tau_{\theta\theta}$ are given by equations (2.91) and (2.92). Let $v_r = \partial \hat{r}/\partial t$ where $\hat{r} \equiv \hat{r}(R,t)$. Using the chain rule

$$\frac{\partial}{\partial r}\left(\frac{\partial \hat{r}}{\partial t}\right) = \frac{\partial R}{\partial r}\frac{\partial^2 \hat{r}}{\partial R \partial t}, \tag{2.123}$$

Equation (2.121) can be rewritten as

$$\rho_o J \left(\frac{\partial^2 \hat{r}}{\partial t^2} + \frac{\partial \hat{r}}{\partial t}\frac{\partial R}{\partial r}\frac{\partial^2 \hat{r}}{\partial R \partial t} \right) e_r = \nabla_r \cdot \tau. \tag{2.124}$$

To nondimensionalise time we use $t = \gamma \hat{t}$ which results in

$$\frac{\partial \hat{r}}{\partial t} = \frac{R_I}{\gamma}\left(\frac{\partial \hat{y}}{\partial \hat{t}}\right),$$

and

$$\frac{\partial^2 \hat{r}}{\partial t^2} = \frac{R_I}{\gamma^2}\frac{\partial^2 \hat{y}}{\partial \hat{t}^2},$$

and the convective derivative (in component form) becomes

$$\left(\frac{\partial \hat{r}}{\partial t}\frac{\partial}{\partial r}\right)\frac{\partial \hat{r}}{\partial t} = \frac{R_I}{\gamma^2}\frac{\partial \hat{y}}{\partial \hat{t}}\frac{\partial Y}{\partial y}\frac{\partial^2 \hat{y}}{\partial Y \partial \hat{t}}.$$

The left hand side of equation (2.121) is

$$\rho\frac{Dv}{Dt} = \frac{\rho_o R_I}{\gamma^2}\frac{y^2}{Y^2}\left(\frac{\partial y}{\partial Y}\right)\left(\frac{\partial^2 \hat{y}}{\partial \hat{t}^2} + \frac{\partial \hat{y}}{\partial \hat{t}}\frac{\partial Y}{\partial y}\frac{\partial^2 \hat{y}}{\partial Y \partial \hat{t}}\right)e_r, \tag{2.125}$$

with the right hand side of equation (2.121) reducing to

$$\begin{aligned}\nabla_r \cdot \tau = \frac{\mu}{R_I J}\left((2\beta+1)J^{-2\beta}\left(\frac{2}{y} + \frac{\partial^2 y}{\partial Y^2}\left(\frac{\partial Y}{\partial y}\right)^2 - \frac{2}{Y}\left(\frac{\partial Y}{\partial y}\right)\right)\right)e_r \\ + \frac{\mu}{R_I J}\left(\frac{\partial^2 y}{\partial Y^2} + \frac{2}{Y}\left(\frac{\partial y}{\partial Y}\right) - \frac{2y}{Y^2}\right)e_r.\end{aligned} \tag{2.126}$$

Setting $\gamma = \sqrt{\rho_o R_I^2/\mu}$ and substituting equations (2.125) and (2.126) into equation (2.121) leads to the nondimensionalised momentum balance

$$\begin{aligned}\frac{y^2}{Y^2}\left(\frac{\partial y}{\partial Y}\right)\left(\frac{\partial^2 \hat{y}}{\partial \hat{t}^2} + \frac{\partial \hat{y}}{\partial \hat{t}}\frac{\partial Y}{\partial y}\frac{\partial^2 \hat{y}}{\partial Y \partial \hat{t}}\right) = (2\beta+1)J^{-2\beta-1}\left(\frac{2}{y} + \frac{\partial^2 y}{\partial Y^2}\left(\frac{\partial Y}{\partial y}\right)^2 - \frac{2}{Y}\left(\frac{\partial Y}{\partial y}\right)\right) \\ + \frac{1}{J}\left(\frac{\partial^2 y}{\partial Y^2} + \frac{2}{Y}\left(\frac{\partial y}{\partial Y}\right) - \frac{2y}{Y^2}\right).\end{aligned} \tag{2.127}$$

Applying the boundary conditions at the inner and outer radii where the stress is set to zero such that $\tau_{yy}(Y_{I/O}) = 0$ gives

$$\left.\frac{\partial y}{\partial Y}\right|_{(1,\hat{t})} = \left(y\left(1,\hat{t}\right)\right)^{-2\beta/(\beta+1)}, \tag{2.128}$$

and

$$\frac{\partial y}{\partial Y}\Big|_{(Y_O,\hat{t})} = \left(\frac{y\left(Y_O,\hat{t}\right)}{Y_O}\right)^{-2\beta/(\beta+1)}, \tag{2.129}$$

where the nondimensionalised initial conditions are given by the inflated solution

$$y(Y,0) = Y + \hat{p}f(Y), \tag{2.130}$$

and

$$\frac{\partial y}{\partial \hat{t}}\Big|_{(Y,0)} = 0. \tag{2.131}$$

Linearisation is performed once again where

$$y = Y + \hat{p}g(Y,\hat{t}). \tag{2.132}$$

Linearising the left hand side of equation (2.127) reduces it to

$$\frac{y^2}{Y^2}\left(\frac{\partial y}{\partial Y}\right)\left(\frac{\partial^2 \hat{y}}{\partial \hat{t}^2} + \frac{\partial \hat{y}}{\partial \hat{t}}\frac{\partial Y}{\partial y}\frac{\partial^2 \hat{y}}{\partial Y \partial \hat{t}}\right) \approx \hat{p}\frac{\partial^2 g}{\partial \hat{t}^2}, \tag{2.133}$$

and the various terms on the right hand side of equation (2.127) are

$$\frac{\partial^2 y}{\partial Y^2}\left(\frac{\partial Y}{\partial y}\right)^2 + \frac{2}{y} - \frac{2}{Y}\left(\frac{\partial Y}{\partial y}\right) \approx \hat{p}\frac{\partial^2 g}{\partial Y^2} - \frac{2\hat{p}g}{Y^2} + \frac{2\hat{p}}{Y}\left(\frac{\partial g}{\partial Y}\right), \tag{2.134}$$

and

$$J^{-2\beta-1} \approx 1 - (2\beta+1)\left(\frac{2\hat{p}g}{Y} + \hat{p}\frac{\partial g}{\partial Y}\right), \tag{2.135}$$

and so

$$(2\beta+1)J^{-2\beta-1}\left(\frac{\partial^2 y}{\partial Y^2}\left(\frac{\partial Y}{\partial y}\right)^2 + \frac{2}{y} - \frac{2}{Y}\left(\frac{\partial Y}{\partial y}\right)\right) \approx (2\beta+1)\left(\hat{p}\frac{\partial^2 g}{\partial Y^2} - \frac{2\hat{p}g}{Y^2} + \frac{2\hat{p}}{Y}\left(\frac{\partial g}{\partial Y}\right)\right). \tag{2.136}$$

Other terms on the right hand side of equation (2.127) linearise to give

$$\frac{\partial^2 y}{\partial Y^2} + \frac{2}{Y}\left(\frac{\partial y}{\partial Y}\right) - \frac{2y}{Y^2} \approx \hat{p}\frac{\partial^2 g}{\partial Y^2} + \frac{2\hat{p}}{Y}\left(\frac{\partial g}{\partial Y}\right) - \frac{2\hat{p}g}{Y^2}. \tag{2.137}$$

Substituting equations (2.136) and (2.137) into the momentum balance law (2.127) and cancelling out the small nondimensional parameter $\hat{p}$ gives us

$$\frac{\partial^2 g}{\partial \hat{t}^2} = (2\beta+2)\frac{\partial^2 g}{\partial Y^2} + \frac{(4\beta+4)}{Y}\left(\frac{\partial g}{\partial Y}\right) - \frac{(4\beta+4)g}{Y^2}. \tag{2.138}$$

The initial conditions are given by

$$g(Y,0) = f(Y), \tag{2.139}$$

and

$$\frac{\partial g}{\partial \hat{t}}\Big|_{(Y,0)} = 0, \tag{2.140}$$

with boundary conditions that are stress free at both the inner and outer radius given by

$$\frac{\partial g}{\partial Y}\Big|_{(1,\hat{t})} + \frac{2\beta}{(\beta+1)}g(1,\hat{t}) = 0, \tag{2.141}$$

and

$$\frac{\partial g}{\partial Y}\Big|_{(Y_O,\hat{t})} + \frac{2\beta}{(\beta+1)}\frac{g(Y_O,\hat{t})}{Y_O} = 0. \tag{2.142}$$

Applying a Laplace transform to equation (2.138) and applying the initial conditions leads to

$$(2\beta+2)\left(\frac{d^2G}{dY^2} + \frac{2}{Y}\frac{dG}{dY} - \frac{2G}{Y^2}\right) = s^2G(Y,s) - sf(Y), \tag{2.143}$$

where $G(Y,s) = \int_0^\infty g(Y,\hat{t})e^{-s\hat{t}}d\hat{t}$. Setting $\alpha^2 = 1/(2\beta+2)$ results in

$$Y^2\frac{d^2G}{dY^2} + 2Y\frac{dG}{dY} - \left(2+\alpha^2Y^2s^2\right)G = -\alpha^2Y^2sf(Y). \tag{2.144}$$

Consider first the case when $s = 0$. Here equation (2.144) becomes

$$Y^2\frac{d^2G}{dY^2} + 2Y\frac{dG}{dY} - 2G = 0, \tag{2.145}$$

which has solution $G(Y,0) = E/Y^2 + FY,$ where $E, F \in \mathbb{R}$. The Laplace transformed boundary conditions arising from equations (2.141) and (2.142) result in $E = F = 0$. Hence the solution pertaining to the case $s = 0$ is the trivial solution $G(Y,0) = 0$. From now on we consider the case when $s \neq 0$. The homogeneous equation has the solution

$$G(Y,s)_{\text{Hom}} = A(s)I_1(\alpha sY) + B(s)K_1(\alpha sY), \tag{2.146}$$

where $I_1(\alpha sY)$ is the modified spherical Bessel function of the first kind of order one and $K_1(\alpha sY)$ is the modified spherical Bessel function of the second kind of order one ([74],p443-445) and ([75],p633-634). The modified spherical Bessel functions can be written in terms of more familiar functions as

$$I_1(x) = \frac{x\cosh x - \sinh x}{x^2},$$
$$K_1(x) = \frac{e^{-x}(x+1)}{x^2}.$$

The particular integral solution is

$$G_{PI}(Y,s) = \frac{f(Y)}{s}, \tag{2.147}$$

since $f(y)$ satifies equation (2.106). The general solution is then given by

$$G(Y,s) = A(s)I_1(\alpha sY) + B(s)K_1(\alpha sY) + \frac{f(Y)}{s}. \tag{2.148}$$

Taking the Laplace transform of the stress free boundary conditions given by equations (2.141) and (2.142) and substituting equation (2.148) into the Laplace transforms of (2.141) and (2.142) gives

$$A(s)\left(\frac{\partial I_1(\alpha sY)}{\partial Y}\Big|_{Y=1} + \frac{2\beta}{(\beta+1)}I_1(\alpha s)\right) + B(s)\left(\frac{\partial K_1(\alpha sY)}{\partial Y}\Big|_{Y=1} + \frac{2\beta}{(\beta+1)}K_1(\alpha s)\right) + \frac{1}{s}\left(\frac{\partial f(Y)}{\partial Y}\Big|_{Y=1} + \frac{2\beta}{(\beta+1)}f(1)\right) = 0, \tag{2.149}$$

and

$$A(s)\left(\frac{\partial I_1(\alpha sY)}{\partial Y}\Big|_{Y=Y_O} + \frac{2\beta}{(\beta+1)}\frac{I_1(\alpha sY_O)}{Y_O}\right) + B(s)\left(\frac{\partial K_1(\alpha sY)}{\partial Y}\Big|_{Y=Y_O} + \frac{2\beta}{(\beta+1)}\frac{K_1(\alpha sY_O)}{Y_O}\right) + \frac{1}{s}\left(\frac{\partial f(Y)}{\partial Y}\Big|_{Y=Y_O} + \frac{2\beta}{(\beta+1)}\frac{f(Y_O)}{Y_O}\right) = 0. \tag{2.150}$$

Using equations (2.112) and (2.113), we can write equations (2.149) and (2.150) as the matrix equation

$$M(s)\begin{pmatrix} A(s) \\ B(s) \end{pmatrix} = \begin{pmatrix} \frac{1}{s(2\beta+2)} \\ 0 \end{pmatrix},$$

where

$$M(s) = \begin{pmatrix} \frac{\partial I_1(\alpha sY)}{\partial Y}\Big|_{Y=1} + \frac{2\beta}{(\beta+1)}I_1(\alpha s) & \frac{\partial K_1(\alpha sY)}{\partial Y}\Big|_{Y=1} + \frac{2\beta}{(\beta+1)}K_1(\alpha s) \\ \frac{\partial I_1(\alpha sY)}{\partial Y}\Big|_{Y=Y_O} + \frac{2\beta}{(\beta+1)}\frac{I_1(\alpha sY_O)}{Y_O} & \frac{\partial K_1(\alpha sY)}{\partial Y}\Big|_{Y=Y_O} + \frac{2\beta}{(\beta+1)}\frac{K_1(\alpha sY_O)}{Y_O} \end{pmatrix}. \tag{2.151}$$

Equation (2.151) leads to

$$A(s) = \frac{1}{\det(M)} \left(\frac{1}{s(2\beta+2)} \right) \left(\frac{\partial K_1(\alpha s Y)}{\partial Y}\Big|_{Y=Y_O} + \frac{2\beta}{(\beta+1)} \frac{K_1(\alpha s Y_O)}{Y_O} \right), \quad (2.152)$$

and

$$B(s) = \frac{1}{\det(M)} \left(\frac{-1}{s(2\beta+2)} \right) \left(\frac{\partial I_1(\alpha s Y)}{\partial Y}\Big|_{Y=Y_O} + \frac{2\beta}{(\beta+1)} \frac{I_1(\alpha s Y_O)}{Y_O} \right), \quad (2.153)$$

where the determinant is given by

$$\begin{aligned} \det(M) = & \left(\frac{\partial I_1(\alpha s Y)}{\partial Y}\Big|_{Y=1} + \frac{2\beta}{(\beta+1)} I_1(\alpha s) \right) \left(\frac{\partial K_1(\alpha s Y)}{\partial Y}\Big|_{Y=Y_O} + \frac{2\beta}{(\beta+1)} \frac{K_1(\alpha s Y_O)}{Y_O} \right) \\ & - \left(\frac{\partial K_1(\alpha s Y)}{\partial Y}\Big|_{Y=1} + \frac{2\beta}{(\beta+1)} K_1(\alpha s) \right) \left(\frac{\partial I_1(\alpha s Y)}{\partial Y}\Big|_{Y=Y_O} + \frac{2\beta}{(\beta+1)} \frac{I_1(\alpha s Y_O)}{Y_O} \right). \end{aligned} \quad (2.154)$$

The matrix M becomes singular when the determinant given by equation (2.154) is equal to zero. This corresponds to the poles of the integrand in the inverse Laplace transform formulation. The location of the poles in the complex plane was empirically observed by producing an exhaustive set of contour plots of $|\det M(s)|$ where $s = re + i\omega$, over an extensive range of real and imaginary values of s and a range of material parameters given by $0 < \beta \leq 25$ and $1.02 \leq Y_O \leq 1.05$ [15]. Figure 2.3 illustrates one of the many contour plots that has been produced for one set of material parameters where $\beta = 12$ and $Y_O = 1.02$.

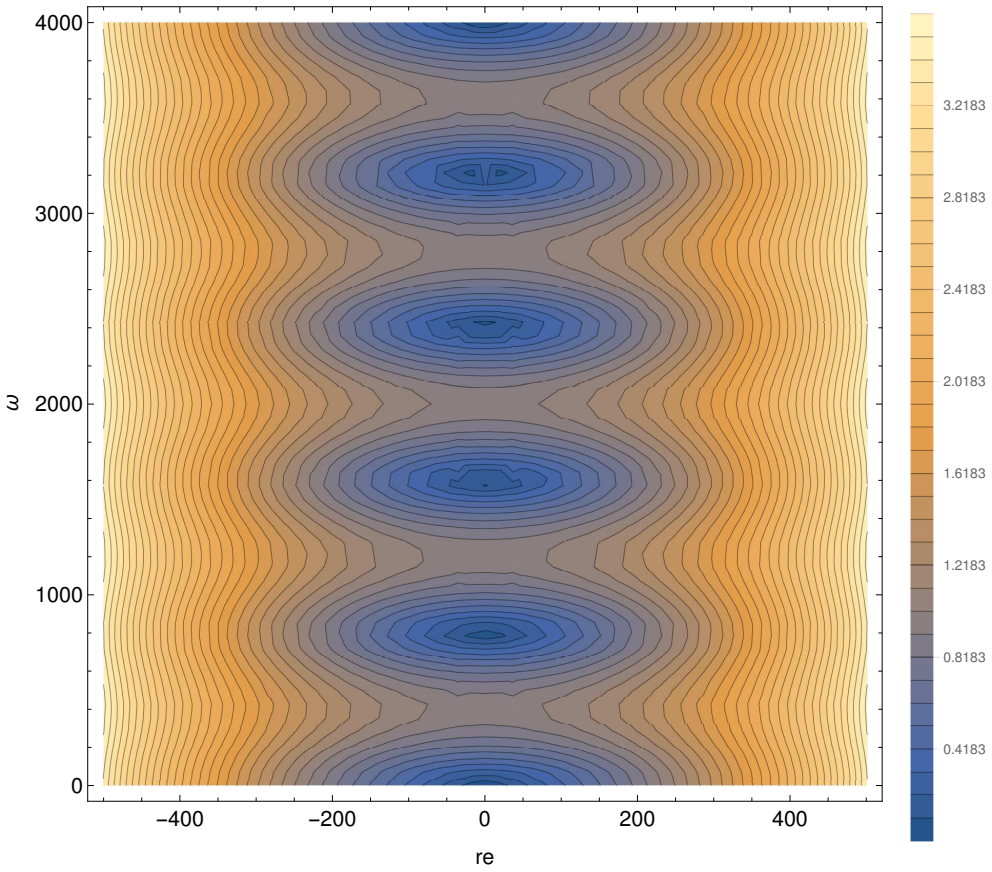

Figure 2.3: Contour plot of $|\det M(s)|$ (evaluated using equation (2.154)) over a range of real and imaginary values where $s = re + i\omega$ for $\beta = 12$ and $Y_O = 1.02$.

Figure 2.3 shows a contour plot of $|\det M(s)|$ over a broad range of s where $s = re + i\omega$ with $\beta = 12$ and $Y_O = 1.02$. The scale on the right hand side of the contour plot corresponds to the values of $|\det M(s)|$ with the dark blue regions of the contour plot indicating values of $|\det M(s)|$ which are below ≈ 0.5 and potentially equal to 0. Note that there is a symmetry in Figure 2.3 along the vertical line $re = 0$. This is characteristic of all the contour plots that were constructed. Constructing three dimensional plots of $\log_e(|\det M(s)|)$ over an extensive range of real and imaginary values with $0 < \beta \leq 25$ and $1.02 \leq Y_O \leq 1.05$ shows that there is a series of approximately periodic minima. Figure 2.4 shows one such plot for the material parameter set $\beta = 12$ and $Y_O = 1.02$.

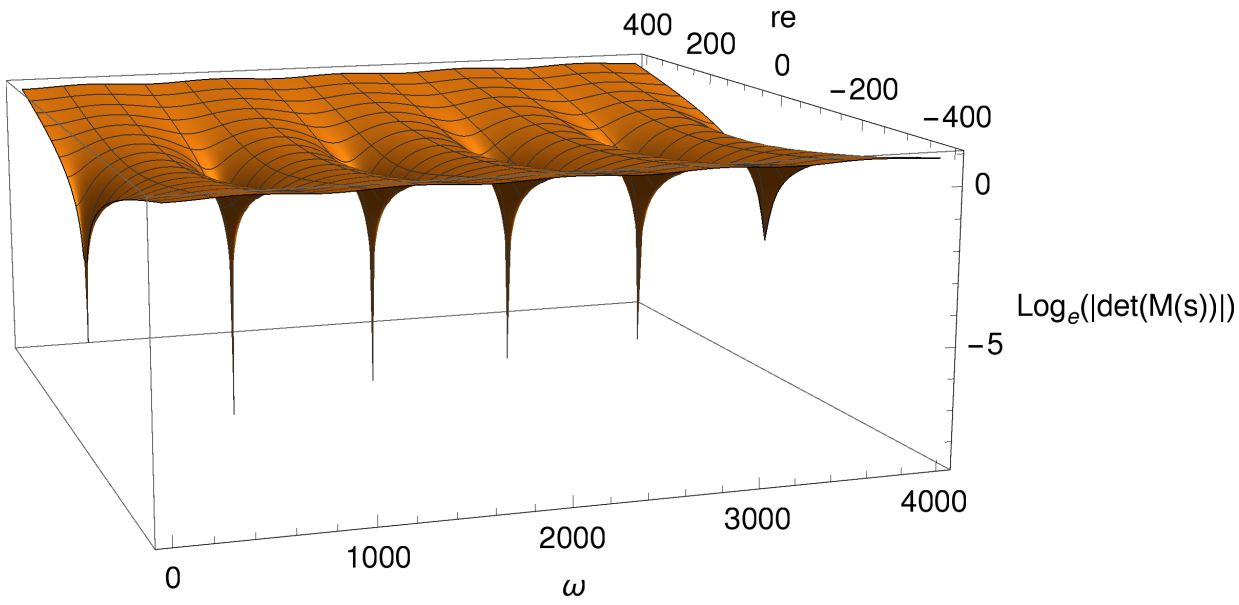

Figure 2.4: Plot of $\log_e(|\det M(s)|)$ (evaluated using equation (2.154)) over a range of real and imaginary values where $s = re + i\omega$ for $\beta = 12$ and $Y_O = 1.02$.

Figure 2.4 highlights the series of approximately periodic minima. Due to the complexity of the expression for the determinant given by (2.154) it is not possible to prove that the poles are all purely imaginary for all of the parameter space and hence we have resorted to this numerical investigation. For the remainder of this study we shall therefore assume that the solutions of equation (2.154) are purely imaginary. Setting $s = i\omega$ in equation (2.154) gives

$$\det(M) = -\frac{2i(Y_O - 1)\left(2 + Y_O\alpha^2(1+\beta)\omega^2\right)\cos((Y_O-1)\alpha\omega)}{Y_O^3\alpha^3(1+\beta)^2\omega^3} + \frac{i\left(8 - 4\alpha^2(1 - 2Y_O + \beta + Y_O^2(1+\beta))\omega^2 + 2Y_O^2\alpha^4(1+\beta)^2\omega^4\right)\sin((Y_O-1)\alpha\omega)}{2Y_O^3\alpha^4(1+\beta)^2\omega^4}. \tag{2.155}$$

To enable some analytic headway we shall consider an asymptotic expansion of

equation (2.155) and examine the limit as $\omega \to \infty$. This results in

$$\det(M) = \frac{i \sin\left((Y_O - 1)\alpha\omega\right)}{Y_O} + \mathcal{O}(\omega^{-1}). \tag{2.156}$$

The poles are therefore approximately periodic and are given by

$$\omega_n \approx (n-1)\pi \frac{\sqrt{2\beta + 2}}{Y_O - 1}, \tag{2.157}$$

where $n \in \mathbb{N}$. Equation (2.157) holds for the typical parameter regime of this study, for example when $\beta = 12$ and $Y_O = 1.02$ then $\omega_2 \approx 800$.

The inverse Laplace transform of $G(Y, s)$, $\mathcal{L}^{-1} : s \to \hat{t}$, is given by

$$g(Y, \hat{t}) = \frac{1}{2\pi i} \int_{a-i\infty}^{a+i\infty} e^{s\hat{t}} G(Y, s) ds. \tag{2.158}$$

The poles can be used to determine the inverse Laplace transform by utilising the Bromwich contour $C = C_1 \cup C_2$ as shown in Figure 2.5 ([76], p151-174).

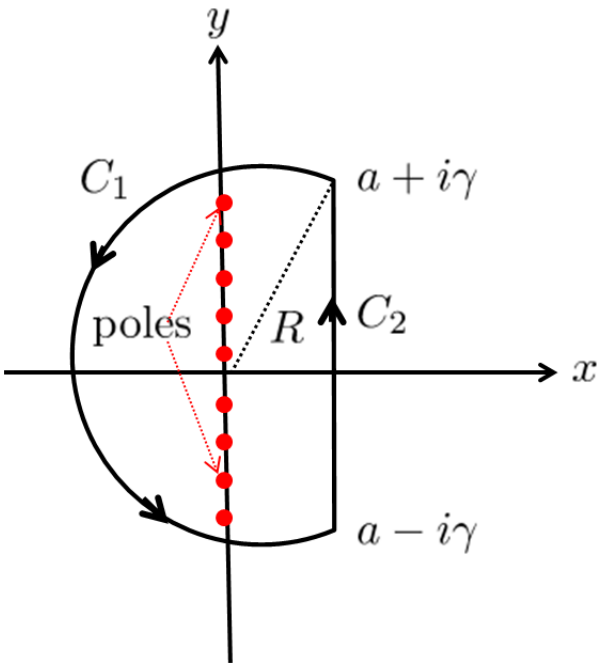

Figure 2.5: Illustration of the Bromwich contour which is required to calculate the inverse Laplace transform.

Here C_1 is the portion of the circle of radius R centred at the origin and C_2 is the vertical line at $x = a$ where $a = \epsilon$ which lies to the right of all the poles (as they lie on the imaginary axis). The integration on equation (2.160) is in the anticlockwise direction (as indicated in Figure 2.5). We must consider $R \to \infty$ to encircle all the poles, and in C_2, $\gamma = \sqrt{R^2 - a^2}$. By the Residue Theorem ([76], p151-174) we have in the limit as $R \to \infty$

$$\frac{1}{2\pi i} \oint_C e^{s\hat{t}} G(Y, s) ds = \sum_{j=-\infty}^{\infty} \text{res}(\omega_j), \tag{2.159}$$

where ω_j are the poles and where $\text{res}(\omega_j)$ is

$$\lim_{R\to\infty} \left(\frac{1}{2\pi i} \int_{C_1} e^{s\hat{t}} G(Y, s) ds \right) + \frac{1}{2\pi i} \int_{a-i\infty}^{a+i\infty} e^{s\hat{t}} G(Y, s) ds = \sum_{j=-\infty}^{\infty} \text{res}(\omega_j). \tag{2.160}$$

If we can show that the first term on the left hand side of equation (2.160) is identically zero then from equation (2.158) we have that

$$g(Y,\hat{t}) = \sum_{j=-\infty}^{\infty} \text{res}(\omega_j). \tag{2.161}$$

In the integral over C_1 the substitution $s = Re^{i\Theta}$ was made in the term $G(Y,s)$ which leads to

$$G(Y,s) = \frac{1}{2R(1+Y_O)^2} e^{-i\Theta} \left(\frac{2Y_O^3}{-1+Y_O^3} + \frac{(1+Y_O)^3}{-2-6\beta+Y_O^3\,(2+6\beta)} - \frac{N_1}{D} + \frac{N_2}{D} \right), \tag{2.162}$$

where

$$N_1 = 8\sqrt{2} e^{-e^{i\Theta}R(1+Y_O)/(2\sqrt{2+2\beta})} \left(1 + \frac{e^{i\Theta}R(1+Y_O)}{2\sqrt{2+2\beta}}\right) \left(\frac{-2\sqrt{2}e^{i\Theta}RY_O}{\sqrt{1+\beta}} \cosh\left(\frac{e^{i\Theta}RY_O}{\sqrt{2+2\beta}}\right) + (4+e^{2i\Theta}R^2Y_O^2)\sinh\left(\frac{e^{i\Theta}RY_O}{\sqrt{2+2\beta}}\right)\right),$$

and

$$N_2 = 8\sqrt{2} e^{-e^{i\Theta}RY_O/\sqrt{2+2\beta}} \left(-4 - e^{2i\Theta}R^2Y_O^2 - \frac{2\sqrt{2}e^{i\Theta}RY_O}{\sqrt{1+\beta}}\right) \left(\frac{e^{i\Theta}R(1+Y_O)}{2\sqrt{2+2\beta}} \cosh\left(\frac{e^{i\Theta}R(1+Y_O)}{2\sqrt{2+2\beta}}\right) - \sinh\left(\frac{e^{i\Theta}R(1+Y_O)}{2\sqrt{2+2\beta}}\right)\right),$$

with

$$D = e^{-e^{i\Theta}RY_O/\sqrt{2+2\beta}}\left(4\sqrt{2}+\sqrt{2}e^{2i\Theta}R^2Y_O^2+\frac{4e^{i\Theta}RY_O}{\sqrt{1+\beta}}\right)$$
$$\left(\frac{2\sqrt{2}e^{i\Theta}R}{\sqrt{1+\beta}}\cosh\left(\frac{e^{i\Theta}R}{\sqrt{2+2\beta}}\right)-\left(4+e^{2i\Theta}R^2\right)\sinh\left(\frac{e^{i\Theta}R}{\sqrt{2+2\beta}}\right)\right)$$
$$-e^{-e^{i\Theta}R/\sqrt{2+2\beta}}\left(4\sqrt{2}+\sqrt{2}e^{2i\Theta}R^2+\frac{4e^{i\Theta}R}{\sqrt{1+\beta}}\right)$$
$$\left(\frac{2\sqrt{2}e^{i\Theta}RY_O}{\sqrt{1+\beta}}\cosh\left(\frac{e^{i\Theta}RY_O}{\sqrt{2+2\beta}}\right)-\left(4+e^{2i\Theta}R^2Y_O^2\right)\sinh\left(\frac{e^{i\Theta}RY_O}{\sqrt{2+2\beta}}\right)\right).$$

We will now consider an asymptotic expansion of equation (2.162) as $|s|\to\infty$. Since there are hyperbolic functions contained within equation (2.162) we will assume that $\mathbb{R}(s)$ is negative. Using Mathematica [77] to perform an asymptotic expansion of equation (2.162) to order $\mathcal{O}(R^{-1})$ gives

$$G(Y,R)=\frac{(2Y_O^3/(Y_O^3-1)+(1+Y_O)^3/(-2-6\beta+Y_O^3(2+6\beta))}{2R(1+Y_O)^2}$$
$$-\frac{e^{R\sqrt{1/(2\beta+2)}-(R(1+Y_O)/2)\sqrt{1/(2\beta+2)}}Y_O\sqrt{1/(2\beta+2)}}{2\sqrt{2}R(1+Y_O)^2\sqrt{1/(1+\beta)}}$$
$$-\frac{e^{R\sqrt{1/(2\beta+2)}-(R(1+Y_O)/2)\sqrt{1/(2\beta+2)}}Y_O\sqrt{1/(2\beta+2)}}{2\sqrt{2}R(1+Y_O)^2\sqrt{1/(1+\beta)}}+\mathcal{O}(R^{-2}). \quad (2.163)$$

Since $Y_O>1$ the resulting exponential terms in equation (2.163) are raised to a negative power which in the limit as $R\to\infty$ tends to zero. This reduces to

$$G(Y,R)\approx\frac{(2Y_O^3/(Y_O^3-1)+(1+Y_O)^3/(-2-6\beta+Y_O^3(2+6\beta))}{2R(1+Y_O)^2}, \quad (2.164)$$

which tends to zero as $R\to\infty$. Hence by applying Jordan's lemma ([76], p54) $\lim_{R\to\infty}\left(\frac{1}{2\pi i}\int_{C_1}e^{s\hat{t}}G(Y,s)ds\right)\to 0$ for $\hat{t}>0$. The poles ω_j were identified numerically using *FindRoot* in Mathematica [77] which uses the Newton method to

identify roots. The residuals were also evaluated numerically using *NResidue* in Mathematica [77] for a range of β and Y_O values. The general form of the solution is given by

$$g(Y,\hat{t}) = \sum_{n=1}^{\infty} A_n(Y) e^{\pm i\omega_n \hat{t}}, \tag{2.165}$$

which simplifies to

$$g(Y,\hat{t}) = \sum_{n=1}^{\infty} 2A_n(Y)\cos(\omega_n \hat{t}), \tag{2.166}$$

where $A_n(Y)$ denotes the amplitude of each residual whose pole is given by $s = \pm i\omega_n$. Now equation (2.166) is a Fourier series. The amplitudes for higher harmonics are very small in comparison to A_1 (refer to Table 2.1).

Table 2.1: Magnitude of residuals at Y_O (outer radius)

Harmonic no.	Magnitude of residual
1	2.24
2	4.12×10^{-7}
3	1.93×10^{-5}
4	1.52×10^{-7}
5	4.82×10^{-6}
6	3.29×10^{-9}
7	2.14×10^{-6}
8	1.20×10^{-9}
9	1.21×10^{-6}
10	5.65×10^{-10}

Table 2.1 shows that the amplitudes of the higher harmonics are very small in comparison to $A_1(Y_O)$. Hence the collapse time is dominated by the first angular frequency ω_1. Every component in expression (2.166) independently satisfies the boundary conditions given by equations (2.141) and (2.142). The collapse time $\hat{t^*}$, which is the time taken for the stressed shell to collapse to its stress free state, is therefore given by $\hat{t^*} = \pi/(2\omega_1)$. To validate this analysis the original linearised PDE given by equation (2.138) is solved numerically using the NDSolve built in solver in Mathematica [77]. This solver uses the method of lines to evaluate

equation (2.138).

2.6 Results for the inflationary phase of the shelled microbubble

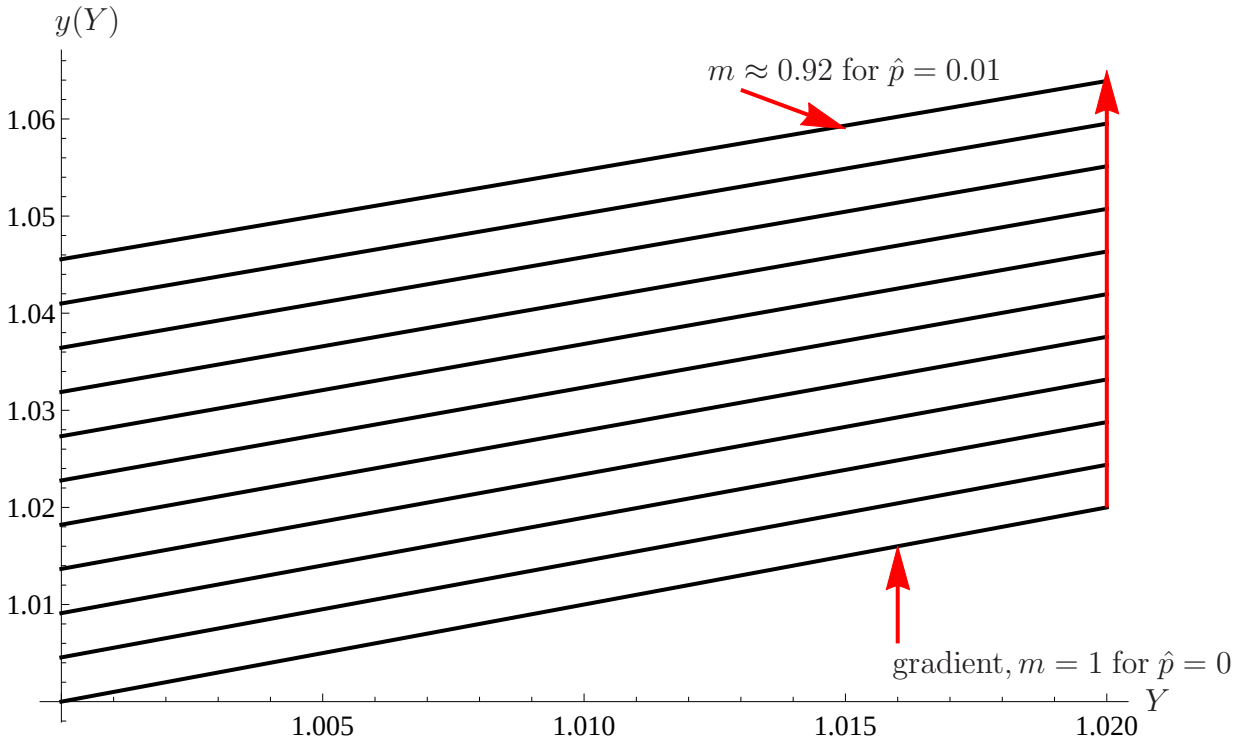

Figure 2.6: Graph of the nondimensionalised radial deformation versus the nondimensionalised reference configuration's radial coordinates for different nondimensionalised internal stress loads given by $\hat{p} = 0, 0.001, 0.002, ..., 0.01$ where $\nu = 0.48$, $\beta = 12$ and the initial thickness is $Y_O - 1 = 0.02$. This is calculated using equation (2.117).

Figure 2.6 plots the radial deformation of the inflated shell given by equation (2.117) as a function of the reference configuration for a series of stresses applied to the inner surface of the shelled microbubble. The red vertical arrow indicates the direction of increasing applied stress. As the applied stress increases the slope

of each successive line decreases slightly. The gradient of $y(Y)$ when $\hat{p} = 0.01$ varies from roughly 0.915 to 0.92 over the range of Y plotted. This is due to the material being compressed more at the inner radius than at the outer radius. Using equation (2.117) we can determine how the change in thickness of the shell for the linearised model depends on the various material parameters of the shell. Evaluating $y(Y_O) - y(1) - (Y_O - 1)$ using (2.117) results in

$$y(Y_O) - y(1) - (Y_O - 1) = \frac{-\hat{p}(-2 + Y_O + 3\beta Y_O + Y_O^2(1 + 3\beta))}{4(1 + Y_O + Y_O^2)(1 + 3\beta)}, \tag{2.167}$$

which shows that the change in thickness of the shell varies linearly with $\hat{p}$. The negative sign highlights that the shell's thickness decreases as the applied stress increases. This is a result of the shelled microbubble expanding radially and the thinning of the shell is indicative of a compressive stress in the radial direction. Equation (2.167) also highlights the slightly more complicated dependency on the Poisson ratio on which β depends and on the thickness of the shell which is given by $Y_O - 1$. The linearised Jacobian which measures the change in the local density of the shell as it inflates can be simplified using equations (2.102), (2.115) and (2.116) to give

$$J \approx 1 + \frac{3\hat{p}}{(6\beta + 2)(Y_O^3 - 1)}. \tag{2.168}$$

Equation (2.168) shows that as $\hat{p}$ increases the Jacobian of the shell increases linearly which implies that the density of the shell is decreasing. The change in density at the final applied stress of $\hat{p} = 0.01$ is approximately 0.7% of its original density which is the same order of magnitude as the nondimensionalised stress load. Note that the Jacobian of the shell is independent of Y but depends on both the Poisson ratio and the thickness of the shell $Y_O - 1$.

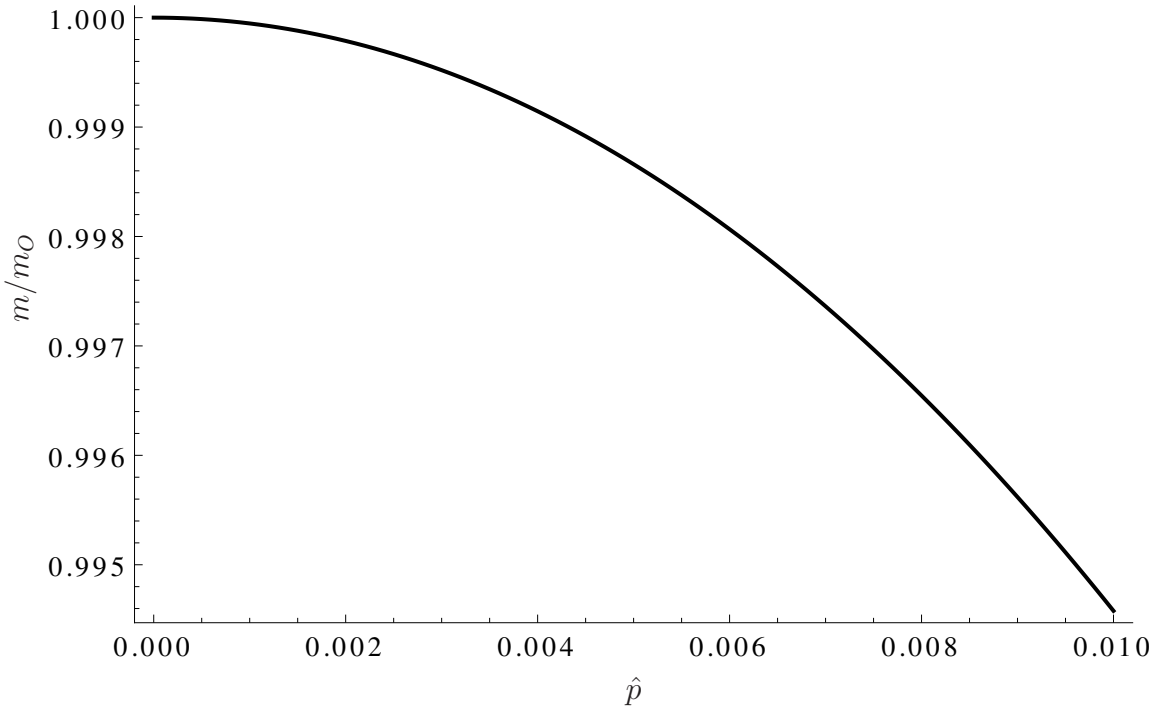

Figure 2.7: Graph of the normalised mass of the shell versus the nondimensionalised stress load where where $\nu = 0.48,\ \beta = 12$ and the initial thickness is $Y_O - 1 = 0.02$. This is calculated using $\rho_0 = \rho J$ alongside equations (2.102) and (2.117)
.

Figure 2.7 plots the normalised mass versus the nondimensionalised applied stress up to a value of $\hat{p} = 0.01$; the normalised mass is obtained by dividing the mass at each stress step by the mass at the initial stress $\hat{p} = 0$ resulting in the equation $m/m_0 = \left(y(Y_O)^3 - y(1)^3\right)/((Y_O^3 - 1)J)$. Figure 2.7 shows that the mass error is approximately proportional to $\hat{p}^2$ as one would expect for a linearised model.

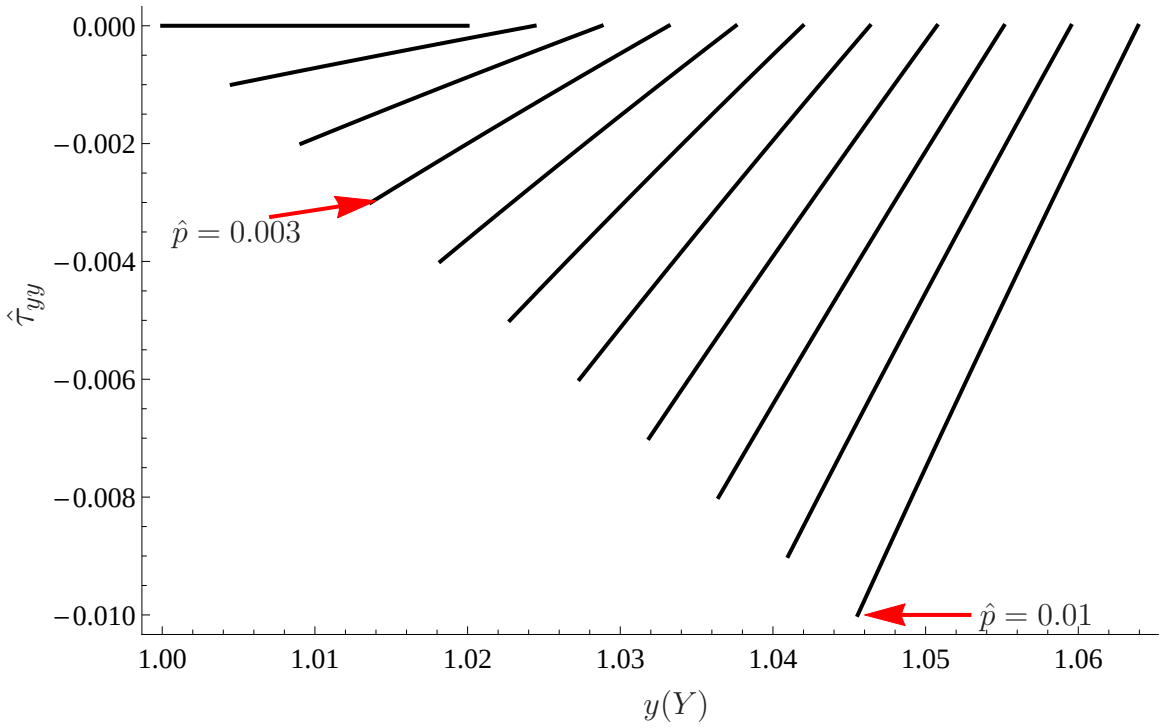

Figure 2.8: Graph of the nondimensionalised radial Cauchy stress of the shell versus the nondimensionalised radial deformation for various nondimensionalised internal stress loads where $\hat{p} = 0, 0.001, 0.002, ..., 0.01$, $\nu = 0.48$, $\beta = 12$ and the initial thickness is $Y_O - 1 = 0.02$. This is calculated using equations (2.117) and (2.118).

Figure 2.8 shows the relationship between the nondimensionalised Cauchy radial stress $\hat{\tau}_{yy}$, and the nondimensionalised radial deformation, $y(Y)$, for a series of stresses applied to the inner surface of the shelled microbubble. The Cauchy radial stress is greater at the inner radius than at the outer radius. This is because the stress is zero at the outer radius and nonzero at the inner radius during the inflationary process. Figure 2.8 illustrates a Cauchy radial stress which is negative, indicating that the stress is compressive. This is a consequence of the shell thinning down during the inflationary process. Note that the Cauchy radial stress at the inner radius is equal in magnitude to the stress applied to the inner radius

of the shell.

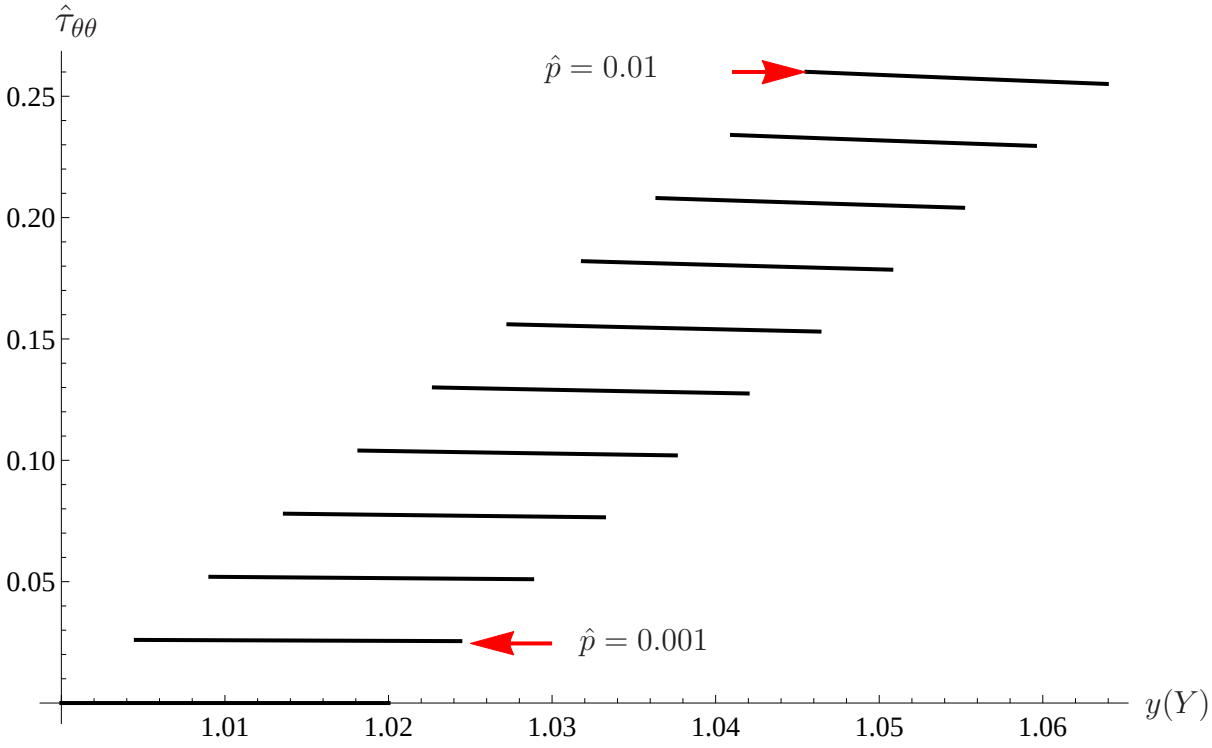

Figure 2.9: Graph of the normalised Cauchy angular stress (hoop stress) of the shell versus the nondimensionalised radial deformation for various nondimensionalised internal stress loads where $\hat{p} = 0, 0.001, 0.002, ..., 0.01$, $\nu = 0.48$, $\beta = 12$ and the initial thickness is $Y_O - 1 = 0.02$. This is calculated using equations (2.117) and (2.119).

Figure 2.9 illustrates the relationship between the nondimensionalised Cauchy angular (hoop) stress ($\hat{\tau}_{\theta\theta}$) and the nondimensionalised radial deformation for a range of applied stress values up to a nondimensionalised inflationary applied stress of $\hat{p} = 0.01$. The graph shows Cauchy hoop stresses that are linear and essentially flat over the range of radial deformations varying from the inner to the outer radii. The Cauchy hoop stress $\tau_{\theta\theta}$ is equal in magnitude to $\tau_{\phi\phi}$ due to the spherically directed nature of the radial deformation and is positive indicating stretching. The Cauchy angular stresses are significantly larger than the Cauchy radial stresses

which were represented by Figure 2.8. This would suggest that the hoop stresses play the key role in dictating the collapsing of the shelled microbubble. It is interesting to note that the Cauchy angular stress is very slightly larger at the inner radius than the outer radius which is a result of the material particle spacing in the shell changing radially.

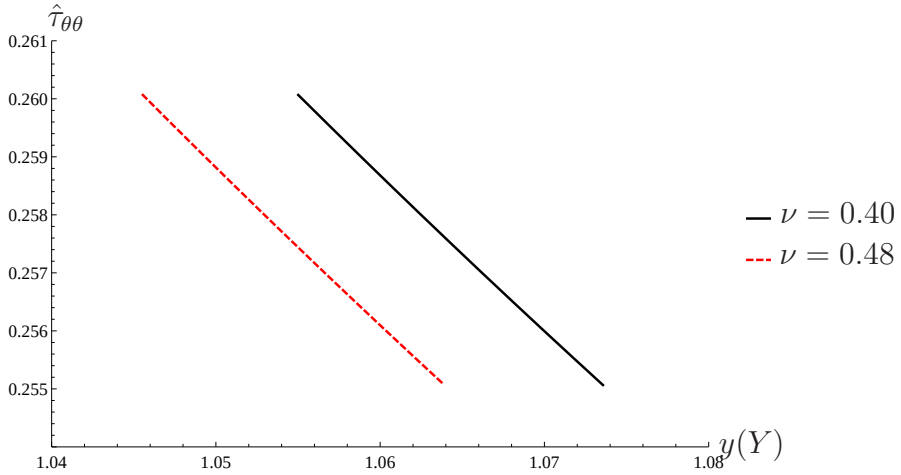

Figure 2.10: Graph of the nondimensionalised hoop stress of the shell versus the nondimensionalised radial deformation for two different Poisson ratios where $\hat{p} = 0.01$ and the initial thickness is $Y_O - 1 = 0.02$. This is calculated using equations (2.117) and (2.119).

Figure 2.10 illustrates how the nondimensionalised hoop stress varies against the nondimensionalised radial deformation for a particular shell thickness but with two different Poisson ratio values for a nondimensionalised radial stress of $\hat{p} = 0.01$. Figure 2.10 shows that the hoop stress is independent of the Poisson ratio and that shells with smaller Poisson ratios experience larger radial displacements.

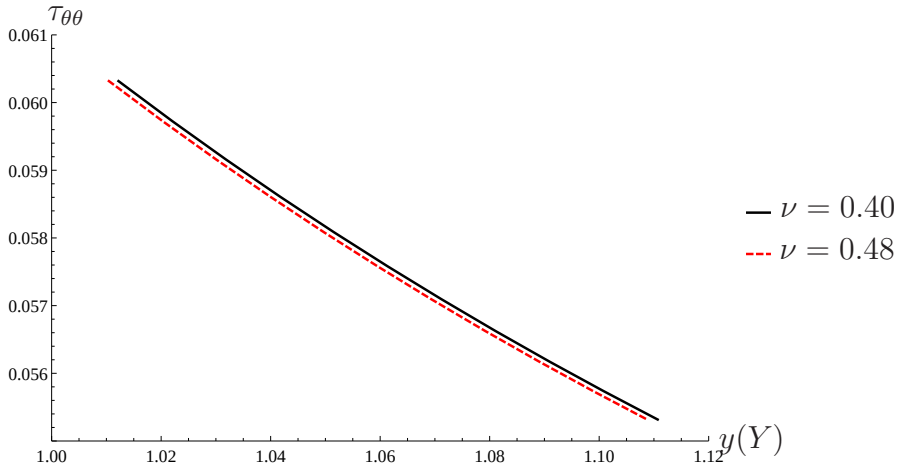

Figure 2.11: Graph of the nondimensionalised hoop stress of the shell versus the nondimensionalised radial deformation for two different Poisson ratios where $\hat{p} = 0.01$ and the initial thickness is $Y_O - 1 = 0.10$. This is calculated using equations (2.117) and (2.119).

Figure 2.11 illustrates how the nondimensionalised hoop stress varies against the nondimensionalised radial deformation for a thicker shell than Figure 2.10 but with the same two Poisson ratio values as Figure 2.10 for a nondimensionalised radial stress of $\hat{p} = 0.01$. Figure 2.11 when compared with Figure 2.10 highlights the relationship between the hoop stress and the thickness of the shell with thinner shells experiencing a significantly larger hoop stress. Note that the hoop stress given by equation (2.119) is influenced by the applied stress $\hat{p}$, the thickness of the shell, and the inner and outer radii.

2.7 Results for the collapse phase of the shelled microbubble

Having produced results for the inflationary phase of the microbubble's evolution, this can be used as an initial condition to model the collapsing shell. The collapse

is achieved by setting the boundary condition on the inner surface of the shell to be stress free.

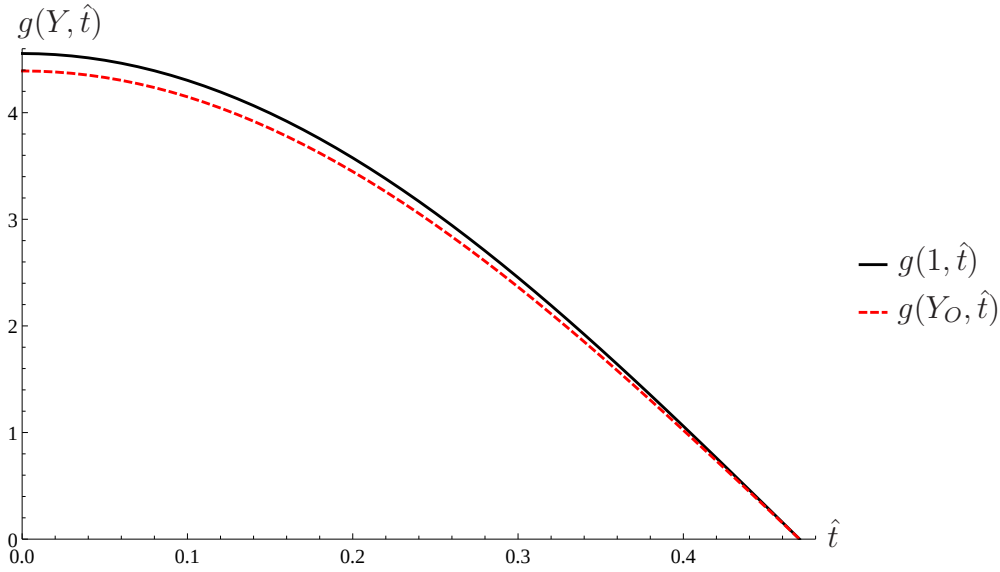

Figure 2.12: Graph of $g(Y,\hat{t})$ at the nondimensionalised inner and outer radius of a collapsing shell versus the nondimensionalised time where $\nu = 0.48$, $\beta = 12$, and the initial thickness is $Y_O - 1 = 0.02$. This is calculated using equations (2.154) and (2.166).

Figure 2.12 plots $g(Y,\hat{t})$ at the nondimensionalised inner and outer radius of a collapsing shell versus the nondimensionalised time for an initial condition based on an inflationary stress load that is 1% of the shear modulus of the shell ($\hat{p} = 0.01$). The resulting nonlinear trend is a sinusoidal function with a collapse time, $\hat{t}^* \approx 0.47$. There are no dissipative, damping terms in the momentum balance law such as viscoelastic terms connected to the viscosity of the shell and the surrounding fluid. Neglecting the fluid resistance results in a simple harmonic behaviour with no resulting energy dissipation to the surrounding medium. Both the inner and outer radius of the shell experience the same collapse time despite their radial deformations being different with the inner radius experiencing a slightly larger radial deformation.

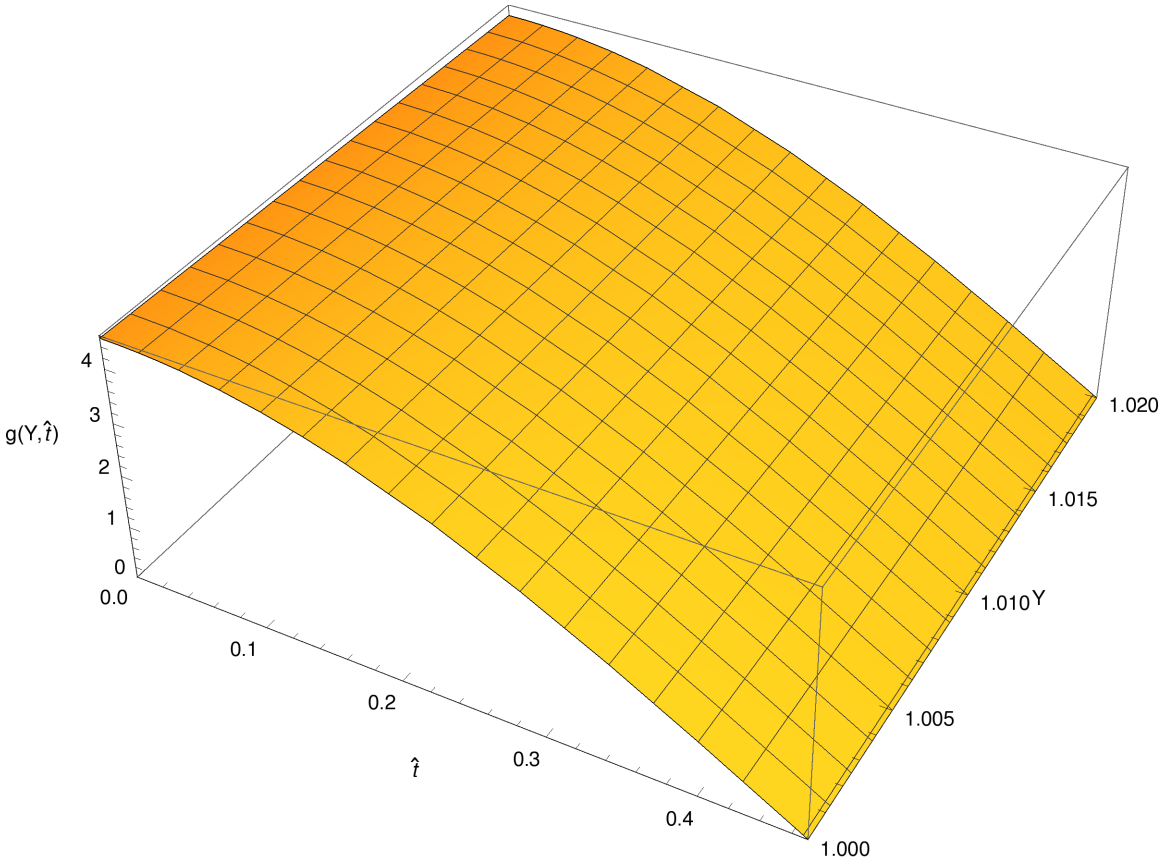

Figure 2.13: Graph of the nondimensionalised numerical solution of a collapsing shell versus the nondimensionalised time where $\nu = 0.48$ and $\beta = 12$. This is calculated using equation (2.138).

Figure 2.13 plots the nondimensionalised numerical solution for the collapsing shell versus the nondimensionalised time for an initial condition based on an inflationary stress load that is 1% of the shear modulus of the shell ($\hat{p} = 0.01$). The resulting nonlinear trend is characteristic of Figure 2.12 with approximately the same collapse time $\hat{t}^*$. Note that the collapse time is the same for each section of the shell lying between $1 \leq Y \leq Y_O$.

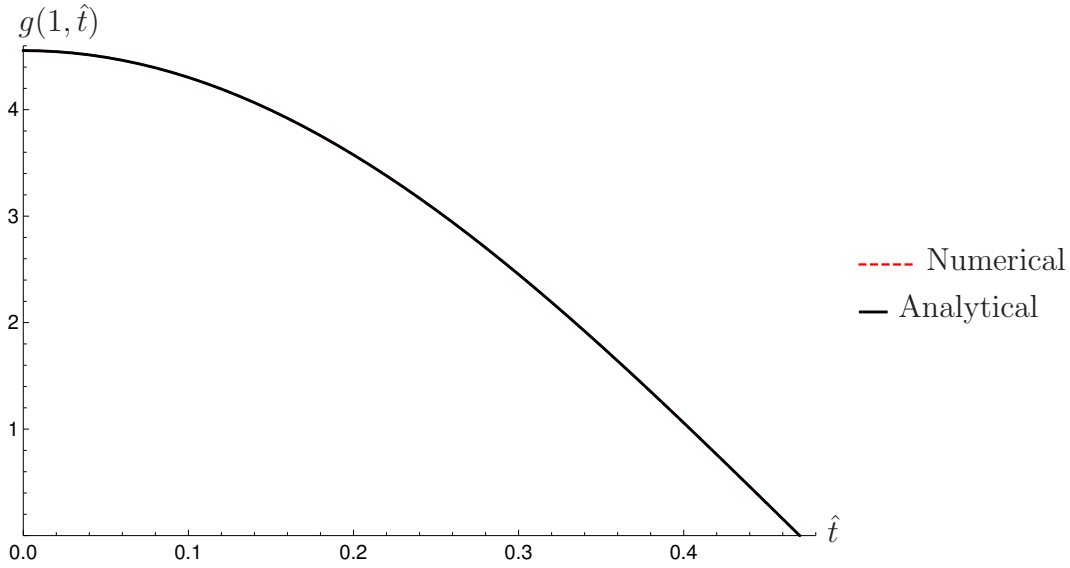

Figure 2.14: Graph comparing the nondimensionalised numerical and analytical solutions of a collapsing shell at the inner radius versus the nondimensionalised time where $\nu = 0.48$ and $\beta = 12$. The analytical solution is calculated using equations (2.154) and (2.166) whereas the numerical solution is calculated using equation (2.138).

Figure 2.14 compares the analytical and numerical solutions to equation (2.138) for the nondimensionalised parameters $\nu = 0.48$ and $\beta = 12$. Figure 2.14 shows that there is good agreement between the numerical and analytical solutions.

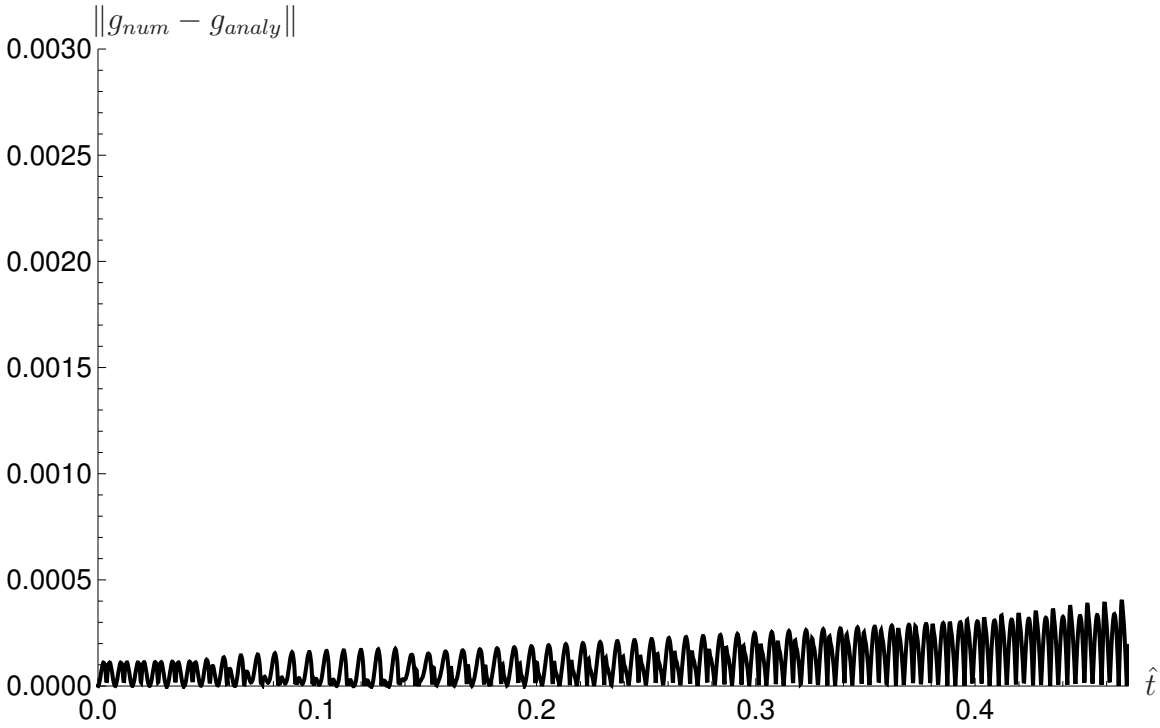

Figure 2.15: Graph of the absolute difference between the nondimensionalised numerical and analytical solutions of a collapsing shell at the outer radius versus the nondimensionalised time where $\nu = 0.48$ and $\beta = 12$. The analytical solution is calculated using equations (2.157) and (2.166) whereas the numerical solution is calculated using equation (2.138).

A series of graphs of $\|g_{num} - g_{analy}\|$ have been produced where the number of modes in the analytical solution were varied between one and nine. Very little change was observed between these plots and the oscillations that can be seen in Figure 2.15 persisted throughout. This suggests that these oscillations are caused by numerical instabilities in the method used to numerically solve equation (2.138).

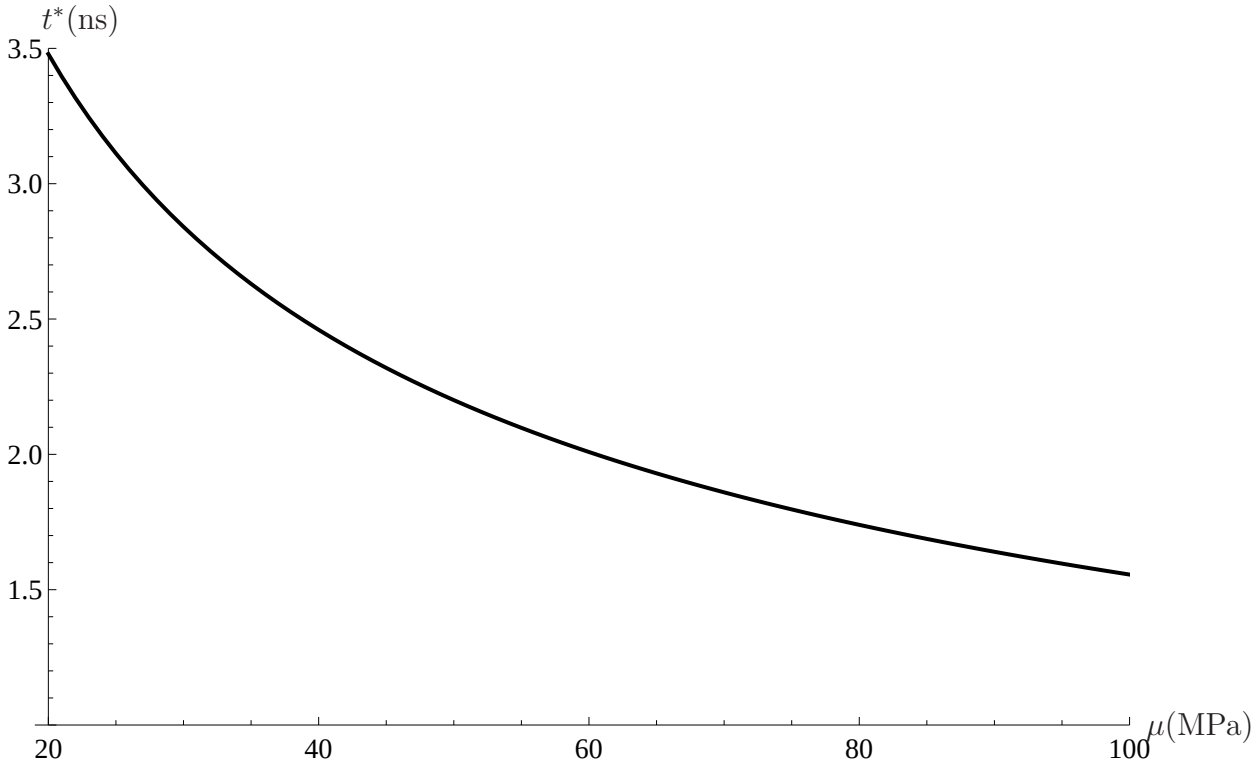

Figure 2.16: Graph of the redimensionalised collapse time of the shell versus the redimensionalised shear modulus where $\beta = 12$, $\nu = 0.48$ and the initial stress free thickness is $R_O - R_I = 0.02$nm. The density of the shell $\rho_o = 1100\text{kg}m^{-3}$ [14] and its inner radius is $R_I = 1\mu$m. Typical shear modulus values are within the range of $\mu = 20 \rightarrow 100$MPa [14,15]. The collapse time is calculated from the zeros of the determinant of the matrix $M(s)$ in equation (2.154) and is redimensionalised using $t = \gamma\hat{t}$ where $\gamma = \sqrt{\rho_o R_I^2/\mu}$.

Figure 2.16 highlights the nonlinear relationship between the redimensionalised collapse time of the shell and the redimensionalised shear modulus. The nondimensionalised angular collapse frequency is evaluated using equation (2.151) where the nondimensionalised collapse time is given by $\hat{t}^* = \pi/(2\omega)$. We redimensionalise the collapse time using $t = \gamma\hat{t}$ where $\gamma = \sqrt{\rho_o R_I^2/\mu}$. Figure 2.16 shows that as the shear modulus increases the microbubble shells experience shorter collapse times.

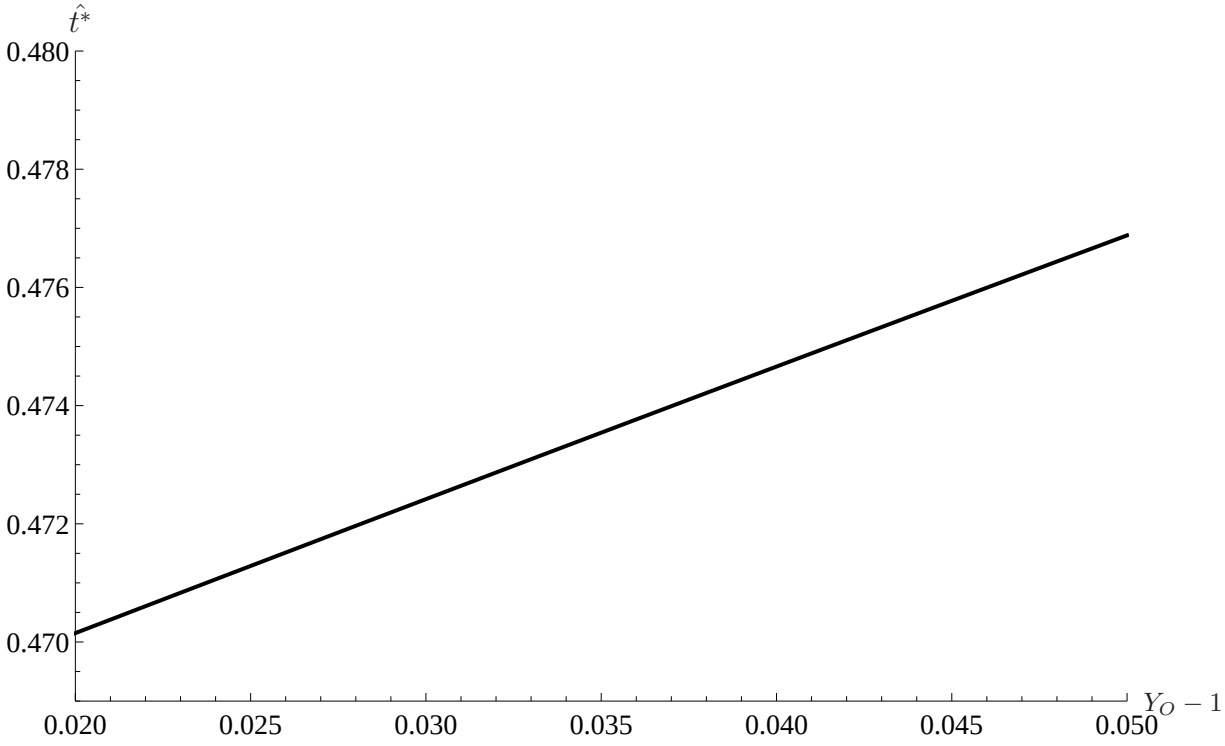

Figure 2.17: Graph of the nondimensionalised collapse time ($\hat{t^*} = \pi/(2\omega_1)$) of the shell versus the nondimensionalised original thickness of the shell ($Y_O - 1$) where $\beta = 12$ and $\nu = 0.48$. This is calculated from the zeros of the determinant of the matrix $M(s)$ in equation (2.154).

Figure 2.17 shows the relationship between the collapse time of the shell and the nondimensionalised original (stress free) thickness of the shell. Thinner shells will strain more to balance the tensions that they are subjected to which will result in larger radial deformations. The hoop stresses play a key role in the collapse phase of the shell with thinner shells experiencing a larger hoop stress as illustrated by Figures 2.10 and 2.11. Thinner shells also possess a smaller mass and it is the combination of the mass and the hoop stress that must be considered when determining the collapse time. Figure 2.17 illustrates that thicker shells have slightly longer collapse times.

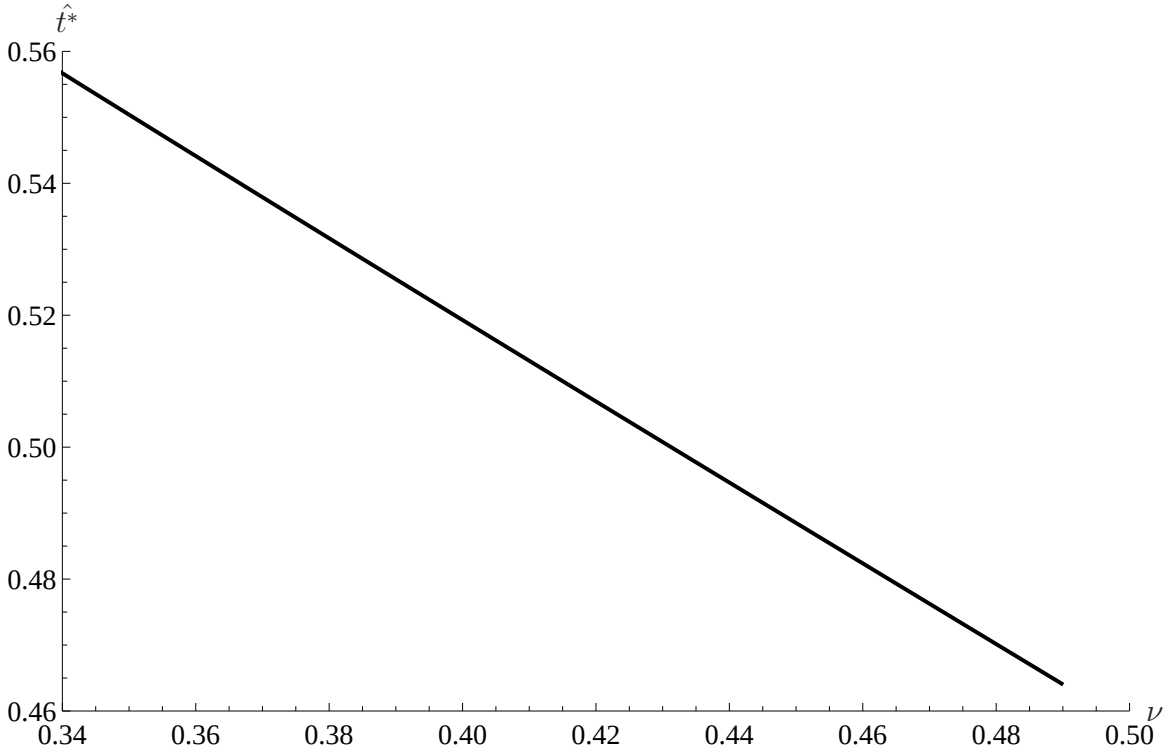

Figure 2.18: Graph of the nondimensionalised collapse time ($\hat{t^*} = \pi/(2\omega_1)$) of the shell versus the Poisson ratio (ν) of the shell's material where the initial stress thickness is $Y_O - 1 = 0.02$. This is calculated from the zeros of the determinant of the matrix $M(s)$ in equation (2.154).

Figure 2.18 highlights the approximately linear relationship between the nondimensionalised collapse time and the Poisson ratio ν. Equation (2.157) shows that the angular frequency is approximately proportional to the square root of β, where $\beta = \nu/(1-2\nu)$. Since $0 < \nu < 1/2$ then $\beta > 0$ and monotonically increases as ν increases and so as the Poisson ratio increases the angular frequency ω, increases which results in a shorter collapse time (as $\hat{t^*} = \pi/(2\omega_1)$).

2.8 Conclusion

This chapter described an analytical approach to modelling the inflationary process of a shelled microbubble via a quasistatic radially directed stress load applied to its inner surface. The stress load was switched off (a stress free boundary condition was applied) and the time for the microbubble's shell to collapse back down to its equilibrium position was determined by applying the momentum balance law and the forward picture's inflated radial deformation as an initial condition. Key material parameters such as the thickness of the shell, its Poisson ratio and the shell's shear modulus were varied to determine their influence on the collapse phase of the shell. A typical redimensionalised collapse time for a shelled microbubble of interior radius 1μm, a shell density of $\rho = 1100kgm^{-3}$, a redimensionalised shear modulus of $\mu = 20$MPa and a Poisson ratio of $\nu = 0.48$, subjected to a redimensionalised stress load of $p = 200$kPa, is of the order $t^* = 0.47 \times \sqrt{(\rho_o R_I^2/\mu)} \approx 3.5$ns where $\hat{t^*} = 0.47$ is the nondimensionalised collapse time. Shells with a larger shear modulus possessed shorter collapse times. As the thickness of the shell increased the collapse time of the shell increased in a linear manner. Shells with a larger Poisson ratio had shorter collapse times. The stress profile within the shell of the microbubble in the radial direction in the inflationary stage (quasistatic) differed from the stress profiles during the collapse phase due to the unloading at the inner shell as a consequence of the change in boundary conditions (switching off of the stress load at the inner shell). The complexity of the Laplace transformed collapsing deformation ($G(Y, s)$) made the process of obtaining an explicit form for $g(Y, \hat{t})$ challenging. The complex integrals were therefore evaluated numerically and a numerical solution of the original PDE used to validate the analysis. It would be extremely advantageous to have a numerical solution for the nonlinear model to not only validate the linearised model's solution but also to enable us to

extend this study into the regimes of higher, non-perturbative stress loads where an asymptotic expansion would be inappropriate. However, the development of a numerical solution for a nonlinear model is a formidable challenge and is a possible area for future study. The chief legacy of this study is the qualitative insight that it gives us into how the material parameters such as the shear modulus, the thickness of the shell and the Poisson ratio influence the collapse time of the shell. This study highlighted the key role that the hoop stresses played in the potential rupture and collapse time of the shell. Figure 2.10 indicated that the hoop stresses were not only larger than the axial (radial) stress but were also positive which is indicative of a stretching behaviour.

Having studied the collapse of a stressed shelled microbubble that remains as an intact sphere throughout the deformations, it seems natural to then extend the analysis to a situation where the shell has ruptured. In the next chapter we will study this situation and observe the static model of a stressed, open shelled microbubble which experiences both a radial and an angular deformation.

Chapter 3

Rupture of a shelled microbubble

3.1 Introduction

In this chapter a theoretical model is proposed to model a ruptured shelled microbubble. A compressible, neo-Hookean [54] hyperelastic strain energy density function is used to model the potential energy per unit volume of the shell which is subjected to a stress via an opening angle [54]. A stress is generated in the shell by deforming a shelled microbubble with a spherical cap removed in the south polar region; the original shelled microbubble represents the reference configuration. An angular stress is applied to the rim of this open shelled microbubble resulting in it experiencing both a radial and a polar angular deformation. This stressed shelled microbubble then represents the current configuration and possesses both radial and hoop stresses which are evaluated using the hyperelastic strain energy density function in conjunction with the relevant boundary conditions and the momentum balance law. The application of the deforming stress is done via a quasistatic process and is thus independent of time. The quasistatic process implies that the divergence of the stress is equal to zero. The radial stresses at both the inner and

outer radii of the compressible shell are set to zero. An opening angle $\pi - \Theta_{op}$ is chosen that is small compared to π (see Figure 3.1).

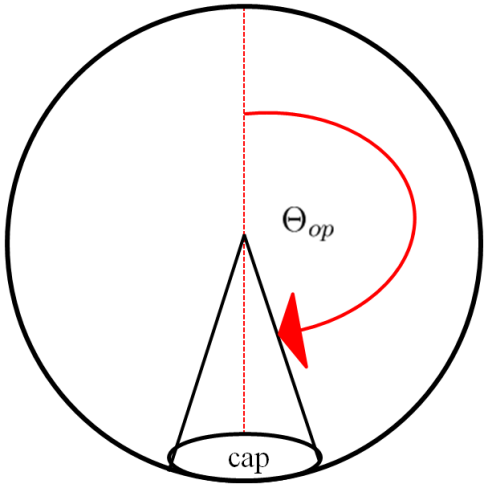

Figure 3.1: Figure illustrating the opening angle, $\pi - \Theta_{op}$.

Since the shell is modelled as compressible this results in a small change in the volume and thickness of the shell as it is deformed. The change in density (and thickness) of the shell is described using the Jacobian of the shell which displays a radial and an angular dependency. The deformation used to link the reference configuration to the current configuration has both an angular and a radial dependency and so produces two differential equations: one describing the angular deformation and the other the radial deformation. This necessitates two different sets of coupled boundary conditions, one set for the polar angle and the other set for the radial behaviour. The process of deforming the initial shelled microbubble will be referred to as the forward picture. Developing a model for the radial and angular deformation of an open angle shelled microbubble is fundamental to studying shelled microbubble rupture and collapse. Future work will use numerical analysis to solve both the forward picture and the collapse phase of a stressed open shelled microbubble and its dependency on various material parameters. A

collapse model for a ruptured shell would capture the unfolding shell imaged by Müller and Stannarius [78].

3.2 Calculating the deformation for the forward picture

Let us consider the reference configuration of a stress free shell. The reference configuration in Cartesian coordinates is defined as (X^1, X^2, X^3) and is more generally denoted as X^i whereas the current configuration, representing the stressed shelled microbubble, is defined using the Cartesian coordinates (x^1, x^2, x^3) which can be generalised to x^i. The stress free, open shell has inner and outer radii described by R_I and R_O respectively whilst the deformed stressed shell has inner and outer radii denoted by $r(R_I, \Theta)$ and $r(R_O, \Theta)$. A deformation acting on the stress free, open shelled microbubble, is represented by

$$\chi = r(R, \Theta)e_r, \tag{3.1}$$

such that the polar angle in the current configuration can be expressesd as a function of the polar angle and the radius in the reference configuration where $\theta = \theta(R, \Theta)$ and e_r represents the radial component of the standard basis in spherical polar coordinates ([70], p66). This implies that for any given angle Θ in the reference configuration, all points within the shell that lie along $R_I \leq R \leq R_O$ are not restricted to move in the same direction in their current configuration since e_r depends on R. However, to reduce the complexity of the analysis we shall place a kinematic constraint on this deformation such that $\theta = \theta(\Theta)$. This simplified assumption means that for a given angle of Θ in the reference configuration, then

all points within the shell that lie along $R_I \leq R \leq R_O$ are constrained to move in the same direction as e_r now only depends on Θ. We will use a mixed tensorial basis and define the deformation gradient as $F = \nabla \otimes \chi$ ([70], p83-84) where F is given by equation (2.41). In spherical polar coordinates the current configuration is transformed into physical components ([70], p64) yielding $\chi_1 = \chi_r$, $\chi_2 = ru_\theta$ and $\chi_3 = r\sin\theta\chi_\phi$ where the physical coordinates preserve the units. Using equation (2.41) we can determine the gradient of the deformation defined by equation (3.1) where $\chi_1 = r(R,\Theta)$ and $\chi_2 = \chi_3 = 0$. For the opening angle approach $\theta = \theta(\Theta)$ and $\phi = \Phi$ resulting in a deformation, F, that is given by

$$\begin{aligned}(\nabla \otimes \chi)_{rR}\, e_r \otimes e_R &= \left(\frac{\partial \chi_1}{\partial X^1} + \chi_1 \frac{\partial g^1}{\partial X^1} \cdot g_1\right) g^1 \otimes G^1, \\ &= \left(\frac{\partial r}{\partial R} + r\frac{\partial e_r}{\partial R} \cdot e_r\right) e_r \otimes e_R, \\ &= \left(\frac{\partial r}{\partial R}\right) e_r \otimes e_R, \end{aligned} \tag{3.2}$$

$$\begin{aligned}(\nabla \otimes \chi)_{r\Theta}\, e_r \otimes e_\Theta &= \left(\frac{\partial \chi_1}{\partial X^2} + \chi_1 \frac{\partial g^1}{\partial X^2} \cdot g_1\right) g^1 \otimes G^2, \\ &= \left(\frac{\partial r}{\partial \Theta} + r\frac{\partial e_r}{\partial \Theta} \cdot e_r\right) \frac{e_r \otimes e_\Theta}{R}, \\ &= \frac{1}{R}\left(\frac{\partial r}{\partial \Theta}\right) e_r \otimes e_\Theta, \end{aligned} \tag{3.3}$$

$$\begin{aligned}(\nabla \otimes \chi)_{r\Phi}\, e_r \otimes e_\Phi &= \left(\frac{\partial \chi_1}{\partial X^3} + \chi_1 \frac{\partial g^1}{\partial X^3} \cdot g_1\right) g^1 \otimes G^3, \\ &= \left(r\frac{\partial e_r}{\partial \Phi} \cdot e_r\right) \frac{e_r \otimes e_\Phi}{R\sin\Phi}, \\ &= \left(r\sin\theta e_\phi \phi' \cdot e_r\right) \frac{e_r \otimes e_\Phi}{R\sin\Theta} = 0, \end{aligned} \tag{3.4}$$

$$(\nabla \otimes \chi)_{\theta R}\, e_\theta \otimes e_R = \left(\frac{\partial \chi_2}{\partial X^1} + \chi_1 \frac{\partial g^1}{\partial X^1} \cdot g_2\right) g^2 \otimes G^1,$$
$$= \left(r\frac{\partial e_r}{\partial R} \cdot r e_\theta\right) \frac{e_\theta \otimes e_R}{r} = 0, \tag{3.5}$$

$$(\nabla \otimes \chi)_{\theta\Theta}\, e_\theta \otimes e_\Theta = \left(\frac{\partial \chi_2}{\partial X^2} + \chi_1 \frac{\partial g^1}{\partial X^2} \cdot g_2\right) g^2 \otimes G^2,$$
$$= \frac{r}{R}\left(e_\theta \frac{\partial \theta}{\partial \Theta} \cdot e_\theta\right) e_\theta \otimes e_\Theta = \frac{r}{R}\left(\frac{\partial \theta}{\partial \Theta}\right) e_\theta \otimes e_\Theta, \tag{3.6}$$

$$(\nabla \otimes \chi)_{\theta\Phi}\, e_\theta \otimes e_\Phi = \left(\frac{\partial \chi_2}{\partial X^3} + \chi_1 \frac{\partial g^1}{\partial X^3} \cdot g_2\right) g^2 \otimes G^3,$$
$$= \left(r\frac{\partial e_r}{\partial \Phi} \cdot r e_\theta\right) \frac{e_\theta \otimes e_\Phi}{rR\sin\Theta} = 0, \tag{3.7}$$

$$(\nabla \otimes \chi)_{\phi R}\, e_\phi \otimes e_R = \left(\frac{\partial \chi_3}{\partial X^1} + \chi_1 \frac{\partial g^1}{\partial X^1} \cdot g_3\right) g^3 \otimes G^1,$$
$$= \left(r\frac{\partial e_r}{\partial R} \cdot r\sin\theta e_\phi\right) \frac{e_\phi \otimes e_R}{r\sin\theta} = 0, \tag{3.8}$$

$$(\nabla \otimes \chi)_{\phi\Theta}\, e_\phi \otimes e_\Theta = \left(\frac{\partial \chi_3}{\partial X^2} + \chi_1 \frac{\partial g^1}{\partial X^2} \cdot g_3\right) g^3 \otimes G^2,$$
$$= \left(r e_\theta \frac{\partial \theta}{\partial \Theta} \cdot r\sin\theta e_\phi\right) \frac{e_\phi \otimes e_\Theta}{rR\sin\theta} = 0, \tag{3.9}$$

and

$$(\nabla \otimes \chi)_{\phi\Phi}\, e_\phi \otimes e_\Phi = \left(\frac{\partial \chi_3}{\partial X^3} + \chi_1 \frac{\partial g^1}{\partial X^3} \cdot g_3\right) g^3 \otimes G^3,$$
$$= \left(r\frac{\partial e_r}{\partial \Phi} \cdot r\sin\theta e_\phi\right) \frac{e_\phi \otimes e_\Phi}{rR\sin\theta\sin\Theta},$$
$$= \left(\frac{r\sin\theta}{R\sin\Theta}\right) e_\phi \otimes e_\Phi. \tag{3.10}$$

Combining equations (3.2) - (3.10) and writing them as a 3×3 matrix, since the gradient of the deformation written as $F = \nabla \otimes \chi$ is a two point tensor, gives

$$F = \begin{pmatrix} \frac{\partial r}{\partial R} & \frac{1}{R}\frac{\partial r}{\partial \Theta} & 0 \\ 0 & \frac{r}{R}\left(\frac{\partial \theta}{\partial \Theta}\right) & 0 \\ 0 & 0 & \frac{r \sin\theta}{R \sin\Theta} \end{pmatrix} \tag{3.11}$$

with an inverse transpose, F^{-T}, given by

$$F^{-T} = \begin{pmatrix} \frac{\partial R}{\partial r} & 0 & 0 \\ -\frac{1}{r}\left(\frac{\partial R}{\partial r}\right)\left(\frac{\partial r}{\partial \Theta}\right)\frac{\partial \Theta}{\partial \theta} & \frac{R}{r}\left(\frac{\partial \Theta}{\partial \theta}\right) & 0 \\ 0 & 0 & \frac{R \sin\Theta}{r \sin\theta} \end{pmatrix}. \tag{3.12}$$

3.3 Hyperelastic strain energy density function

Let us assume that the shell's material is hyperelastic so that there exists a strain energy density function (expressing the potential energy per unit volume), that is neo-Hookean [54,58,71], $W(F)$, and let it include a compressible term that is used to model the change in volume of the shell as it is stressed. The determinant of F gives a measure of how the volume of the spherical shell changes as it maps from the stress free, reference configuration to the stressed, current configuration. From equation (3.12), the Jacobian (determinant of F) is

$$J = \frac{r^2}{R^2}\left(\frac{\partial r}{\partial R}\right)\left(\frac{\partial \theta}{\partial \Theta}\right)\frac{\sin\theta}{\sin\Theta}. \tag{3.13}$$

The neo-Hookean strain energy density function is given by equation (2.54) ([54], equation(5)). Substituting equations (3.11) and (3.12) into equation (2.61) leads

to the first Piola-Kirchoff stress

$$\begin{aligned} S &= S_{rR}e_r \otimes e_R + S_{\theta\Theta}e_\theta \otimes e_\Theta + S_{\phi\Phi}e_\phi \otimes e_\Phi + S_{r\Theta}e_r \otimes e_\Theta + S_{\theta R}e_\theta \otimes e_R, \\ &= \mu\left(-J^{-2\beta}\frac{\partial R}{\partial r} + \frac{\partial r}{\partial R}\right)e_r \otimes e_R + \mu\left(-J^{-2\beta}\frac{R}{r}\left(\frac{\partial \Theta}{\partial \theta}\right) + \frac{r}{R}\left(\frac{\partial \theta}{\partial \Theta}\right)\right)e_\theta \otimes e_\Theta \\ &\quad + \mu\left(-J^{-2\beta}\frac{R\sin\Theta}{r\sin\theta} + \frac{r\sin\theta}{R\sin\Theta}\right)e_\phi \otimes e_\Phi + \frac{\mu}{R}\left(\frac{\partial r}{\partial \Theta}\right)e_r \otimes e_\Theta \\ &\quad + \frac{\mu J^{-2\beta}}{r}\left(\frac{\partial R}{\partial r}\right)\left(\frac{\partial r}{\partial \Theta}\right)\frac{\partial \Theta}{\partial \theta}e_\theta \otimes e_R. \quad (3.14) \end{aligned}$$

Note that equation (3.14) identifies the physical components for $S_{rR}, S_{\theta\Theta}, S_{\phi\Phi}$ and so on.

3.4 Calculating the divergence of the first Piola-Kirchoff stress tensor for the forward picture

The reference configuration shelled microbubble is deformed by applying a stress directed towards the pole and applied on the rim of the open surface at the opening angle. The applied stress causes a quasistatic deformation. This implies that the divergence of the first Piola-Kirchoff stress tensor must satisfy $\nabla \cdot S = 0$. We need to be able to relate the physical coordinates for the mixed tensorial basis to the general basis vectors represented by the components g_i and G_i where $i \in \{1, 2, 3\}$. The first Piola-Kirchhoff stress tensor is represented by ([70], p34), $S = S_i^{\ j} g^i \otimes G_j$ where $S_i^{\ j}$ are the left-covariant components of S. Converting physical coordinates into generalised coordinates using equation (3.14) yields

$$S_1^{\ 1} g^1 \otimes G_1 = S_1^{\ 1} e_r \otimes e_R = S_{rR} e_r \otimes e_R,$$

where

$$S_1^{\ 1} = S_{rR} = \mu\left(-J^{-2\beta}\frac{\partial R}{\partial r} + \frac{\partial r}{\partial R}\right), \tag{3.15}$$

and

$$S_2^{\ 2} g^2 \otimes G_2 = S_2^{\ 2}\left(\frac{R}{r}\right) e_\theta \otimes e_\Theta = S_{\theta\Theta} e_\theta \otimes e_\Theta,$$

thus

$$S_2^{\ 2} = \mu\left(-J^{-2\beta}\left(\frac{\partial\Theta}{\partial\theta}\right) + \frac{r^2}{R^2}\left(\frac{\partial\theta}{\partial\Theta}\right)\right), \tag{3.16}$$

and

$$S_3^{\ 3} g^3 \otimes G_3 = S_3^{\ 3}\left(\frac{R\sin\Theta}{r\sin\theta}\right) e_\phi \otimes e_\Phi = S_{\phi\Phi} e_\phi \otimes e_\Phi,$$

resulting in

$$S_3^{\ 3} = \mu\left(-J^{-2\beta} + \left(\frac{r\sin\theta}{R\sin\Theta}\right)^2\right). \tag{3.17}$$

Similarly

$$S_1^{\ 2} g^1 \otimes G_2 = S_1^{\ 2} e_r \otimes R e_\Theta = S_{r\Theta} e_r \otimes e_\Theta,$$

where

$$S_1^{\ 2} = \frac{\mu}{R^2}\left(\frac{\partial r}{\partial\Theta}\right), \tag{3.18}$$

and

$$S_2^{\ 1} g^2 \otimes G_1 = S_2^{\ 1}\frac{e_\theta}{r} \otimes e_R = S_{\theta R} e_\theta \otimes e_R,$$

resulting in

$$S_2^{\ 1} = \mu J^{-2\beta}\left(\frac{\partial R}{\partial r}\right)\left(\frac{\partial r}{\partial\Theta}\right)\frac{\partial\Theta}{\partial\theta}. \tag{3.19}$$

Calculating the divergence of S,

$$\nabla \cdot S = \frac{\partial}{\partial X^k} \left(S_i^{\ j} g^i \otimes G_j \right) \cdot G^k, \tag{3.20}$$

requires the quantity

$$\frac{\partial}{\partial X^1} \left(S_1^{\ 1} g^1 \otimes G_1 \right) \cdot G^1 = \frac{\partial S_1^{\ 1}}{\partial R} \left(e_r \otimes e_R \right) \cdot e_R = \frac{\partial S_1^{\ 1}}{\partial R} e_r. \tag{3.21}$$

Similarly we get

$$\begin{aligned} \frac{\partial}{\partial X^1} \left(S_2^{\ 2} g^2 \otimes G_2 \right) \cdot G^1 &= \frac{\partial}{\partial R} \left(S_2^{\ 2} \frac{e_\theta}{r} \otimes R e_\Theta \right) \cdot e_R, \\ &= \frac{\partial}{\partial R} \left(S_2^{\ 2} \frac{R}{r} \right) \left(e_\theta \otimes e_\Theta \right) \cdot e_R = 0. \end{aligned} \tag{3.22}$$

Similarly

$$\begin{aligned} \frac{\partial}{\partial X^1} \left(S_3^{\ 3} g^3 \otimes G_3 \right) \cdot G^1 &= \frac{\partial}{\partial R} \left(S_3^{\ 3} \frac{e_\phi}{r \sin\theta} \otimes R \sin\Theta e_\Phi \right) \cdot e_R, \\ &= \frac{\partial}{\partial R} \left(S_3^{\ 3} \frac{R \sin\Theta}{r \sin\theta} \right) \left(e_\phi \otimes e_\Phi \right) \cdot e_R = 0. \end{aligned} \tag{3.23}$$

The off diagonal terms are

$$\frac{\partial}{\partial X^1} \left(S_1^{\ 2} g^1 \otimes G_2 \right) \cdot G^1 = 0, \tag{3.24}$$

and

$$\frac{\partial}{\partial X^1} \left(S_2^{\ 1} g^2 \otimes G_1 \right) \cdot G^1 = \left(\frac{\partial S_2^{\ 1}}{\partial R} \right) \frac{e_\theta}{r} - \frac{S_2^{\ 1}}{r^2} \left(\frac{\partial r}{\partial R} \right) e_\theta. \tag{3.25}$$

Other terms are

$$\frac{\partial}{\partial X^2}\left(S_1{}^1 g^1 \otimes G_1\right)\cdot G^2 = \frac{S_1{}^1}{R}\left(e_r \otimes e_\Theta\right)\cdot e_\Theta,$$
$$= \frac{S_1{}^1}{R}\left(e_r \otimes e_\Theta\right)\cdot e_\Theta = \frac{S_1{}^1}{R} e_r, \tag{3.26}$$

also

$$\frac{\partial}{\partial X^2}\left(S_2{}^2 g^2 \otimes G_2\right)\cdot G^2 = \frac{\partial S_2{}^2}{\partial \Theta}\left(\frac{e_\theta}{r}\right) + S_2{}^2\frac{\partial}{\partial \Theta}\left(\frac{e_\Theta}{r}\right),$$
$$= \frac{\partial S_2{}^2}{\partial \Theta}\left(\frac{e_\theta}{r}\right) - \frac{S_2{}^2}{r^2}\left(\frac{\partial r}{\partial \Theta}\right)e_\theta - \frac{S_2{}^2}{r}\left(\frac{\partial \theta}{\partial \Theta}\right)e_r, \tag{3.27}$$

similarly

$$\frac{\partial}{\partial X^2}\left(S_3{}^3 g^3 \otimes G_3\right)\cdot G^2 = \left(S_3{}^3\frac{e_\phi}{r\sin\theta}\otimes\frac{\partial}{\partial \Theta}\left(R\sin\Theta e_\Phi\right)\right)\cdot\frac{e_\Theta}{R} = 0, \tag{3.28}$$

and

$$\frac{\partial}{\partial X^2}\left(S_1{}^2 g^1 \otimes G_2\right)\cdot G^2 = \frac{\partial S_1{}^2}{\partial X^2} g^1 + S_1{}^2\frac{\partial g^1}{\partial X^2} + S_1{}^2 g^1 \otimes \frac{\partial}{\partial \Theta}\left(R e_\Theta\right)\cdot G^2,$$
$$= \frac{\partial S_1{}^2}{\partial \Theta} e_r + S_1{}^2\left(\frac{\partial \theta}{\partial \Theta}\right)e_\theta, \tag{3.29}$$

with

$$\frac{\partial}{\partial X^2}\left(S_2{}^1 g^2 \otimes G_1\right)\cdot G^2 = \left(S_2{}^1 g^2 \otimes \frac{\partial G_1}{\partial X^2}\right)\cdot G^2,$$
$$= \left(S_2{}^1\frac{e_\theta}{r}\otimes\frac{\partial}{\partial \Theta} e_R\right)\cdot\frac{e_\Theta}{R} = \frac{S_2{}^1}{Rr} e_\theta. \tag{3.30}$$

Other components are

$$\frac{\partial}{\partial X^3}\left(S_1{}^1 g^1 \otimes G_1\right)\cdot G^3 = \left(S_1{}^1 g^1 \otimes \frac{\partial e_R}{\partial \Phi}\right)\cdot G^3,$$
$$= \left(S_1{}^1 e_r \otimes \sin\Theta e_\Phi\right)\cdot \frac{e_\Phi}{R\sin\Theta} = \frac{S_1{}^1}{R} e_r, \tag{3.31}$$

and

$$\frac{\partial}{\partial X^3}\left(S_2{}^2 g^2 \otimes G_2\right)\cdot G^3 = S_2{}^2 \frac{e_\theta}{r} \otimes \frac{\partial}{\partial \Phi}\left(R e_\Theta\right)\cdot \frac{e_\Phi}{R\sin\Theta},$$
$$= S_2{}^2 \frac{e_\theta}{r} \otimes R\cos\Theta e_\Phi \cdot \frac{e_\Phi}{R\sin\Theta} = \frac{S_2{}^2\cot\Theta}{r} e_\theta, \tag{3.32}$$

also

$$\frac{\partial}{\partial X^3}\left(S_3{}^3 g^3 \otimes G_3\right)\cdot G^3 = S_3{}^3 \frac{\partial}{\partial \Phi}\left(\frac{e_\phi}{r\sin\theta}\right),$$
$$= -\frac{S_3{}^3}{r} e_r - \frac{S_3{}^3\cot\theta}{r} e_\theta, \tag{3.33}$$

similarly

$$\frac{\partial}{\partial X^3}\left(S_1{}^2 g^1 \otimes G_2\right)\cdot G^3 = S_1{}^2 e_r \otimes \frac{\partial}{\partial \Phi}\left(R e_\Theta\right)\cdot \frac{e_\Phi}{R\sin\Theta},$$
$$= S_1{}^2 e_r \otimes \cos\Theta e_\Phi \cdot \frac{e_\Phi}{\sin\Theta} = \cot\Theta S_1{}^2 e_r, \tag{3.34}$$

and

$$\frac{\partial}{\partial X^3}\left(S_2{}^1 g^2 \otimes G_1\right)\cdot G^3 = S_2{}^1 g^2 \otimes \frac{\partial G_1}{\partial X^3}\cdot G^3,$$
$$= S_2{}^1 \frac{e_\theta}{r} \otimes \frac{\partial e_R}{\partial \Phi}\cdot \frac{e_\Phi}{R\sin\Theta} = \frac{S_2{}^1}{rR} e_\theta. \tag{3.35}$$

3.5 Radial and angular equations

Combining equations (3.21) to (3.35) and substituting into equation (3.20) results in the radial and angular equations

$$\frac{\partial S_1^{\ 1}}{\partial R} + \frac{2S_1^{\ 1}}{R} - \frac{S_2^{\ 2}}{r}\left(\frac{\partial \theta}{\partial \Theta}\right) - \frac{S_3^{\ 3}}{r} + \frac{\partial S_1^{\ 2}}{\partial \Theta} + \cot\Theta S_1^{\ 2} = 0, \tag{3.36}$$

and

$$\frac{1}{r}\left(\frac{\partial S_2^{\ 1}}{\partial R}\right) - \frac{S_2^{\ 1}}{r^2}\left(\frac{\partial r}{\partial R}\right) + \frac{1}{r}\left(\frac{\partial S_2^{\ 2}}{\partial \Theta}\right) - \frac{S_2^{\ 2}}{r^2}\left(\frac{\partial r}{\partial \Theta}\right) + S_1^{\ 2}\left(\frac{\partial \theta}{\partial \Theta}\right) + \frac{2S_2^{\ 1}}{Rr} + \frac{S_2^{\ 2}\cot\Theta}{r} - \frac{S_3^{\ 3}\cot\theta}{r} = 0. \tag{3.37}$$

The first Piola-Kirchoff tensor is related to the Cauchy stress tensor via

$$\tau = \frac{1}{J}\left(SF^T\right), \tag{3.38}$$

where J, the Jacobian, is given by equation (3.13) and F is described by equation (3.11) [54]. Using equation (3.38) in conjunction with equations (3.15) to (3.19), alongside equations (3.11) and (3.38) results in Cauchy stress terms that are given by the expressions

$$\begin{aligned}\tau_{rr} &= \frac{1}{J}\left(S_{rR}\frac{\partial r}{\partial R} + \frac{S_{r\Theta}}{R}\left(\frac{\partial r}{\partial \Theta}\right)\right), \\ &= \frac{\mu}{J}\left(-J^{-2\beta} + \left(\frac{\partial r}{\partial R}\right)^2 + \frac{1}{R^2}\left(\frac{\partial r}{\partial \Theta}\right)^2\right),\end{aligned} \tag{3.39}$$

alongside

$$\begin{aligned}\tau_{\theta\theta} &= \frac{1}{J}\left(S_{\theta\Theta}\left(\frac{r}{R}\right)\frac{\partial\theta}{\partial\Theta}\right), \\ &= \frac{\mu}{J}\left(-J^{-2\beta}+\left(\frac{r}{R}\right)^{2}\left(\frac{\partial\theta}{\partial\Theta}\right)^{2}\right),\end{aligned} \tag{3.40}$$

and

$$\tau_{\phi\phi} = \frac{S_{\phi\Phi}}{J}\left(\frac{r\sin\theta}{R\sin\Theta}\right) = \frac{\mu}{J}\left(-J^{-2\beta}+\left(\frac{r\sin\theta}{R\sin\Theta}\right)^{2}\right). \tag{3.41}$$

The off diagonal term is given by

$$\tau_{r\theta} = \frac{1}{J}\left(S_{r\Theta}\right)\frac{r}{R}\left(\frac{\partial\theta}{\partial\Theta}\right) = \frac{\mu r}{JR^{2}}\left(\frac{\partial\theta}{\partial\Theta}\right)\frac{\partial r}{\partial\Theta}. \tag{3.42}$$

The radial equation can be written in terms of $r(R,\Theta)$ and $\theta(\Theta)$ by substituting equations (3.15) to (3.19) into equation (3.36), where

$$\frac{\partial J}{\partial R} = J\left(\frac{2}{r}\left(\frac{\partial r}{\partial R}\right)+\left(\frac{\partial R}{\partial r}\right)\frac{\partial^{2}r}{\partial R^{2}}-\frac{2}{R}\right), \tag{3.43}$$

and

$$\frac{\partial S_{1}^{\,1}}{\partial R} = \mu\left(\frac{\partial^{2}r}{\partial R^{2}}\left(1+(2\beta+1)J^{-2\beta}\left(\frac{\partial R}{\partial r}\right)^{2}\right)+J^{-2\beta}\left(\frac{4\beta}{r}-\frac{4\beta}{R}\left(\frac{\partial R}{\partial r}\right)\right)\right). \tag{3.44}$$

Similarly

$$\frac{2S_{1}^{\,1}}{R} = \mu\left(\frac{-2J^{-2\beta}}{R}\left(\frac{\partial R}{\partial r}\right)+\frac{2}{R}\left(\frac{\partial r}{\partial R}\right)\right), \tag{3.45}$$

also

$$-\frac{S_{2}^{\,2}}{r}\left(\frac{\partial\theta}{\partial\Theta}\right) = \mu\left(\frac{J^{-2\beta}}{r}-\frac{r}{R^{2}}\left(\frac{\partial\theta}{\partial\Theta}\right)^{2}\right), \tag{3.46}$$

and

$$-\frac{S_3^{\,3}}{r} = \mu\left(\frac{J^{-2\beta}}{r} - \frac{r\sin^2\theta}{R^2\sin^2\Theta}\right). \tag{3.47}$$

The off diagonal terms are

$$\frac{\partial S_1^{\,2}}{\partial\Theta} = \frac{\mu}{R^2}\left(\frac{\partial^2 r}{\partial\Theta^2}\right), \tag{3.48}$$

and

$$\cot\Theta S_1^{\,2} = \frac{\mu\cot\Theta}{R^2}\left(\frac{\partial r}{\partial\Theta}\right). \tag{3.49}$$

Substituting equations (3.44) to (3.49) into equation (3.36) yields

$$\begin{aligned}\frac{\partial^2 r}{\partial R^2}\left(1+(2\beta+1)J^{-2\beta}\left(\frac{\partial R}{\partial r}\right)^2\right) + J^{-2\beta}\left(\frac{4\beta}{r} - \frac{4\beta}{R}\left(\frac{\partial R}{\partial r}\right) - \frac{2}{R}\left(\frac{\partial R}{\partial r}\right) + \frac{2}{r}\right)\\ + \frac{2}{R}\left(\frac{\partial r}{\partial R}\right) - \frac{r}{R^2}\left(\frac{\partial\theta}{\partial\Theta}\right)^2 - \frac{r\sin^2\theta}{R^2\sin^2\Theta} + \frac{1}{R^2}\left(\frac{\partial^2 r}{\partial\Theta^2}\right) + \frac{\cot\Theta}{R^2}\left(\frac{\partial r}{\partial\Theta}\right) = 0.\end{aligned} \tag{3.50}$$

For the angular equation given by equation (3.37), the following is required

$$\begin{aligned}\frac{\partial J}{\partial\Theta} &= \frac{\partial}{\partial\Theta}\left(\frac{r^2}{R^2}\left(\frac{\partial r}{\partial R}\right)\left(\frac{\partial\theta}{\partial\Theta}\right)\frac{\sin\theta}{\sin\Theta}\right),\\ &= J\left(\frac{2}{r}\frac{\partial r}{\partial\Theta} + \left(\frac{\partial R}{\partial r}\right)\frac{\partial^2 r}{\partial\Theta\partial R} + \frac{\partial^2\theta}{\partial\Theta^2}\left(\frac{\partial\Theta}{\partial\theta}\right) + \frac{\partial\theta}{\partial\Theta}\cot\theta - \cot\Theta\right),\end{aligned} \tag{3.51}$$

and

$$\begin{aligned}\frac{1}{r}\frac{\partial S_2^{\,2}}{\partial\Theta} = \mu\left(J^{-2\beta}\left(\frac{4\beta}{r^2}\left(\frac{\partial\Theta}{\partial\theta}\right)\left(\frac{\partial r}{\partial\Theta}\right) + \frac{2\beta}{r}\left(\frac{\partial\Theta}{\partial\theta}\right)\left(\frac{\partial R}{\partial r}\right)\frac{\partial^2 r}{\partial\Theta\partial R} + \frac{(2\beta+1)}{r}\frac{\partial^2\theta}{\partial\Theta^2}\left(\frac{\partial\Theta}{\partial\theta}\right)^2\right)\right)\\ + \mu\left(J^{-2\beta}\left(\frac{2\beta\cot\theta}{r} - \frac{2\beta\cot\Theta}{r}\frac{\partial\Theta}{\partial\theta}\right) + \frac{2}{R^2}\left(\frac{\partial\theta}{\partial\Theta}\right)\frac{\partial r}{\partial\Theta} + \frac{r}{R^2}\frac{\partial^2\theta}{\partial\Theta^2}\right),\end{aligned} \tag{3.52}$$

also

$$\frac{1}{r}\frac{\partial S_2^{\,1}}{\partial R} = \mu J^{-2\beta}\left(-\frac{4\beta}{r^2}\left(\frac{\partial\Theta}{\partial\theta}\right)\left(\frac{\partial r}{\partial\Theta}\right) - \frac{2\beta}{r}\left(\frac{\partial\Theta}{\partial\theta}\right)\left(\frac{\partial R}{\partial r}\right)^2\left(\frac{\partial r}{\partial\Theta}\right)\frac{\partial^2 r}{\partial R^2}\right)$$
$$+\mu J^{-2\beta}\left(\frac{4\beta}{rR}\left(\frac{\partial\Theta}{\partial\theta}\right)\left(\frac{\partial R}{\partial r}\right)\frac{\partial r}{\partial\Theta} + \frac{1}{r}\left(\frac{\partial\Theta}{\partial\theta}\right)\frac{\partial^2 r}{\partial R\partial\Theta}\left(\frac{\partial R}{\partial r}\right) - \frac{1}{r}\left(\frac{\partial\Theta}{\partial\theta}\right)\left(\frac{\partial R}{\partial r}\right)^2\frac{\partial r}{\partial\Theta}\left(\frac{\partial^2 r}{\partial R^2}\right)\right), \tag{3.53}$$

similarly

$$-\frac{S_2^{\,2}}{r^2}\frac{\partial r}{\partial\Theta} = \mu\left(\frac{J^{-2\beta}}{r^2}\left(\frac{\partial\Theta}{\partial\theta}\right)\frac{\partial r}{\partial\Theta} - \frac{1}{R^2}\frac{\partial\theta}{\partial\Theta}\left(\frac{\partial r}{\partial\Theta}\right)\right), \tag{3.54}$$

and

$$-\frac{S_2^{\,1}}{r^2}\left(\frac{\partial r}{\partial R}\right) = -\frac{\mu J^{-2\beta}}{r^2}\left(\frac{\partial r}{\partial\Theta}\right)\frac{\partial\Theta}{\partial\theta}, \tag{3.55}$$

where

$$\frac{2S_2^{\,1}}{Rr} = \frac{2\mu J^{-2\beta}}{Rr}\left(\frac{\partial\Theta}{\partial\theta}\right)\frac{\partial R}{\partial r}\left(\frac{\partial r}{\partial\Theta}\right), \tag{3.56}$$

and

$$\frac{S_2^{\,2}\cot\Theta}{r} = \mu\left(-\frac{J^{-2\beta}}{r}\cot\Theta\frac{\partial\Theta}{\partial\theta} + \frac{r}{R^2}\cot\Theta\frac{\partial\theta}{\partial\Theta}\right). \tag{3.57}$$

Other angular terms lead to

$$\frac{-S_3^{\,3}\cot\theta}{r} = \mu\left(\frac{J^{-2\beta}\cot\theta}{r} - \frac{r\sin\theta\cos\theta}{R^2\sin^2\Theta}\right), \tag{3.58}$$

and

$$S_1^{\,2}\left(\frac{\partial\theta}{\partial\Theta}\right) = \frac{\mu}{R^2}\left(\frac{\partial r}{\partial\Theta}\right)\frac{\partial\theta}{\partial\Theta}. \tag{3.59}$$

Combining equations (3.51) to (3.59) and substituting into equation (3.37) gives

$$J^{-2\beta}\left(\frac{(2\beta+1)}{r}\frac{\partial\Theta}{\partial\theta}\left(\frac{\partial R}{\partial r}\right)\frac{\partial^2 r}{\partial\Theta\partial R}+\frac{(2\beta+1)}{r}\left(\frac{\partial\Theta}{\partial\theta}\right)^2\frac{\partial^2\theta}{\partial\Theta^2}+\frac{(2\beta+1)\cot\theta}{r}\right)$$
$$+J^{-2\beta}\left(-\frac{(2\beta+1)\cot\Theta}{r}\left(\frac{\partial\Theta}{\partial\theta}\right)-\frac{(2\beta+1)}{r}\left(\frac{\partial\Theta}{\partial\theta}\right)\left(\frac{\partial R}{\partial r}\right)^2\left(\frac{\partial r}{\partial\Theta}\right)\frac{\partial^2 r}{\partial R^2}\right)$$
$$+J^{-2\beta}\left(\frac{2(2\beta+1)}{rR}\left(\frac{\partial\Theta}{\partial\theta}\right)\frac{\partial R}{\partial r}\left(\frac{\partial r}{\partial\Theta}\right)\right)+\frac{2}{R^2}\left(\frac{\partial\theta}{\partial\Theta}\right)\frac{\partial r}{\partial\Theta}+\frac{r}{R^2}\frac{\partial^2\theta}{\partial\Theta^2}$$
$$+\frac{r}{R^2}\left(\frac{\partial\theta}{\partial\Theta}\right)\cot\Theta-\frac{r\sin\theta\cos\theta}{R^2\sin^2\Theta}=0. \quad (3.60)$$

Both the radial and angular equations given by (3.50) and (3.60) can be rearranged and expressed in terms of their respective second partial derivatives with respect to Θ resulting in

$$\frac{\partial^2 r}{\partial\Theta^2}=-R^2\frac{\partial^2 r}{\partial R^2}\left(1+(2\beta+1)J^{-2\beta}\left(\frac{\partial R}{\partial r}\right)^2\right)$$
$$+J^{-2\beta}\left(-\frac{4\beta R^2}{r}+4\beta R\left(\frac{\partial R}{\partial r}\right)+2R\left(\frac{\partial R}{\partial r}\right)-\frac{2R^2}{r}\right)$$
$$-2R\left(\frac{\partial r}{\partial R}\right)+r\left(\frac{\partial\theta}{\partial\Theta}\right)^2+\frac{r\sin^2\theta}{\sin^2\Theta}-\cot\Theta\frac{\partial r}{\partial\Theta}, \quad (3.61)$$

and

$$\left(\frac{(2\beta+1)}{r}J^{-2\beta}\left(\frac{\partial\Theta}{\partial\theta}\right)^2+\frac{r}{R^2}\right)\frac{\partial^2\theta}{\partial\Theta^2}$$
$$=J^{-2\beta}\left(-\frac{(2\beta+1)}{r}\left(\frac{\partial\Theta}{\partial\theta}\right)\left(\frac{\partial R}{\partial r}\right)\frac{\partial^2 r}{\partial\Theta\partial R}-\frac{(2\beta+1)\cot\theta}{r}+\frac{(2\beta+1)\cot\Theta}{r}\left(\frac{\partial\Theta}{\partial\theta}\right)\right)$$
$$+J^{-2\beta}\left(\frac{(2\beta+1)}{r}\left(\frac{\partial\Theta}{\partial\theta}\right)\left(\frac{\partial R}{\partial r}\right)^2\left(\frac{\partial r}{\partial\Theta}\right)\frac{\partial^2 r}{\partial R^2}-\frac{2(2\beta+1)}{rR}\left(\frac{\partial\Theta}{\partial\theta}\right)\left(\frac{\partial R}{\partial r}\right)\frac{\partial r}{\partial\Theta}\right)$$
$$-\frac{2}{R^2}\left(\frac{\partial\theta}{\partial\Theta}\right)\frac{\partial r}{\partial\Theta}-\frac{r\cot\Theta}{R^2}\left(\frac{\partial\theta}{\partial\Theta}\right)+\frac{r\sin\theta\cos\theta}{R^2\sin^2\Theta}. \quad (3.62)$$

The radial and angular equations are nondimensionalised using $y = r/R_I$ and $Y = R/R_I$. The equation for the quasistatic radial momentum represented by equation (3.61) gives

$$\begin{aligned}\frac{\partial^2 y}{\partial \Theta^2} = -Y^2 \frac{\partial^2 y}{\partial Y^2}\left(1 + (2\beta+1)J^{-2\beta}\left(\frac{\partial Y}{\partial y}\right)^2\right) \\ + J^{-2\beta}\left(-\frac{4\beta Y^2}{y} + 4\beta Y\left(\frac{\partial Y}{\partial y}\right) + 2Y\left(\frac{\partial Y}{\partial y}\right) - \frac{2Y^2}{y}\right) \\ - 2Y\left(\frac{\partial y}{\partial Y}\right) + y\left(\frac{\partial \theta}{\partial \Theta}\right)^2 + \frac{y\sin^2\theta}{\sin^2\Theta} - \cot\Theta\frac{\partial y}{\partial \Theta}, \quad (3.63)\end{aligned}$$

where the Jacobian given by equation (3.13) becomes

$$J = \frac{y^2}{Y^2}\left(\frac{\partial y}{\partial Y}\right)\left(\frac{\partial \theta}{\partial \Theta}\right)\frac{\sin\theta}{\sin\Theta}. \quad (3.64)$$

The quasistatic polar momentum equation represented by equation (3.62) reduces to

$$\begin{aligned}&\left(\frac{(2\beta+1)}{y}J^{-2\beta}\left(\frac{\partial \Theta}{\partial \theta}\right)^2 + \frac{y}{Y^2}\right)\frac{\partial^2 \theta}{\partial \Theta^2} \\ &= J^{-2\beta}\left(-\frac{(2\beta+1)}{y}\left(\frac{\partial \Theta}{\partial \theta}\right)\left(\frac{\partial Y}{\partial y}\right)\frac{\partial^2 y}{\partial \Theta \partial Y} - \frac{(2\beta+1)\cot\theta}{y} + \frac{(2\beta+1)\cot\Theta}{y}\left(\frac{\partial \Theta}{\partial \theta}\right)\right) \\ &+ J^{-2\beta}\left(\frac{(2\beta+1)}{y}\left(\frac{\partial \Theta}{\partial \theta}\right)\left(\frac{\partial Y}{\partial y}\right)^2\left(\frac{\partial y}{\partial \Theta}\right)\frac{\partial^2 y}{\partial Y^2} - \frac{2(2\beta+1)}{yY}\left(\frac{\partial \Theta}{\partial \theta}\right)\left(\frac{\partial Y}{\partial y}\right)\frac{\partial y}{\partial \Theta}\right) \\ &- \frac{2}{Y^2}\left(\frac{\partial \theta}{\partial \Theta}\right)\frac{\partial y}{\partial \Theta} - \frac{y\cot\Theta}{Y^2}\left(\frac{\partial \theta}{\partial \Theta}\right) + \frac{y\sin\theta\cos\theta}{Y^2\sin^2\Theta}, \quad (3.65)\end{aligned}$$

and the Cauchy stresses given by equations (3.39), (3.40), (3.41) and (3.42) lead to

$$\hat{\tau}_{yy} = \frac{\tau_{yy}}{\mu} = \frac{1}{J}\left(-J^{-2\beta} + \left(\frac{\partial y}{\partial Y}\right)^2 + \frac{1}{Y^2}\left(\frac{\partial y}{\partial \Theta}\right)^2\right), \quad (3.66)$$

alongside

$$\hat{\tau}_{\theta\theta} = \frac{\tau_{\theta\theta}}{\mu} = \frac{1}{J}\left(-J^{-2\beta} + \left(\frac{y}{Y}\right)^2 \left(\frac{\partial\theta}{\partial\Theta}\right)^2\right), \tag{3.67}$$

and

$$\hat{\tau}_{\phi\phi} = \frac{\tau_{\phi\phi}}{\mu} = \frac{1}{J}\left(-J^{-2\beta} + \left(\frac{y\sin\theta}{Y\sin\Theta}\right)^2\right), \tag{3.68}$$

with the off diagonal stress term given by

$$\hat{\tau}_{y\theta} = \frac{\tau_{y\theta}}{\mu} = \frac{y}{JY^2}\left(\frac{\partial\theta}{\partial\Theta}\right)\frac{\partial y}{\partial\Theta}. \tag{3.69}$$

At the opening angle Θ_{op} the polar hoop stress represented by equation (3.107) is subjected to the nondimensionalised stress $\hat{p}$ where $\hat{p} = p/\mu$. The boundary condition is then

$$\hat{\tau}_{\theta\theta}\left(\Theta_{op}\right) = \hat{p}. \tag{3.70}$$

The boundary conditions at the inner and outer radii of the shell are that the Cauchy radial stresses vanish,

$$\tau_{rr}(R_I) = \tau_{rr}(R_O) = 0. \tag{3.71}$$

3.6 Linearisation

Linearisation can be applied to both the radial and angular equations provided that the applied stress p is small compared to μ. Now consider the linearisation of the nondimensionalised radial equation (3.61) where

$$y(Y,\Theta) = Y + \hat{p}f(Y,\Theta), \tag{3.72}$$

and

$$\theta(\Theta) = \Theta + \hat{p}g(\Theta), \tag{3.73}$$

where $\hat{p} = p/\mu$ and is small in magnitude, $\hat{p}f(Y,\Theta)$ represents a small radial perturbation and $\hat{p}g(\Theta)$ denotes a small angular perturbation. Linearising the Jacobian, J, given by equation (3.64) gives

$$\begin{aligned} J &= \frac{(Y+\hat{p}f)^2}{Y^2}\left(1+\hat{p}\frac{\partial f}{\partial Y}\right)\left(1+\hat{p}\frac{dg}{d\Theta}\right)(1+\hat{p}g\cot\Theta), \\ &\approx 1 + \frac{2\hat{p}f}{Y} + \hat{p}\frac{\partial f}{\partial Y} + \hat{p}\frac{dg}{d\Theta} + \hat{p}g\cot\Theta, \end{aligned} \tag{3.74}$$

and hence

$$J^{-2\beta} \approx 1 - 2\beta\hat{p}\left(\frac{2f}{Y} + \frac{\partial f}{\partial Y} + \frac{dg}{d\Theta} + g\cot\Theta\right). \tag{3.75}$$

Terms in equation (3.63) become

$$\begin{aligned} 1 + (2\beta+1)\,J^{-2\beta}\left(\frac{\partial Y}{\partial y}\right)^2 &\approx 1 + (2\beta+1)\left(1 - 2\beta\hat{p}\left(\frac{2f}{Y} + \frac{\partial f}{\partial Y} + \frac{dg}{d\Theta} + g\cot\Theta\right)\right)\left(1 - 2\hat{p}\frac{\partial f}{\partial Y}\right), \\ &\approx 2(\beta+1) - 2(2\beta+1)\hat{p}\left(\frac{2\beta f}{Y} + (\beta+1)\frac{\partial f}{\partial Y} + \beta\frac{dg}{d\Theta} + \beta g\cot\Theta\right), \end{aligned} \tag{3.76}$$

and

$$-Y^2\frac{\partial^2 y}{\partial Y^2}\left(1 + (2\beta+1)J^{-2\beta}\left(\frac{\partial Y}{\partial y}\right)^2\right) \approx -2Y^2(1+\beta)\hat{p}\frac{\partial^2 f}{\partial Y^2}. \tag{3.77}$$

To linearise the following term in equation (3.63)

$$J^{-2\beta}\left(-\frac{4\beta Y^2}{y} + 4\beta Y\left(\frac{\partial Y}{\partial y}\right) + 2Y\left(\frac{\partial Y}{\partial y}\right) - \frac{2Y^2}{y}\right), \tag{3.78}$$

we use the linearised terms

$$\frac{-4\beta Y^2}{y} = \frac{-4\beta Y^2}{(Y+\hat{p}f)} \approx -4\beta Y + 4\hat{p}\beta f, \tag{3.79}$$

and

$$4\beta Y\left(\frac{\partial Y}{\partial y}\right) = \frac{4\beta Y}{\left(1+\hat{p}\frac{\partial f}{\partial Y}\right)} \approx 4\beta Y - 4\beta\hat{p}Y\left(\frac{\partial f}{\partial Y}\right), \tag{3.80}$$

also

$$2Y\left(\frac{\partial Y}{\partial y}\right) = \frac{2Y}{\left(1+\hat{p}\frac{\partial f}{\partial Y}\right)} \approx 2Y - 2\hat{p}Y\frac{\partial f}{\partial Y}, \tag{3.81}$$

similarly

$$\frac{-2Y^2}{y} = \frac{-2Y^2}{(Y+\hat{p}f)} \approx -2Y + 2\hat{p}f, \tag{3.82}$$

to give

$$J^{-2\beta}\left(-\frac{4\beta Y^2}{y} + 4\beta Y\left(\frac{\partial Y}{\partial y}\right) + 2Y\left(\frac{\partial Y}{\partial y}\right) - \frac{2Y^2}{y}\right) \approx 2\left(2\beta+1\right)\hat{p}\left(f - Y\left(\frac{\partial f}{\partial Y}\right)\right). \tag{3.83}$$

Linearising the following terms from equation (3.61) results in

$$-2Y\left(\frac{\partial y}{\partial Y}\right) \approx -2Y - 2\hat{p}Y\left(\frac{\partial f}{\partial Y}\right), \tag{3.84}$$

also

$$y\left(\frac{\partial\theta}{\partial\Theta}\right)^2 = (Y+\hat{p}f)\left(1+\hat{p}\frac{dg}{d\Theta}\right)^2 \approx Y + 2\hat{p}Y\left(\frac{dg}{d\Theta}\right) + \hat{p}f, \tag{3.85}$$

similarly

$$\frac{y\sin^2\theta}{\sin^2\Theta} = (Y+\hat{p}f)\left(1+\hat{p}g\cot\Theta\right)^2 \approx Y + 2\hat{p}Yg\cot\Theta + \hat{p}f, \tag{3.86}$$

and

$$-\cot\Theta\left(\frac{\partial y}{\partial\Theta}\right)\approx-\cot\Theta\left(\hat{p}\frac{\partial f}{\partial\Theta}\right). \tag{3.87}$$

Collecting the expressions (3.77) and (3.83) to (3.87) reduces equation (3.63) on rearrangement to

$$-(4\beta+4)\,Y\frac{\partial f}{\partial Y}+(4\beta+4)\,f+2Yg\cot\Theta+2Y\frac{dg}{d\Theta} \\ -\cot\Theta\frac{\partial f}{\partial\Theta}-\frac{\partial^2 f}{\partial\Theta^2}-2Y^2\,(\beta+1)\,\frac{\partial^2 f}{\partial Y^2}=0, \tag{3.88}$$

which can be further rearranged and results in

$$(4\beta+4)\,f-(4\beta+4)\,Y\frac{\partial f}{\partial Y}-\cot\Theta\frac{\partial f}{\partial\Theta}-\frac{\partial^2 f}{\partial\Theta^2}-2Y^2\,(\beta+1)\,\frac{\partial^2 f}{\partial Y^2} \\ =-2Yg\cot\Theta-2Y\frac{dg}{d\Theta}. \tag{3.89}$$

Linearising the angular equation given by equation (3.65) requires the following expressions

$$J^{-2\beta}\left(\frac{-(2\beta+1)}{y}\right)\left(\frac{\partial\Theta}{\partial\theta}\right)\left(\frac{\partial Y}{\partial y}\right)\frac{\partial^2 y}{\partial\Theta\partial Y}\approx\frac{-(2\beta+1)}{Y}\hat{p}\frac{\partial^2 f}{\partial Y\partial\Theta}, \tag{3.90}$$

simplifying $\cot\theta$ yields

$$\cot\theta=\frac{\cos\left(\Theta+\hat{p}g\right)}{\sin\left(\Theta+\hat{p}g\right)}, \\ \approx\cot\Theta-\hat{p}g\csc^2\Theta, \tag{3.91}$$

leading to

$$\frac{-(2\beta+1)\cot\theta}{y} = \frac{-(2\beta+1)(\cot\Theta - \hat{p}g\csc^2\Theta)}{(Y+\hat{p}f)},$$
$$\approx \frac{-(2\beta+1)}{Y}\left(\cot\Theta - \hat{p}g\csc^2\Theta - \hat{p}\frac{f}{Y}\cot\Theta\right), \tag{3.92}$$

which results in

$$-J^{-2\beta}\frac{(2\beta+1)\cot\theta}{y} \approx \frac{-(2\beta+1)\cot\Theta}{Y} + \frac{(2\beta+1)(4\beta+1)\hat{p}f\cot\Theta}{Y^2}$$
$$+\frac{(2\beta+1)\hat{p}g}{Y}(\beta+1+\beta\cos 2\Theta)\csc^2\Theta$$
$$+\frac{2\beta(2\beta+1)}{Y}\hat{p}\left(\cot\Theta\frac{dg}{d\Theta}+\cot\Theta\frac{\partial f}{\partial Y}\right). \tag{3.93}$$

Consider

$$\frac{(2\beta+1)\cot\Theta}{y}\left(\frac{\partial\Theta}{\partial\theta}\right) \approx \frac{(2\beta+1)\cot\Theta}{Y}\left(1-\hat{p}\frac{f}{Y}-\hat{p}\frac{dg}{d\Theta}\right), \tag{3.94}$$

and combining expression (3.94) with $J^{-2\beta}$ gives

$$J^{-2\beta}\frac{(2\beta+1)\cot\Theta}{y}\left(\frac{\partial\Theta}{\partial\theta}\right) \approx \frac{(2\beta+1)\cot\Theta}{Y}$$
$$-\hat{p}\frac{(2\beta+1)\cot\Theta}{Y^2}\left((1+4\beta)f+Y\left((2\beta+1)\frac{dg}{d\Theta}+2\beta g\cot\Theta+2\beta\frac{\partial f}{\partial Y}\right)\right). \tag{3.95}$$

On the third line of equation (3.65) the following term can be approximated as follows

$$\frac{(2\beta+1)}{y}\left(\frac{\partial\Theta}{\partial\theta}\right)\left(\frac{\partial Y}{\partial y}\right)^2\left(\frac{\partial y}{\partial\Theta}\right)\frac{\partial^2 y}{\partial Y^2} \approx \frac{(2\beta+1)}{(Y+\hat{p}f)}\left(1-\hat{p}\frac{dg}{d\Theta}\right)\left(1-2\hat{p}\frac{\partial f}{\partial Y}\right)\left(\hat{p}\frac{\partial f}{\partial\Theta}\right)\hat{p}\frac{\partial^2 f}{\partial Y^2}\approx 0. \tag{3.96}$$

Similarly, the next term

$$\frac{-2(2\beta+1)}{yY}\left(\frac{\partial\Theta}{\partial\theta}\right)\left(\frac{\partial Y}{\partial y}\right)\frac{\partial y}{\partial\Theta}\approx\frac{-2(2\beta+1)}{Y^2}\hat{p}\left(\frac{\partial f}{\partial\Theta}\right), \tag{3.97}$$

which on combining with $J^{-2\beta}$ results in

$$J^{-2\beta}\left(\frac{-2(2\beta+1)}{yY}\left(\frac{\partial\Theta}{\partial\theta}\right)\left(\frac{\partial Y}{\partial y}\right)\frac{\partial y}{\partial\Theta}\right)\approx\frac{-2(2\beta+1)}{Y^2}\hat{p}\left(\frac{\partial f}{\partial\Theta}\right). \tag{3.98}$$

Terms on the fourth line of equation (3.65) become

$$\frac{-2}{Y^2}\left(\frac{\partial\theta}{\partial\Theta}\right)\left(\frac{\partial y}{\partial\Theta}\right)\approx\frac{-2\hat{p}}{Y^2}\left(\frac{\partial f}{\partial\Theta}\right), \tag{3.99}$$

and

$$\frac{-y\cot\Theta}{Y^2}\left(\frac{\partial\theta}{\partial\Theta}\right)\approx\frac{-\cot\Theta}{Y}-\frac{\hat{p}\cot\Theta}{Y}\left(\frac{dg}{d\Theta}\right)-\frac{\hat{p}f\cot\Theta}{Y^2}. \tag{3.100}$$

Now since $\sin\theta\approx\sin\Theta+\hat{p}g\cos\Theta$ similarly, $\cos\theta\approx\cos\Theta-\hat{p}g\sin\Theta$, resulting in

$$\sin\theta\cos\theta\approx\sin\Theta\cos\Theta+\hat{p}g\left(1-2\sin^2\Theta\right), \tag{3.101}$$

then

$$\frac{y\sin\theta\cos\theta}{Y^2\sin^2\Theta}\approx\frac{1}{Y}\left(\left(1+\frac{\hat{p}f}{Y}\right)\cot\Theta+\hat{p}g(\cot^2\Theta-1)\right), \tag{3.102}$$

also, on the first line of equation (3.65)

$$\begin{aligned}&\frac{(2\beta+1)}{y}J^{-2\beta}\left(\frac{\partial\Theta}{\partial\theta}\right)^2+\frac{y}{Y^2},\\&\approx\frac{(2\beta+1)}{Y}\left(1-\frac{\hat{p}f}{Y}-2\hat{p}\frac{dg}{d\Theta}-2\beta\hat{p}\left(\frac{2f}{Y}+\frac{\partial f}{\partial Y}+\frac{dg}{d\Theta}+g\cot\Theta\right)\right)+\frac{1}{Y}\left(1+\frac{\hat{p}f}{Y}\right),\end{aligned} \tag{3.103}$$

which on combining equation (3.103) with $\partial^2\theta/\partial\Theta^2$ leads to

$$\frac{(2\beta+1)\hat{p}}{Y}\left(\frac{d^2g}{d\Theta^2}\right)+\frac{\hat{p}}{Y}\left(\frac{d^2g}{d\Theta^2}\right)\approx\frac{2(\beta+1)\hat{p}}{Y}\left(\frac{d^2g}{d\Theta^2}\right). \tag{3.104}$$

Combining and substituting equations (3.90), (3.92), (3.93), (3.95) to (3.100) and (3.102) and (3.104) into the angular equation (3.65) results in

$$\begin{aligned}-Y\left(1+2\beta+\cos^2\Theta\right)g\csc^2\Theta+2Y(1+\beta)\cot\Theta\left(\frac{dg}{d\Theta}\right)\\+2Y(1+\beta)\frac{d^2g}{d\Theta^2}+4(1+\beta)\left(\frac{\partial f}{\partial\Theta}\right)\\+Y(1+2\beta)\frac{\partial^2 f}{\partial Y\partial\Theta}=0.\end{aligned} \tag{3.105}$$

The Cauchy radial, polar and azimuthal stresses given by equations (3.66), (3.67) and (3.68) respectively are linearised using equations (3.72) and (3.73) which results in

$$\hat{\tau}_{yy}\approx\hat{p}\left(\frac{4\beta f}{Y}+(2\beta+2)\frac{\partial f}{\partial Y}+2\beta\frac{dg}{d\Theta}+2\beta g\cot\Theta\right), \tag{3.106}$$

alongside

$$\hat{\tau}_{\theta\theta}\approx\hat{p}\left((4\beta+2)\frac{f}{Y}+2\beta\left(\frac{\partial f}{\partial Y}\right)+(2\beta+2)\left(\frac{dg}{d\Theta}\right)+2\beta g\cot\Theta\right), \tag{3.107}$$

and

$$\hat{\tau}_{\phi\phi}\approx\hat{p}\left((4\beta+2)\frac{f}{Y}+2\beta\left(\frac{\partial f}{\partial Y}\right)+2\beta\left(\frac{dg}{d\Theta}\right)+(2\beta+2)g\cot\Theta\right), \tag{3.108}$$

respectively. Equations (3.106) and (3.107) will be used to evaluate the boundary conditions for the deformation of the open shell (forward picture).

The boundary conditions at the nondimensionalised inner and outer radii of the shell (which are represented by 1 and Y_O respectively) are obtained using the nondimensionalised Cauchy radial stresses, $\hat{\tau}_{yy}(1) = 0$ and $\hat{\tau}_{yy}(Y_O) = 0$. Using equation (3.106) and setting $\hat{\tau}_{yy} = 0$ at both the nondimensionalised inner and outer radii $Y_{1/O}$ leads to

$$\frac{4\beta f(Y_{1/O}, \Theta)}{Y_{1/O}} + (2\beta + 2)\left.\frac{\partial f}{\partial Y}\right|_{(Y_{1/O},\Theta)} + 2\beta\frac{dg}{d\Theta} + 2\beta g\cot\Theta = 0. \tag{3.109}$$

The angular boundary condition at the rim, Θ_{op}, is given by equation (3.70). This simplifies using equation (3.107) to give

$$\frac{(4\beta + 2)f}{Y} + 2\beta\frac{\partial f}{\partial Y} + (2\beta + 2)\left.\frac{dg}{d\Theta}\right|_{\Theta=\Theta_{op}} + 2\beta g\cot\Theta_{op} = 1. \tag{3.110}$$

To solve the coupled linearised radial and angular PDEs for the quasistatic phase denoted by equations (3.89) and (3.105) respectively, we have to use the linearised boundary conditions given by equations (3.109) and (3.110). Future work will focus on solving both the radial and angular equations numerically using a relaxation scheme.

3.7 Conclusion

Chapter 3 discussed the deformation of an open shelled microbubble. The opening angle approach was used with the original stress free configuration represented by an open, deformed and incomplete shelled microbubble. This can be thought of as a spherical shelled microbubble with a spherical cap removed. A radial and angular deformation was applied via a polar hoop stress and an asymptotic expansion was used to simplify the complex radial and angular equations. This model was

developed in order to study the rupture of a shelled microbubble. The opening angle approach attempted to model the change in geometry of a deformed shell. Future work will focus on modelling numerically the linearised quasistatic phase using a numerical relaxation scheme. A similar approach could be used to solve the collapsing, perturbed shell. Solving both the quasistatic stage and the collapse phase of the open shelled microbubble would represent a formidable challenge due to the coupled nature of the angular and radial PDE equations as well as the boundary conditions for both the radial and hoop (angular) stresses.

Literature pertaining to the modelling of UCAs adopts a Rayleigh-Plesset approach [36,39,44,45,50–52], modelling the shell as linearly elastic and viscoelastic in nature. Certain proteins are smectic A liquid crystals implying that some thin protein shelled UCA microbubbles could possibly be modelled using continuum liquid crystal theory. Understanding how the material parameters influence the natural frequency and relaxation time of the shelled liquid-crystal microbubbles is of considerable importance. To this end, Chapter 4 develops a Rayleigh-Plesset model for such a liquid-crystal shelled microbubble.

Chapter 4

Liquid-crystal shelled microbubble

4.1 Derivation of the Rayleigh-Plesset equation

One particular type of shelled microbubble displays the physical behaviour that is characteristic of a liquid crystal and such shelled microbubbles could have potential advantages as drug carrying vehicles [39]. This chapter uses the Leslie-Ericksen theory for liquid crystals to build up a model for the dynamics of such a shelled microbubble. This is the first study that has used liquid crystal theory to model UCAs.

The research literature pertaining to the mathematical modelling of ultrasound contrast agents involves the use of some modified version of the Rayleigh-Plesset equation [36–39,42–45,50–52]. Despite the extensive use of this well known equation and the numerous modifications made to it, most of the published literature fails to derive the Rayleigh-Plesset equation using arguments based on the mo-

mentum balance law [44,50–52]. The derivation of the Rayleigh-Plesset equation by applying the momentum balance law is included in Appendix A on the grounds of completeness. This derivation will be used in conjunction with liquid crystal theory to develop a Rayleigh-Plesset model for a shelled microbubble that exhibits mesophase type behaviour.

4.2 Calculating the viscous stress of a liquid-crystal shell

This section focusses on deriving an expression for the viscous stress of an incompressible liquid-crystal shell of known inner and outer radii. It is assumed that the shell's composition is a liquid crystal that can be described dynamically using the nematic theory developed by Leslie and Ericksen ([65], p133-159) where five Leslie viscosities [79] are required to determine the stress in the shell. Certain ultrasound contrast agent shells exhibit both solid and fluid like characteristics and, therefore, can be described as a mesophase [39]. Some proteins [67] exhibit the characteristic behaviour of a smectic A liquid-crystal where the molecules are arranged in layers and exhibit greater long range positional ordering than a nematic liquid-crystal ([65], p6). Smectic A liquid-crystals are slightly more viscous than nematic liquid-crystals due to the layer interactions within the smectic [66]. However, the model in this chapter will use nematic theory as an approximation to smectic A [66]. Continuum modelling of liquid-crystal theory assumes that the molecules are rod like in nature and are described by a unit vector n which is called the director. The molecules are arranged in layers with the director aligning perpendicular to the layers and parallel to the layer normal ([65],p6). We shall assume spherical symmetry of the liquid-crystalline shell with the director pointing radially out-

ward everywhere and the smectic layers consisting of concentric spherical shells. The director describes the local direction of the average molecular alignment and is a unit vector (so $n = e_i x_i/r$) ([65],p6). The viscous stress τ_{ij} for a nematic liquid-crystal is given by

$$\tau_{ij} = \alpha_1 n_k A_{kp} n_p n_i n_j + \alpha_2 N_i n_j + \alpha_3 n_i N_j + \alpha_4 A_{ij} + \alpha_5 n_j A_{ik} n_k + \alpha_6 n_i A_{jk} n_k, \quad (4.1)$$

where $\alpha_1, \alpha_2, ..., \alpha_6$ are the Leslie viscosities, A_{ij} is the rate of strain tensor and N_i is the co-rotational time flux of the director n ([65], p151). The co-rotational time flux is a measure of the rotation of the director, n, relative to the material. These terms are explicitly defined as $n_i = x_i/r$, $A_{ik} = (v_{i,k} + v_{k,i})/2$ where $v_{i,j} = \partial v_i/\partial x_j$, $N_i = \dot{n}_i - W_{ij} n_j$ where the superposed dot signifies the material time derivative $\dot{n}_i = \partial n_i/\partial t + v_j \partial n_i/\partial x_j$ and $W_{ij} = (v_{i,j} - v_{j,i})/2$ is the vorticity tensor. For the spherically symmetric case we have a velocity profile given by $\mathbf{v} = v e_r = v\hat{r}$ which is rewritten as

$$v_i = \frac{v x_i}{r}. \quad (4.2)$$

Hence

$$v_{i,k} = \frac{\partial}{\partial x_k}\left(\frac{x_i v}{r}\right) = \frac{v\delta_{ik}}{r} + x_i \frac{\partial}{\partial x_k}\left(\frac{v}{r}\right) = \frac{v\delta_{ik}}{r} + x_i \frac{\partial}{\partial r}\left(\frac{v}{r}\right)\frac{\partial r}{\partial x_k}.$$

Since $r^2 = x_k x_k$,

$$2r\frac{\partial r}{\partial x_k} = 2x_k,$$

and so

$$\frac{\partial r}{\partial x_k} = \frac{x_k}{r}. \quad (4.3)$$

Equation (4.2) can then be written

$$v_{i,k} = \frac{v\delta_{ik}}{r} + \frac{x_i x_k}{r}\frac{\partial}{\partial r}\left(\frac{v}{r}\right), \tag{4.4}$$

and since $\delta_{kp} = \delta_{pk}$

$$A_{kp} = \frac{v\delta_{kp}}{r} + \frac{x_k x_p}{r}\frac{\partial}{\partial r}\left(\frac{v}{r}\right). \tag{4.5}$$

Substituting equations (4.4) and (4.5) into the first term on the right hand side of equation (4.1) gives

$$\frac{\alpha_1 x_i x_j v}{r^3} + \frac{\alpha_1 x_i x_j}{r}\frac{\partial}{\partial r}\left(\frac{v}{r}\right). \tag{4.6}$$

Calculating the second term on the right hand side of equation (4.1) using $N_i = \dot{n}_i - W_{ij}n_j$ requires an expression for W_{ij}. From equation (4.4)

$$W_{i,j} = \frac{1}{2}\left(v_{i,j} - v_{j,i}\right) = 0. \tag{4.7}$$

Using this to calculate N_i leads to

$$\begin{aligned}
N_i = \dot{n}_i &= \frac{\partial n_i}{\partial t} + v_k\frac{\partial n_i}{\partial x_k}, \\
&= \frac{\partial}{\partial t}\left(\frac{x_i}{r}\right) + v_k\frac{\partial}{\partial x_k}\left(\frac{x_i}{r}\right), \\
&= 0 + v_k\left(\frac{\delta_{ik}}{r} + x_i\frac{\partial}{\partial x_k}\left(\frac{1}{r}\right)\right), \\
&= v_k\left(\frac{\delta_{ik}}{r} - \frac{x_i x_k}{r^3}\right), \\
&= \frac{v_i}{r} - \frac{v_k x_i x_k}{r^3}, \\
&= \frac{v x_i}{r^2} - \frac{v x_k x_i x_k}{r^4}, \\
&= \frac{v x_i}{r^2} - \frac{v x_i}{r^2} = 0.
\end{aligned} \tag{4.8}$$

Therefore the second term on the right hand side of equation (4.1) is

$$\alpha_2 N_i n_j = 0.$$

Similarly, the next term in equation (4.1) is

$$\alpha_3 n_i N_j = 0. \tag{4.9}$$

Continuing in this way for the next term in equation (4.1) we use equation (4.4) to give

$$\begin{aligned}
\alpha_4 A_{ij} &= \frac{\alpha_4}{2}\left(v_{i,j} + v_{j,i}\right), &(4.10)\\
&= \frac{\alpha_4}{2}\left(\frac{v\delta_{ij}}{r} + \frac{x_i x_j}{r}\frac{\partial}{\partial r}\left(\frac{v}{r}\right) + \frac{v\delta_{ji}}{r} + \frac{x_j x_i}{r}\frac{\partial}{\partial r}\left(\frac{v}{r}\right)\right),\\
&= \alpha_4\left(\frac{v\delta_{ij}}{r} + \frac{x_i x_j}{r}\frac{\partial}{\partial r}\left(\frac{v}{r}\right)\right),\\
&= \frac{\alpha_4 v\delta_{ij}}{r} + \frac{\alpha_4 x_i x_j}{r}\frac{\partial}{\partial r}\left(\frac{v}{r}\right). &(4.11)
\end{aligned}$$

For the next term in equation (4.1) we use equation (4.5) to give

$$\begin{aligned}
\alpha_5 n_j A_{ik} n_k &= \alpha_5\left(\frac{x_j}{r}\right)\left(\frac{v\delta_{ik}}{r} + \frac{x_i x_k}{r}\frac{\partial}{\partial r}\left(\frac{v}{r}\right)\right)\frac{x_k}{r},\\
&= \frac{\alpha_5 x_j x_k}{r^2}\left(\frac{v\delta_{ik}}{r} + \frac{x_i x_k}{r}\frac{\partial}{\partial r}\left(\frac{v}{r}\right)\right),\\
&= \frac{\alpha_5 v x_j x_i}{r^3} + \frac{\alpha_5 x_j x_i}{r}\frac{\partial}{\partial r}\left(\frac{v}{r}\right), &(4.12)
\end{aligned}$$

and finally the last term in equation (4.1) is

$$\alpha_6 n_i A_{jk} n_k = \frac{\alpha_6 x_i x_j v}{r^3} + \frac{\alpha_6 x_i x_j}{r}\frac{\partial}{\partial r}\left(\frac{v}{r}\right). \tag{4.13}$$

4.3 Determining the Leslie viscosity terms in spherical polar coordinates

In this section we will calculate an expression for the right hand side of the momentum equation (A.13). This will be achieved by taking the divergence of the viscous stress given by equation (4.1) and then integrating this in the radial direction between the inner and outer radii of the shelled microsphere. The microbubble's shell is assumed to be incompressible and consists of a thin liquid-crystal shell with a radially directed flow. Since the shell is incompressible its volume, V, and density will be time independent. For a shelled microbubble with inner and outer radii given by R_1 and R_2 respectively, the following relationship holds

$$\frac{dV}{dt} = \frac{d}{dt}\left(\frac{4}{3}\pi\left(R_2^3 - R_1^3\right)\right) = 0.$$

This results in $R_2^2\dot{R}_2 - R_1^2\dot{R}_1 = 0$ from which we can deduce that

$$R_1^2\dot{R}_1 = R_2^2\dot{R}_2. \tag{4.14}$$

Equation (A.3) can be rewritten in terms of the inner radius of the shelled microbubble R_1 as

$$\frac{v}{r} = \frac{R_1^2\dot{R}_1}{r^3}. \tag{4.15}$$

Hence

$$\frac{\partial}{\partial r}\left(\frac{v}{r}\right) = \frac{\partial}{\partial r}\left(\frac{R_1^2\dot{R}_1}{r^3}\right) = \frac{-3R_1^2\dot{R}_1}{r^4}. \tag{4.16}$$

So let us calculate the contributions to the right hand side of equation (A.13) by systematically working through each of the Leslie viscosity terms. The Leslie viscosity contribution due to α_1 given by equation (4.6) on substituting in equations (4.15) and (4.16), becomes

$$\begin{aligned}\frac{\alpha_1 v x_i x_j}{r^3} + \frac{\alpha_1 x_i x_j}{r}\frac{\partial}{\partial r}\left(\frac{v}{r}\right) &= \alpha_1\left(\frac{R_1^2\dot{R}_1}{r^2}\right)\frac{x_i x_j}{r^3} + \frac{\alpha_1 x_i x_j}{r}\left(\frac{-3R_1^2\dot{R}_1}{r^4}\right), \\ &= \frac{\alpha_1 x_i x_j}{r^5}\left(R_1^2\dot{R}_1\right) - \frac{3\alpha_1 x_i x_j}{r^5}\left(R_1^2\dot{R}_1\right), \\ &= \frac{-2\alpha_1 x_i x_j R_1^2\dot{R}_1}{r^5}. \end{aligned} \tag{4.17}$$

Calculating the divergence of the viscous stress associated with α_1 in component form gives

$$\begin{aligned}\frac{\partial}{\partial x_i}\left(\frac{-2\alpha_1 x_i x_j R_1^2\dot{R}_1}{r^5}\right) &= -2\alpha_1 R_1^2\dot{R}_1\frac{\partial}{\partial x_i}\left(\frac{x_i x_j}{r^5}\right), \\ &= -2\alpha_1 R_1^2\dot{R}_1\left(\frac{\delta_{ii}x_j}{r^5} + \frac{x_i\delta_{ij}}{r^5} - \frac{5x_i x_j}{r^6}\left(\frac{x_i}{r}\right)\right), \\ &= -2\alpha_1 R_1^2\dot{R}_1\left(\frac{3x_j}{r^5} + \frac{x_j}{r^5} - \frac{5x_j}{r^5}\right), \\ &= \frac{2\alpha_1 R_1^2\dot{R}_1 x_j}{r^5}. \end{aligned} \tag{4.18}$$

Since the shelled microbubble moves solely in the radial direction then in spherical polar coordinates $\mathbf{r} = re_r$, with $r^2 = x_j x_j$. The jth Cartesian component of e_r is given by x_j/r. Equation (4.18) is integrated between the inner and outer radii of the shelled microbubble to give one component of the right hand side of equation

(A.13) (see Appendix)

$$\int_{R_1}^{R_2} \frac{2\alpha_1 R_1^2 \dot{R}_1}{r^4} dr = \frac{-2\alpha_1 R_1^2 \dot{R}_1}{3} \left(\frac{1}{R_2^3} - \frac{1}{R_1^3} \right), \\ = \frac{-2\alpha_1}{3} \left(\frac{R_1^2 \dot{R}_1}{R_2^3} - \frac{\dot{R}_1}{R_1} \right). \tag{4.19}$$

The stresses for the viscosities α_2 and α_3 are both zero since $N_i = 0$ and $N_j = 0$. The α_4 term is associated with a conventional Newtonian fluid, and so it will exhibit purely isotropic behaviour. Combining equations (4.11) and (4.15) results in

$$\frac{\alpha_4 v \delta_{ij}}{r} + \frac{\alpha_4 x_i x_j}{r} \frac{\partial}{\partial r} \left(\frac{v}{r} \right) = \frac{\alpha_4 R_1^2 \dot{R}_1 \delta_{ij}}{r^3} + \frac{\alpha_4 x_i x_j}{r} \frac{\partial}{\partial r} \left(\frac{R_1^2 \dot{R}_1}{r^3} \right), \\ = \frac{\alpha_4 R_1^2 \dot{R}_1 \delta_{ij}}{r^3} - \frac{3\alpha_4 x_i x_j}{r} \left(\frac{R_1^2 \dot{R}_1}{r^4} \right), \\ = \frac{\alpha_4 R_1^2 \dot{R}_1 \delta_{ij}}{r^3} - \frac{3\alpha_4 x_i x_j R_1^2 \dot{R}_1}{r^5}. \tag{4.20}$$

Calculating the divergence of the stress associated with α_4 using equation (4.20) and equation (4.3) and writing it in component form gives

$$\frac{\partial}{\partial x_i} \left(\frac{\alpha_4 R_1^2 \dot{R}_1 \delta_{ij}}{r^3} - \frac{3\alpha_4 x_i x_j R_1^2 \dot{R}_1}{r^5} \right) = \frac{-3\alpha_4 R_1^2 \dot{R}_1 x_i \delta_{ij}}{r^5} - 3\alpha_4 R_1^2 \dot{R}_1 \frac{\partial}{\partial x_i} \left(\frac{x_i x_j}{r^5} \right), \\ = \frac{-3\alpha_4 R_1^2 \dot{R}_1 x_j}{r^5} - 3\alpha_4 R_1^2 \dot{R}_1 \left(\frac{\delta_{ii} x_j}{r^5} + \frac{x_i \delta_{ij}}{r^5} - \frac{5 x_i x_i x_j}{r^7} \right), \\ = \frac{-3\alpha_4 R_1^2 \dot{R}_1 x_j}{r^5} - 3\alpha_4 R_1^2 \dot{R}_1 \left(\frac{3x_j}{r^5} + \frac{x_j}{r^5} - \frac{5x_j}{r^5} \right), \\ = 0.$$

This is consistent with Brennan ([80], p49-50).

Determining the contribution to the viscous stress from α_5 using equations (4.12) and (4.15) gives

$$\begin{aligned}\frac{\alpha_5 v x_i x_j}{r^3} + \frac{\alpha_5 x_i x_j}{r}\frac{\partial}{\partial r}\left(\frac{R_1^2\dot{R}_1}{r^3}\right) &= \frac{\alpha_5 x_i x_j R_1^2\dot{R}_1}{r^5} + \frac{\alpha_5 x_i x_j}{r}\frac{\partial}{\partial r}\left(\frac{R_1^2\dot{R}_1}{r^3}\right), \\ &= \frac{\alpha_5 x_i x_j R_1^2\dot{R}_1}{r^5} - \frac{3\alpha_5 x_i x_j R_1^2\dot{R}_1}{r^5}, \\ &= \frac{-2\alpha_5 R_1^2\dot{R}_1 x_i x_j}{r^5}. \end{aligned} \tag{4.21}$$

Evaluating the divergence of the stress contribution associated with α_5 results in

$$\begin{aligned}\frac{\partial}{\partial x_i}\left(\frac{-2\alpha_5 R_1^2\dot{R}_1 x_i x_j}{r^5}\right) &= -2\alpha_5 R_1^2\dot{R}_1\frac{\partial}{\partial x_i}\left(\frac{x_i x_j}{r^5}\right), \\ &= -2\alpha_5 R_1^2\dot{R}_1\left(\frac{\delta_{ii}x_j}{r^5} + \frac{x_i\delta_{ij}}{r^5} - \frac{5x_i x_i x_j}{r^7}\right), \\ &= -2\alpha_5 R_1^2\dot{R}_1\left(\frac{3x_j}{r^5} + \frac{x_j}{r^5} - \frac{5x_j}{r^5}\right) \\ &= \frac{2\alpha_5 R_1^2\dot{R}_1 x_j}{r^5}. \end{aligned} \tag{4.22}$$

Integrating this expression to give another term in the right hand side of equation (A.13) where $r^2 = x_j x_j$ and the jth Cartesian component of e_r is given by x_j/r leads to

$$\begin{aligned}\int_{R_1}^{R_2}\frac{2\alpha_5 R_1^2\dot{R}_1}{r^4}dr &= \frac{-2\alpha_5 R_1^2\dot{R}_1}{3}\left(\frac{1}{R_2^3} - \frac{1}{R_1^3}\right), \\ &= -\frac{2\alpha_5}{3}\left(\frac{R_1^2\dot{R}_1}{R_2^3} - \frac{\dot{R}_1}{R_1}\right). \end{aligned} \tag{4.23}$$

Determining the contribution to the viscous stress from α_6 using equation (4.13) follows a similar derivation to give

$$\int_{R_1}^{R_2} \frac{2\alpha_6 R_1^2 \dot{R}_1}{r^4} dr = \frac{-2\alpha_6}{3} \left(\frac{R_1^2 \dot{R}_1}{R_2^3} - \frac{\dot{R}_1}{R_1} \right). \tag{4.24}$$

Collecting all the contributing viscous stresses from equations (4.19), (4.23) and (4.24) results in a stress contribution on the right hand side of equation (A.13) given by

$$\int_{R_1}^{R_2} (\nabla \cdot \tau)\, dr = \frac{2}{3} (\alpha_1 + \alpha_5 + \alpha_6) \left(\frac{\dot{R}_1}{R_1} - \frac{R_1^2 \dot{R}_1}{R_2^3} \right) e_r. \tag{4.25}$$

where $\nabla \cdot \tau$ is the viscous stress. The Miesowicz viscosities are the physically measurable quantities ([81], p209-231) and can be related to the Leslie viscosities using the expressions for the Miesowicz viscosities given in ([65], p158), [82] which allows this equation to be rewritten in radial component form as

$$\int_{R_1}^{R_2} (\nabla \cdot \tau)\, dr = \frac{2}{3} (\eta_{12} + 2\eta_1 + 2\eta_2 - 4\eta_3 - \gamma_1) \left(\frac{\dot{R}_1}{R_1} - \frac{R_1^2 \dot{R}_1}{R_2^3} \right) e_r. \tag{4.26}$$

Note that γ_1 is the rotational viscosity which determines the rate of relaxation of the director whereas $\eta_1, \eta_2,$ and η_3 are related to the orientation of the director and the flow velocity of the liquid crystal.

4.4 The elastic energy density for a shelled microbubble

The liquid-crystal shell has both a viscous stress associated with the Miesowicz viscosities and a stress due to the elastic energy of the liquid crystal. This latter stress will add a further term to equation (4.1) as calculated below. The following

strain energy density function was proposed for a bilipid membrane by De Vita and Stewart [67]

$$W = \frac{1}{2}K_{1a}\left(\nabla \cdot a\right)^2 + \frac{1}{2}K_{1n}\left(\nabla \cdot n\right)^2 + \frac{1}{2}B_0|\nabla\Psi|^{-2}\left(1 - |\nabla\Psi|\right)^2 + \frac{1}{2}B_1\left(1 - (n \cdot a)^2\right) + B_2\left(\nabla \cdot n\right)\left(1 - |\nabla\Psi|^{-1}\right), \tag{4.27}$$

where K_{1a}, K_{1n}, B_0, B_1 and B_2 are material constants, a is the unit normal to the layer, Ψ defines the layer structure of a smectic A liquid crystal and $|\nabla\Psi|^{-1}$ represents the current local interlayer distance. The first term on the right hand side of equation (4.27) refers to the bending energy while the second term represents the splay energy contribution. The B_0 term represents the compression-expansion energy, B_1 is the energy associated with the coupling between n and a, and B_2 is the term associated with the coupling between the splay and compression-expansion of the layer. Note that the strain energy density represented by equation (4.27) is associated with smectic A liquid crystals rather than nematic. This strain energy density function has been chosen since it is the simplest model available requiring only a splay contribution. It is assumed that the shelled microbubble is a bilipid membrane with a typical thickness of 4nm ([65], p4). Generally $|\nabla\Psi|^{-1} \neq 1$ although for an undistorted liquid-crystal such as planar layers it is useful to define $|\nabla\Psi|^{-1}$ such that $|\nabla\Psi|^{-1} = 1$. Assuming that $|\nabla\Psi|^{-1} = 1$ implies that the energy density of the bilipid layer given by equation (4.27) reduces to

$$W = \frac{1}{2}K_{1a}\left(\nabla \cdot a\right)^2 + \frac{1}{2}K_{1n}\left(\nabla \cdot n\right)^2 + \frac{1}{2}B_1\left(1 - (n_i a_i)^2\right). \tag{4.28}$$

For an undistorted smectic A liquid-crystal $n = a$ [66]. Since $n \cdot a = n_i a_i = 1$ the energy term associated with the coupling between n and a becomes

$$\frac{1}{2} B_1 \left(1 - (n \cdot a)\right) = 0. \tag{4.29}$$

The strain energy density equation represented by equation (4.27) reduces to

$$W = \frac{1}{2} K_{1a} \left(\nabla \cdot a\right)^2 + \frac{1}{2} K_{1n} \left(\nabla \cdot n\right)^2. \tag{4.30}$$

where we assume that $K_{1a} = K_{1n} = K_1$. Assuming that $n = a$ then we can conclude that the contribution from the elastic energy density reduces to

$$W = K_1 \left(\nabla \cdot n\right)^2. \tag{4.31}$$

The stress associated with the elastic constant arising from the splay and the bending energies given by $K_1 (n_{i,i})^2$ is determined via $\left(-\partial W / \partial n_{p,j}\right) n_{p,i}$ and is represented by τ_{elastic} ([65],p151) where W is given by equation (4.31). So

$$\begin{aligned} \left(\tau_{\text{elastic}}\right)_{ij} &= -\frac{\partial W}{\partial n_{p,j}} n_{p,i}, \\ &= -2K_1 \left(n_{p,p}\right) n_{j,i}, \\ &= -2K_1 \frac{\partial}{\partial x_p} \left(\frac{x_p}{r}\right) \frac{\partial}{\partial x_i} \left(\frac{x_j}{r}\right). \end{aligned}$$

Using equation (4.3) gives

$$\begin{aligned}(\tau_{\text{elastic}})_{ij} &= -2K_1\left(\frac{\delta_{pp}}{r}-\frac{x_p x_p}{r^3}\right)\left(\frac{\delta_{ij}}{r}-\frac{x_i x_j}{r^3}\right),\\ &= -2K_1\left(\frac{3}{r}-\frac{1}{r}\right)\left(\frac{\delta_{ij}}{r}-\frac{x_i x_j}{r^3}\right),\\ &= -4K_1\left(\frac{\delta_{ij}}{r^2}-\frac{x_i x_j}{r^4}\right). \end{aligned} \tag{4.32}$$

Calculating the divergence of equation (4.32) using equation (4.3) gives (in component form)

$$\begin{aligned}\frac{\partial}{\partial x_i}(\tau_{\text{elastic}})_{ij} &= -4K_1\frac{\partial}{\partial x_i}\left(\frac{\delta_{ij}}{r^2}-\frac{x_i x_j}{r^4}\right),\\ &= -4K_1\left(\frac{-2\delta_{ij}x_i}{r^4}-\frac{\delta_{ii}x_j}{r^4}-\frac{x_i\delta_{ij}}{r^4}+\frac{4x_i^2 x_j}{r^6}\right),\\ &= -4K_1\left(\frac{-2x_j}{r^4}-\frac{3x_j}{r^4}-\frac{x_j}{r^4}+\frac{4x_j}{r^4}\right)=\frac{8K_1x_j}{r^4}. \end{aligned} \tag{4.33}$$

The integral of the divergence of the stress associated with the elastic energy density contributions due to n and a is

$$\int_{R_1}^{R_2}(\nabla\cdot\tau_{\text{elastic}})\,dr = -4K_1\left(\frac{1}{R_2^2}-\frac{1}{R_1^2}\right)e_r. \tag{4.34}$$

Combining equations (4.25) and (4.34) gives the total stress in the shell as

$$\int_{R_1}^{R_2}(\nabla\cdot\tau_S)\,dr = \frac{2}{3}(\alpha_1+\alpha_5+\alpha_6)\left(\frac{\dot{R}_1}{R_1}-\frac{\dot{R}_2}{R_2}\right)e_r + 4K_1\left(\frac{1}{R_1^2}-\frac{1}{R_2^2}\right)e_r, \tag{4.35}$$

where τ_S represents the total stress in the shell.

4.5 A Rayleigh-Plesset model for a liquid-crystal shelled microbubble

In this section we will now bring together all the different stress contributions to find a form for the momentum balance law (A.13).

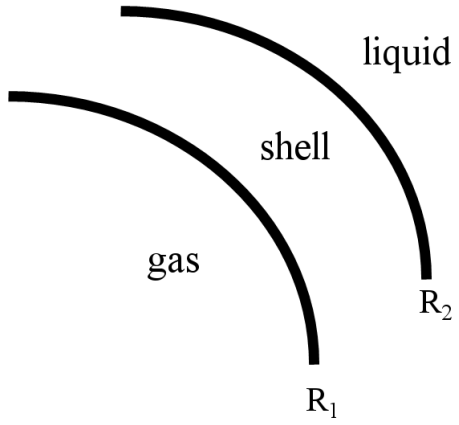

Figure 4.1: Illustration of the three media of a shelled microbubble.

Calculating the left hand side of equation (A.12) with reference to Figure 4.1 gives

$$\rho_S \left(\frac{-2R\dot{R}^2 - R^2\ddot{R}}{r} + \frac{R^4\dot{R}^2}{2r^4} \right)_{R_1}^{R_2} + \rho_L \left(\frac{-2R\dot{R}^2 - R^2\ddot{R}}{r} + \frac{R^4\dot{R}^2}{2r^4} \right)_{R_2}^{\infty}.$$

This gives a revised version of the momentum balance law (A.13) as

$$\left(R_1\ddot{R}_1 + \frac{3}{2}\dot{R}_1{}^2 + \frac{R_1^4\dot{R}_1{}^2}{2R_2^4} - \frac{2R_1\dot{R}_1{}^2}{R_2} - \frac{R_1^2\ddot{R}_1}{R_2} + \frac{\rho_L}{\rho_S}\left(\frac{2R_1\dot{R}_1{}^2}{R_2} + \frac{R_1^2\ddot{R}_1}{R_2} - \frac{R_1^4\dot{R}_1{}^2}{2R_2^4} \right) \right) e_r = \frac{1}{\rho_S}\int_{R_1}^{\infty} (\nabla\cdot\sigma)\, dr.$$

That is

$$\left(R_1\ddot{R}_1 \left(1 - \left(\frac{\rho_S - \rho_L}{\rho_S} \right) \frac{R_1}{R_2} \right) + \dot{R}_1{}^2 \left(\frac{3}{2} - \left(\frac{\rho_S - \rho_L}{\rho_S} \right) \left(\frac{4R_1R_2^3 - R_1^4}{2R_2^4} \right) \right) \right) e_r = \frac{1}{\rho_S}\int_{R_1}^{\infty} (\nabla\cdot\sigma)\, dr. \tag{4.36}$$

A pressure balance has to be applied in order to determine the right hand side of

equation (4.36). The pressure of the gas phase inside the shell and the surrounding ambient fluid pressure have to be considered as do the surface tensions and the shell and fluid viscosities we have defined in Sections 4.3 and 4.4. The divergence of the stress σ can be expressed as

$$\nabla \cdot \sigma = -\nabla P + \nabla \cdot \tau,$$

where P denotes a pressure term and τ represents the stress in the shell and the stress due to the surrounding Newtonian fluid. Rewriting the right-hand side of equation (4.36) in terms of $\nabla \cdot \sigma = -\nabla P + \nabla \cdot \tau$ and integrating over the various media leads to

$$\begin{aligned}\int_{R_1}^{\infty} (\nabla \cdot \sigma)\, dr &= \int_{R_1}^{\infty} (-\nabla P + \nabla \cdot \tau)\, dr \\ &= (P_S(R_1,t) - P_S(R_2,t) + P_L(R_2,t) - P_\infty(t))\, e_r + \int_{R_1}^{R_2} (\nabla \cdot \tau_S)\, dr + \int_{R_2}^{\infty} (\nabla \cdot \tau_L)\, dr,\end{aligned} \tag{4.37}$$

where P_S, P_L and P_∞ are the pressures in the shell, the surrounding Newtonian fluid, and at infinity, respectively. The viscous stresses in the shell and the stress associated with the surrounding fluid viscosity are denoted by τ_S and τ_L respectively. It is assumed that there is no mass exchange at the shell's interface. The boundary conditions on the momentum at the inner and outer radii of the shell's surface [50] which are obtained by balancing forces and using the Young-Laplace law for surface tension, are

$$P_S(R_1,t) = P_g \left(\frac{R_{o1}}{R_1}\right)^{3\kappa} + \tau_{S,rr}(R_1,t) - \frac{2\gamma_1}{R_1}, \tag{4.38}$$

and

$$P_S(R_2,t) = P_L(R_2,t) + \tau_{S,rr}(R_2,t) + \frac{2\gamma_2}{R_2} - \tau_L(R_2,t), \tag{4.39}$$

where $\tau_{S,rr}$ denotes the stress in the radial direction. Note that P_∞ in equation (4.37) describes the atmospheric pressure plus any external applied pressures and is given by $P_\infty = P_o + P_A \sin \omega t$ where P_A and ω represent the externally applied pressure and angular frequency respectively. Substituting equations (4.38) and (4.39) into equation (4.37) gives

$$\int_{R_1}^{\infty} (\nabla \cdot \sigma)\, dr = \left(P_g \left(\frac{R_{o1}}{R_1} \right)^{3\kappa} + \tau_{S,rr}\,(R_1, t) - \tau_{S,rr}(R_2, t) - \frac{2\gamma_1}{R_1} - \frac{2\gamma_2}{R_2} - P_o \right) e_r + \left(-P_A \sin \omega t + \tau_L(R_2, t) \right) e_r + \int_{R_1}^{R_2} (\nabla \cdot \tau_S)\, dr + \int_{R_2}^{\infty} (\nabla \cdot \tau_L)\, dr. \quad (4.40)$$

The stress due to the viscosity of the surrounding Newtonian fluid at the outer surface is denoted by $\tau_L(R_2, t)$ where ([50], [80] p50)

$$\tau_L(R_2, t) = 2\mu_L \frac{\partial v}{\partial r}\Big|_{r=R_2} = 2\mu_L \frac{\partial}{\partial r} \left(\frac{R_2^2 \dot{R}_2}{r^2} \right) \Big|_{r=R_2} = -4\mu_L \frac{\dot{R}_2}{R_2}, \quad (4.41)$$

whereas the term $\int_{R_2}^{\infty} (\nabla \cdot \tau_L)\, dr$ in equation (4.40) ([73], p354-p355) becomes

$$\int_{R_2}^{\infty} (\nabla \cdot \tau_L)\, dr = \mu_L \int_{R_2}^{\infty} \left(\frac{1}{r^2} \frac{\partial}{\partial r} \left(r^2 \frac{\partial v}{\partial r} \right) - \frac{2v}{r^2} \right) e_r dr = 0. \quad (4.42)$$

It is important to recognise that the term $\int_{R_2}^{\infty} (\nabla \cdot \tau_L)\, dr$ is zero for a velocity profile given by $v = R_2^2 \dot{R}_2 / r^2$. Substitututing equations (4.35), (4.41) and (4.42) into equation (4.40) and using equations (4.17), (4.20), (4.21) and (4.32) to calculate

$\tau_{S,rr}(R_1,t)$ and $\tau_{S,rr}(R_2,t)$ results in

$$\int_{R_1}^{\infty}(\nabla\cdot\sigma)\,dr=\left(P_g\left(\frac{R_{o1}}{R_1}\right)^{3\kappa}-\frac{4}{3}\left(\alpha_1+\alpha_5+\alpha_6\right)\left(\frac{\dot{R}_1}{R_1}-\frac{\dot{R}_2}{R_2}\right)-4K_1\left(\frac{1}{R_1^2}-\frac{1}{R_2^2}\right)\right)e_r + \left(-4\mu_L\frac{\dot{R}_2}{R_2}-P_o-P_A\sin\omega t-\frac{2\gamma_1}{R_1}-\frac{2\gamma_2}{R_2}\right)e_r, \quad (4.43)$$

where R_{o1} is the unperturbed inner radius. To simplify the notation let $\alpha=\frac{4}{3}\left(\alpha_1+\alpha_5+\alpha_6\right)$. Substituting equation (4.43) into the right-hand side of equation (4.36) leads to

$$R_1\ddot{R}_1\left(1-\left(\frac{\rho_S-\rho_L}{\rho_S}\right)\frac{R_1}{R_2}\right)+\dot{R_1}^2\left(\frac{3}{2}-\left(\frac{\rho_S-\rho_L}{\rho_S}\right)\left(\frac{4R_1R_2^3-R_1^4}{2R_2^4}\right)\right)$$
$$=\frac{1}{\rho_S}\left(\left(P_o+\frac{2\gamma_1}{R_{o1}}+\frac{2\gamma_2}{R_{o2}}+4K_1\left(\frac{1}{R_{o1}^2}-\frac{1}{R_{o2}^2}\right)\right)\left(\frac{R_{o1}}{R_1}\right)^{3\kappa}-\frac{2\gamma_1}{R_1}-\frac{2\gamma_2}{R_2}-P_o-P_A\sin\left(\omega t\right)\right)$$
$$-\frac{1}{\rho_S}\left(\alpha\left(\frac{\dot{R}_1}{R_1}-\frac{\dot{R}_2}{R_2}\right)+4K_1\left(\frac{1}{R_1^2}-\frac{1}{R_2^2}\right)+\frac{4\mu_L\dot{R}_2}{R_2}\right). \quad (4.44)$$

4.6 Linearisation and time-dependent perturbation theory

The technique of linearisation is used to determine the natural frequency and relaxation time for the shelled microbubble whose dynamic behaviour is described by equation (4.44). The time-dependent perturbations for the inner and outer radii are

$$R_1=R_{o1}\left(1+x\left(t\right)\right), \quad (4.45)$$

and

$$R_2=R_{o2}\left(1+y\left(t\right)\right), \quad (4.46)$$

respectively, where $R_2^3 - R_1^3 = R_{o2}^3 - R_{o1}^3$, since the shell is assumed to be incompressible, and $|x|, |y| \ll 1$. Hence

$$R_2^3 - R_1^3 \approx R_{o2}^3 (1 + 3y) - R_{o1}^3 (1 + 3x),$$

which can be simplified to give

$$y = \left(\frac{R_{o1}}{R_{o2}}\right)^3 x. \tag{4.47}$$

To linearise equation (4.44) we have to assume that the externally applied forcing pressure P_A (in some appropriate sense) is of the same order of magnitude as $|x|$ and $|y|$. Consider a small parameter ϵ such that $|x| = O(\epsilon)$ and $|y| = O(\epsilon)$ where $x = \epsilon X, y = \epsilon Y$ and $P_A = \epsilon P_A^* P_o$ where X, Y and P_A^* are $O(1)$ quantities. Then linearising equation (4.44) leads to

$$\begin{aligned} &R_{o1}^2 \ddot{x} \left(1 - \left(\frac{\rho_S - \rho_L}{\rho_S}\right) \frac{R_{o1}}{R_{o2}}\right) \\ &= \frac{1}{\rho_S} \left(-3\kappa x \left(P_o + \frac{2\gamma_1}{R_{o1}} + \frac{2\gamma_2}{R_{02}} + 4K_1 \left(\frac{1}{R_{o1}^2} - \frac{1}{R_{o2}^2}\right)\right) + \frac{2\gamma_1 x}{R_{o1}} + \frac{2\gamma_2 y}{R_{o2}} - P_A \sin(\omega t)\right) \\ &\qquad - \frac{1}{\rho_S} \left(\alpha \dot{x} \left(1 - \left(\frac{R_{o1}}{R_{o2}}\right)^3\right) + \frac{8K_1 y}{R_{o2}^2} - \frac{8K_1 x}{R_{o1}^2} + 4\mu_L \dot{y}\right). \end{aligned} \tag{4.48}$$

Dividing equation (4.48) throughout by R_{o1}^2 and substituting equation (4.47) into it gives

$$\begin{aligned} &\ddot{x} \left(1 - \left(\frac{\rho_S - \rho_L}{\rho_S}\right) \frac{R_{o1}}{R_{o2}}\right) \\ &= \frac{1}{\rho_S R_{o1}^2} \left(-3\kappa x \left(P_o + \frac{2\gamma_1}{R_{o1}} + \frac{2\gamma_2}{R_{02}} + 4K_1 \left(\frac{1}{R_{o1}^2} - \frac{1}{R_{o2}^2}\right)\right) + \frac{2\gamma_1 x}{R_{o1}} + \frac{2\gamma_2}{R_{o2}} \left(\frac{R_{o1}}{R_{o2}}\right)^3 x - P_A \sin(\omega t)\right) \\ &\qquad - \frac{1}{\rho_S R_{o1}^2} \left(\alpha \dot{x} \left(1 - \left(\frac{R_{o1}}{R_{o2}}\right)^3\right) + \frac{8K_1}{R_{o2}^2} \left(\frac{R_{o1}}{R_{o2}}\right)^3 x - \frac{8K_1 x}{R_{o1}^2} + 4\mu_L \left(\frac{R_{o1}}{R_{o2}}\right)^3 \dot{x}\right). \end{aligned} \tag{4.49}$$

Dividing equation (4.49) throughout by $1-((\rho_S-\rho_L)/\rho_S)\,R_{o1}/R_{o2}$ and rearranging reduces equation (4.49) to

$$\ddot{x}+2\gamma_d\dot{x}+\omega_o^2 x=\frac{P\left(t\right)}{\rho_S R_{o1}^2\left(1-\left(\left(\rho_S-\rho_L\right)/\rho_S\right)R_{o1}/R_{o2}\right)}, \tag{4.50}$$

where γ_d represents a damping coefficient where $P(t)=P_A\sin\left(\omega t\right)$, and ω_o is the natural angular frequency of the shelled microbubble. The term, $P(t)$, represents the sinusoidal, external ultrasound signal which forces the shelled microbubble. The damping coefficient is given as

$$\gamma_d=\frac{\alpha\left(1-\left(R_{o1}/R_{o2}\right)^3\right)+4\mu_L\left(R_{o1}/R_{o2}\right)^3}{2\rho_S R_{o1}^2\left(1-\left(\left(\rho_S-\rho_L\right)/\rho_S\right)R_{o1}/R_{o2}\right)}, \tag{4.51}$$

which is related to the relaxation time by

$$t_{\text{relax}}=\frac{1}{\gamma_d}. \tag{4.52}$$

The natural frequency, $f_o=\omega_o/(2\pi)$, is given by

$$f_o=\frac{1}{2\pi}\sqrt{\frac{\mathrm{N}}{\mathrm{D}}}, \tag{4.53}$$

where

$$\begin{aligned}\mathrm{N}=3\kappa R_{o1}R_{o2}^5\left(P_o+2\gamma_1/R_{o1}+2\gamma_2/R_{o2}\right)-2\gamma_1R_{o2}^5-2\gamma_2R_{o1}^4R_{o2}\\+\left(12\kappa-8\right)K_1R_{o2}^5/R_{o1}+8K_1R_{o1}^4-12\kappa K_1R_{o2}^3R_{o1},\end{aligned} \tag{4.54}$$

and

$$\mathrm{D}=\left(\rho_S R_{o1}^3R_{o2}^5-\left(\rho_S-\rho_L\right)R_{o1}^4R_{o2}^4\right). \tag{4.55}$$

4.7 Results

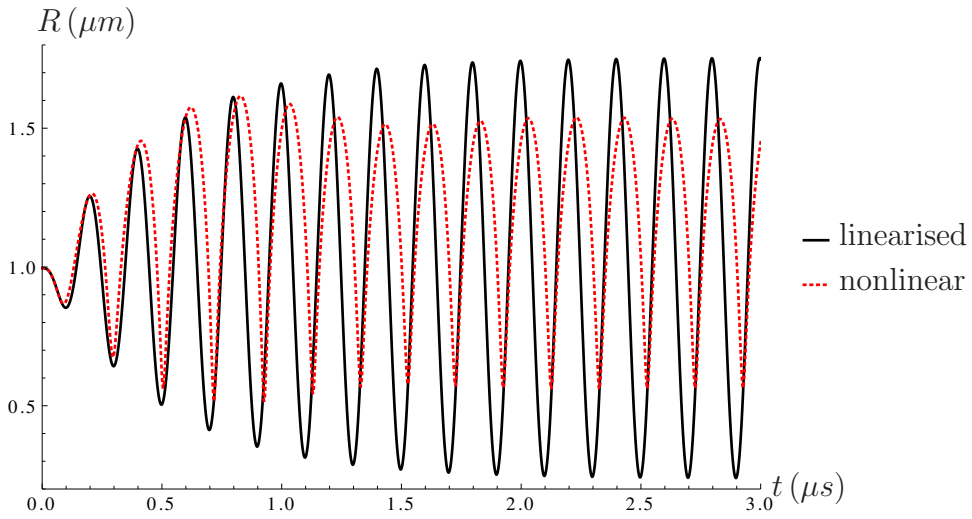

Figure 4.2: The linearised and nonlinear models of the radial displacement of a 1μm shelled microbubble versus time for a shell thickness of 4nm which is subjected to an acoustic pressure of $P_A = 100$kPa at a forcing frequency of $f = \omega/(2\pi) = 5$MHz which is very close to the natural frequency. The Leslie viscosities for MBBA are α=0.035Pa s ([65], p330) and the densities of the liquid-crystal shell and the surrounding fluid are $\rho_S = 1060$ kgm^{-3} and $\rho_L = 1000$kgm^{-3} respectively. The polytropic index of the gas, the viscosity of the surrounding fluid and the interfacial surface tension and the exterior radius' surface tension are $\kappa = 1.095, \mu_L = 10^{-3}$Pa s, $\gamma_1 = \gamma_2 = 0.072Nm^{-1}$ respectively. The graph is produced numerically by solving the ordinary differential equation (4.44) and from equation (4.49).

Figure 4.2 illustrates how the radius of a $1\mu m$ shelled microbubble with a thickness of 4nm varies with time when it is subjected to a forcing frequency of $f = 5$MHz (calculated using equation (4.53)) and an external acoustic pressure of amplitude $P_A = 100$kPa. Figure 4.2 displays a characteristic transient growth during the first couple of oscillations of the shelled microbubble. The linear model has a larger amplitude than the nonlinear model at a forcing frequency that is very close to the linearised model's natural frequency ($f_o = 5.03$MHz). Figure 4.2 shows that there is also a time lag between the nonlinear and the linear models.

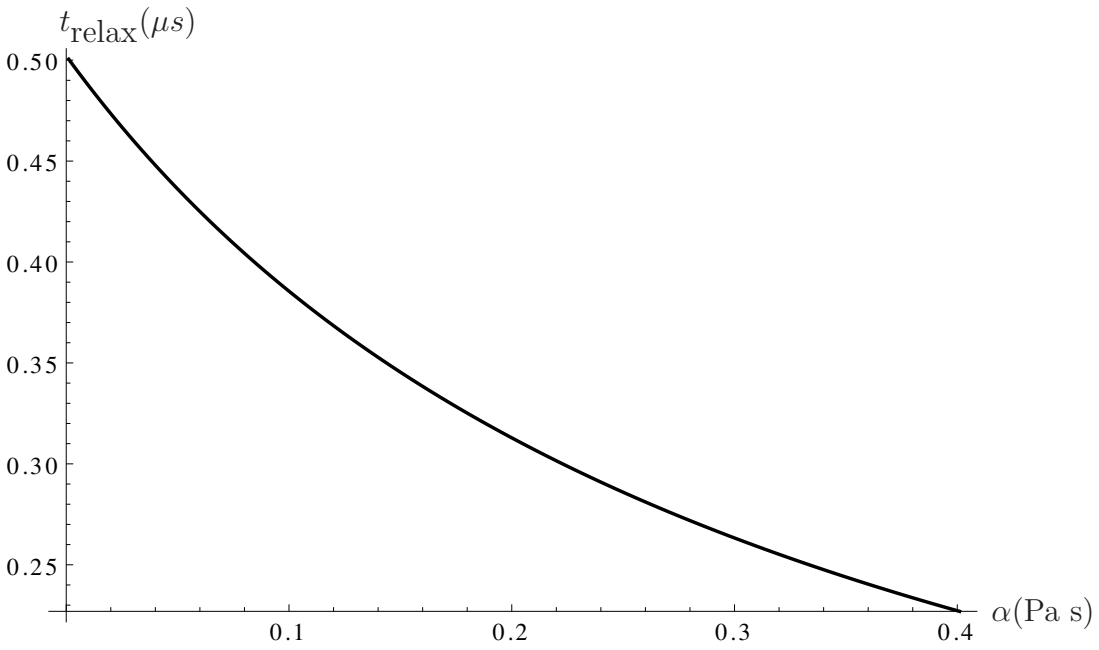

Figure 4.3: The relaxation time of a shelled microbubble of exterior radius $1\mu m$ (thickness 4nm) versus the Leslie viscosities α where $\alpha = \frac{4}{3}(\alpha_1 + \alpha_5 + \alpha_6)$. The densities of the liquid-crystal shell and the surrounding fluid are $\rho_S = 1060$ kgm^{-3} and $\rho_L = 1000$kgm^{-3} respectively. The polytropic index of the gas, the viscosity of the surrounding fluid and the interfacial surface tension and the exterior radius' surface tension are $\kappa = 1.095, \mu_L = 10^{-3}$Pa s, $\gamma_1 = \gamma_2 = 0.072Nm^{-1}$ respectively. The graph is constructed using equations (4.51) and (4.52).

Figure 4.3 illustrates the relaxation time's dependency on the Leslie viscosities where $\alpha = \frac{4}{3}(\alpha_1 + \alpha_5 + \alpha_6)$. As α increases the relaxation time t_{relax} decreases in a nonlinear manner. This is because a more viscous shell will dampen the oscillatory motion of the shell faster.

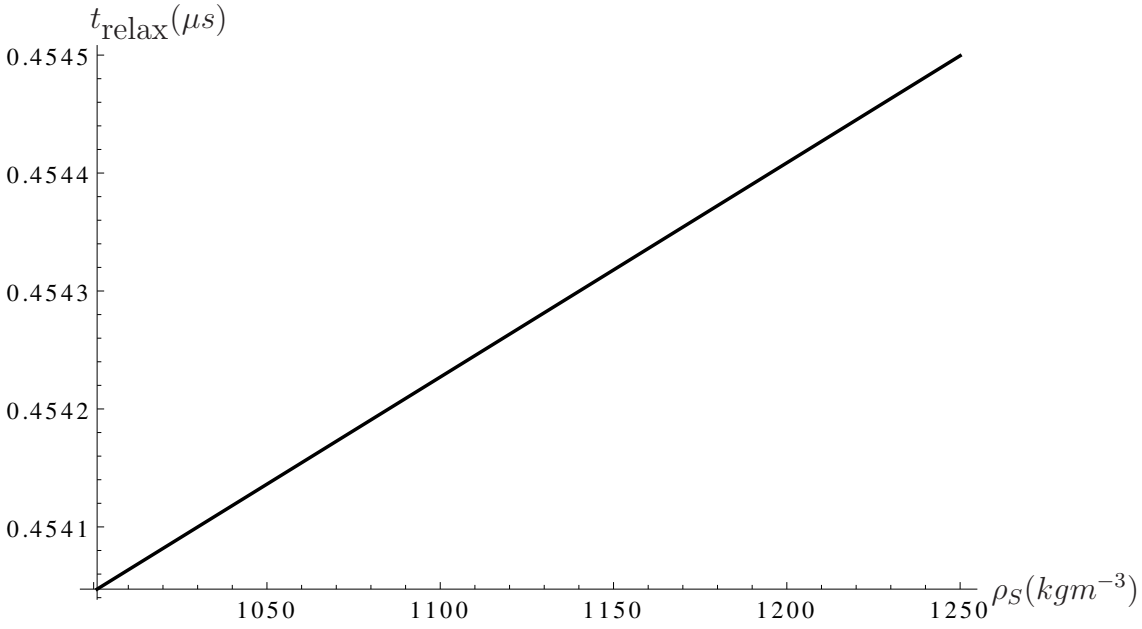

Figure 4.4: The relaxation time of a shelled microbubble of exterior radius $R_{o2} = 1\mu m$ (and thickness 4nm) versus the density of the shell ρ_S. The density of the surrounding fluid is $\rho_L = 1000\text{kg}m^{-3}$ and the Leslie viscosities are $\alpha = 0.035$Pa s. The polytropic index of the gas, the viscosity of the surrounding fluid and the interfacial surface tension and the exterior radius' surface tension are $\kappa = 1.095, \mu_L = 10^{-3}$Pa s, $\gamma_1 = \gamma_2 = 0.072\text{N}m^{-1}$ respectively. The graph is constructed using equations (4.51) and (4.52).

Figure 4.4 shows the relaxation time's dependency on the density of the shell ρ_S. The relaxation time increases by a very small amount in an approximately linear manner as the shell's density increases . The increase in relaxation time is so small that it is almost independent of ρ_S. This is due to the thinness of the shell which can be seen by substituting $R_{o2} = R_{o1}(1+\epsilon)$ where $\epsilon \ll 1$ into equation

(4.51) giving

$$\begin{aligned}\gamma_d &\approx \frac{\alpha(1-(1+\epsilon)^{-3})+4\mu_L(1+\epsilon)^{-3}}{2\rho_S R_{o1}^2(1-(1-\rho_L/\rho_S)(1+\epsilon)^{-1}},\\ &\approx \frac{3\alpha\epsilon+4\mu_L(1-3\epsilon)}{2\rho_L R_{o1}^2(1-\epsilon)},\\ &\approx \left(\frac{3\alpha\epsilon+4\mu_L(1-3\epsilon)}{2\rho_L R_{o1}^2}\right)(1+\epsilon),\\ &\approx \frac{2\mu_L}{\rho_L R_{o1}^2}+O(\epsilon). \qquad (4.56)\end{aligned}$$

Equation (4.56) shows that the damping is dominated by the viscous fluid.

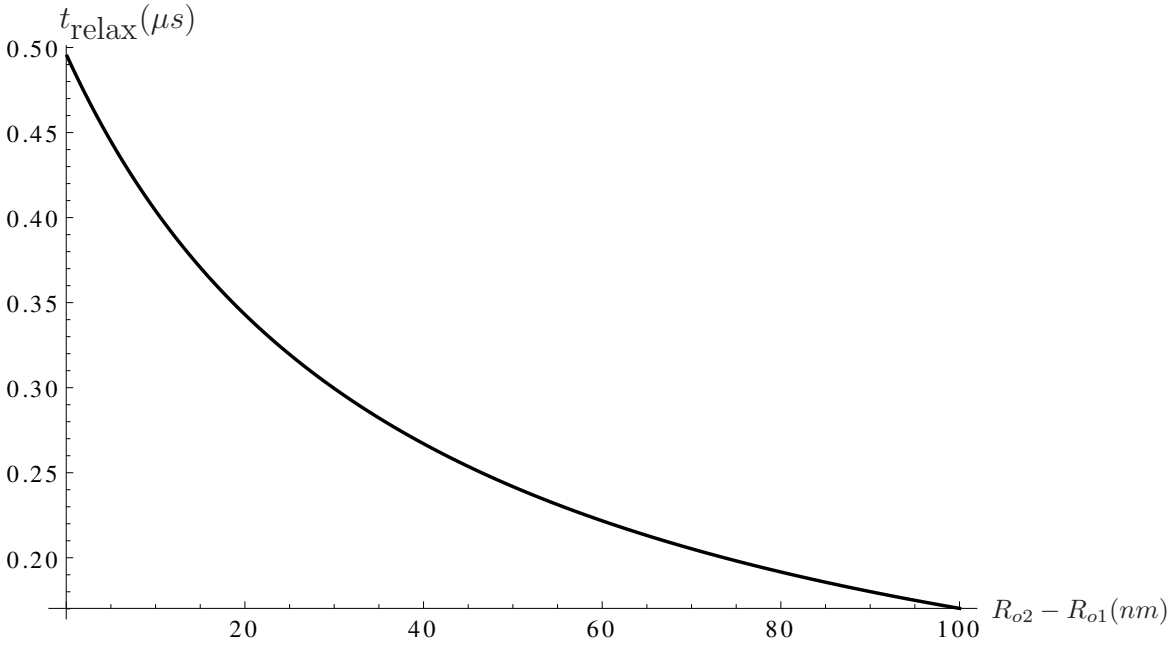

Figure 4.5: The relaxation time of a shelled microbubble of exterior radius $R_{o2} = 1\mu m$ versus the thickness of the shell $R_{o2} - R_{o1}$. The density of the surrounding fluid and the shell are $\rho_L = 1000\text{kg}m^{-3}$ and $\rho_S = 1060\text{kg}m^{-3}$ respectively and the Leslie viscosities are $\alpha = 0.035$Pa s. The polytropic index of the gas, the viscosity of the surrounding fluid and the interfacial surface tension and the exterior radius' surface tension are $\kappa = 1.095, \mu_L = 10^{-3}$Pa s, $\gamma_1 = \gamma_2 = 0.072\text{N}m^{-1}$ respectively. The graph is plotted using equations (4.51) and (4.52).

Figure 4.5 shows how the relaxation time decreases nonlinearly as the thick-

ness ($R_{o2} - R_{o1}$) of the shell increases. Equations (4.51) and (4.52) highlight the dependency of the damping coefficient and the relaxation time on the radii of the shell. Rewriting equation (4.51) as

$$\gamma_d = \frac{\alpha(1 - (R_{o1}/R_{o2})^3(1 - 4\mu_L/\alpha))}{2\rho_S R_{o1}^2 \left(1 - ((\rho_S - \rho_L)/\rho_S)R_{o1}/R_{o2}\right)}, \tag{4.57}$$

and rearranging for a fixed $\alpha, \mu_L, R_{o1}, \rho_S$ and ρ_L gives

$$\hat{\gamma}_d = \frac{1 - a\hat{R}^{-3}}{1 - b\hat{R}^{-1}}, \tag{4.58}$$

where $a = 1 - 4\mu_L/\alpha$, $b = (\rho_S - \rho_L)/\rho_S$, $\hat{R} = R_{o2}/R_{o1}$ and $\hat{\gamma}_d = 2\rho_S R_{o1}^2 \gamma_d/\alpha$. Note that $\hat{\gamma}_d$ can increase or decrease as a function of $\hat{R}$ depending on the values of a and b. Substituting the values of μ_L, α, ρ_S and ρ_L that are used to construct Figure 4.5 (see caption) satisfies the condition $a \gg b$. Hence as $\hat{R}$ increases and the shell thickens, the damping coefficient γ_d increases which results in a shorter relaxation time (since $t_{\text{relax}} = 1/\gamma_d$).

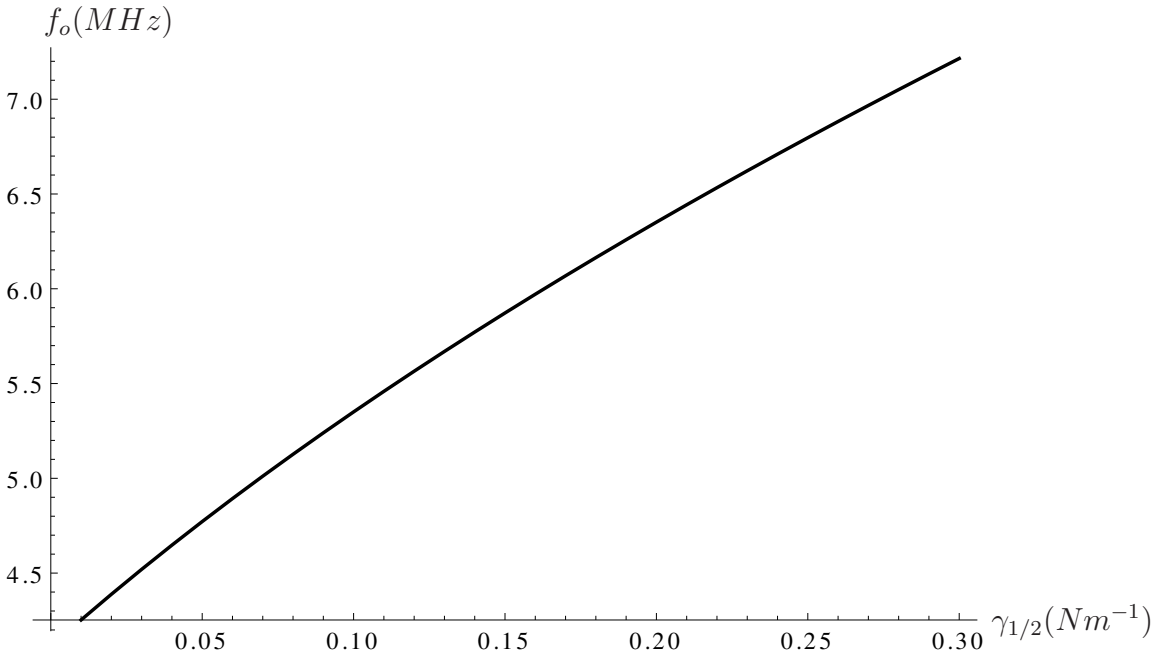

Figure 4.6: The natural frequency f_o of a shelled microbubble of exterior radius $R_{o2} = 1\mu m$ and thickness 4nm versus the surface tension of the shell $\gamma = \gamma_1 = \gamma_2$. The polytropic index of the gas is $\kappa = 1.095$ and $K_1 = 6 \times 10^{-12}$N. The density of the surrounding fluid and shell are $\rho_L = 1000\text{kg}m^{-3}$ and $\rho_S = 1060\text{kg}m^{-3}$; and the Leslie viscosities are $\alpha = 0.035$Pa s. The graph is plotted using equation (4.53).

Figure 4.6 illustrates how the natural frequency f_o of the shell increases as the inner γ_1 and outer γ_2 surface tensions of the shell increase where $\gamma_1 = \gamma_2$. This is due to a greater restoring force arising from a larger surface tension acting on the surface of the shell.

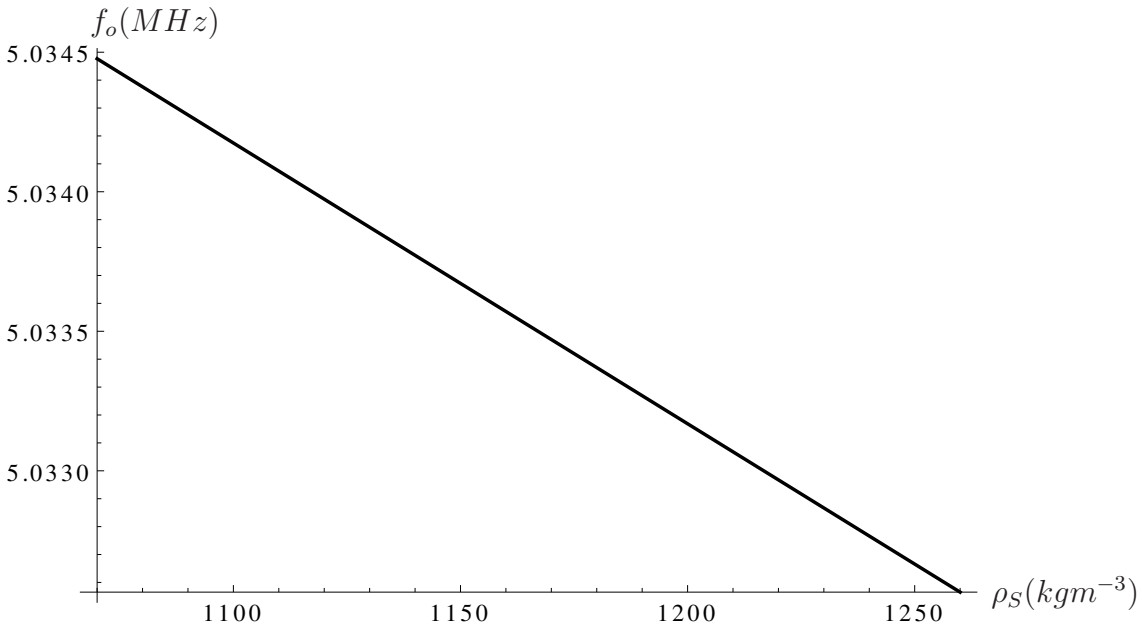

Figure 4.7: Natural frequency f_o of a shelled microbubble of exterior radius $R_{o2} = 1\mu m$ and thickness 4nm versus the density of the shell ρ_S. The polytropic index of the gas is $\kappa = 1.095$ and $K_1 = 6 \times 10^{-12}$N. The density of the surrounding fluid is $\rho_L = 1000\text{kg}m^{-3}$ and the Leslie viscosities are $\alpha = 0.035$Pa s. The graph is plotted using equation (4.53).

Figure 4.7 illustrates how the natural frequency f_o of the shell decreases by a very small amount as the density of the shell ρ_S increases.

4.8 Conclusion

A modified Rayleigh-Plesset equation has been derived for a shelled microbubble with an incompressible shell composed of a liquid-crystal material, surrounded by a Newtonian fluid. The model considers the gas inside the shelled microbubble, the shell's material and the surrounding Newtonian fluid. This model is then linearised using time-dependent perturbation theory to determine the relaxation time and the natural frequency of the shelled microbubble. The relaxation time exhibits a dependency on both the thickness of the shell and the Leslie viscosities (these are

dependent on the type of liquid-crystal material that the shell is made from). This model is anisotropic unlike previous Rayleigh-Plesset equations which model the shell of the microbubble as an isotropic solid. Liquid crystals are non-Newtonian fluids, exhibiting shear thinning whereas all previous Rayleigh-Plesset models use Newtonian fluid mechanics. Current experimental evidence indicates that some contrast agents are viscoelastic with mesophase type behaviour [51] which, by definition, constitutes a liquid-crystal material. The radial displacement exhibited a symmetrical oscillatory pattern. As the Leslie viscosities increased in value the relaxation time decreased in a nonlinear manner. The relaxation time increased linearly as the density of the shell increased. As the thickness of the shell increased the relaxation time decreased nonlinearly. The natural frequency increased linearly as the surface tension increased.

Chapter 5

Conclusion

5.1 Motivation

The aim of this PhD thesis was to understand and identify how various material parameters such as the shear modulus, Poisson ratio and thickness of the shell influenced the collapse, relaxation times and natural frequency of shelled microbubbles. Chapter 2 proposed an analytical model for a stressed, compressible shelled microbubble that oscillated about its equilibrium position and considered how varying the shear modulus, Poisson ratio and shell thickness influenced the period of oscillation. Chapter 3 discussed the physical model for the deformation of an open shelled microbubble whose geometry evolves. An opening angle approach was used to model this geometrical change (folding shell) with the original stress free configuration being represented by an open, deformed and incomplete sphere which was stressed via a hoop stress in order to deform the shell's surface both radially and angularly. This model used an asymptotic expansion (linearisation) to model the quasistatic phase. Chapter 4 developed a Rayleigh-Plesset equation describing an incompressible, thin shelled, gas loaded microbubble with a shell

composed of a liquid-crystalline material. Time-dependent perturbation theory was used to linearise the physical model and the relaxation time and natural frequency of the shelled microbubble and its dependency on the material parameters (Leslie viscosities [64]) of the shell was considered.

5.2 Results

Chapter 2 described an analytical approach to modelling the inflationary process of a shelled microbubble via a quasistatic radially directed stress load applied to its inner surface. The stress load was switched off and the time for the microbubble to collapse back down to its equilibrium position was determined by using the Cauchy momentum equation and the inflated radial deformation as an initial condition. Key material parameters such as the thickness of the shell, its Poisson ratio and the shell's shear modulus were varied to determine their influence on the collapse phase of the shell. A typical collapse time for a shell with a shear modulus of $\mu = 20$MPa and a Poisson ratio of $\nu = 0.48$, subjected to a stress load of $p = 200$kPa, was $t^* \approx 3.5$ns. Shells with a larger shear modulus results in shorter collapse times. As the thickness of the shell increased the collapse time of the shell increased in a linear manner. Shells with a larger Poisson ratio possess smaller initial radial deformations and therefore exhibited shorter collapse times.

Chapter 3 considered a deformed open shelled microbubble with a spherical cap removed. The stress free, open angle shelled microbubble was subjected to a polar directed stress which was applied to the rim of the shell. The deformation had both a radial and angular dependency. This model attempts to consider the change in geometry of a ruptured shelled microbubble.

In Chapter 4, a modified Rayleigh-Plesset equation was derived for a shelled microbubble with an incompressible shell composed of a liquid-crystalline material, surrounded by a Newtonian fluid. The model considered the three physical media of the shell; inside the microbubble, the shell's liquid-crystalline material and the surrounding Newtonian fluid. This model was then linearised using time-dependent perturbation theory to determine the relaxation time and the natural frequency of the shelled microbubble. The relaxation time exhibited a dependency on both the thickness of the shell and the Leslie viscosities. The relaxation time decreased nonlinearly as the Leslie viscosities increased in magnitude. It also increased linearly by a very small amount as the density of the shell increased. For thickening shells the relaxation time decreased nonlinearly. The natural frequency increased linearly as the surface tension of the shell increased. The natural frequency decreased linearly by a very small amount as the density of the shell increased. The radial displacement of the oscillatory shelled microbubble was symmetric whereas the experimental results for UCAs exhibit an asymmetric behaviour [44].

5.3 Further work

Chapter 2 could be extended by applying an external stress load to the outside surface of the shell to represent atmospheric pressure. The viscoelastic behaviour of the shell and the influence of the surrounding fluid could be modelled by using a Maxwell fluid model. Future work could also focus on solving numerically both the forward and collapse phases for the nonlinear model.

The linearisation of Chapter 3 could be evaluated numerically to solve the radial and angular partial differential equations in conjunction with their respective coupled boundary conditions. Further work could consist of solving the linearised collapse phase numerically. The influence of varying material parameters on the collapse time could also be considered.

Chapter 4 models the shell using nematic viscosities rather than smectic A viscosities. A Rayleigh-Plesset model could be developed for a smectic A shell which requires thirteen viscosities rather than the five Leslie viscosities associated with a nematic. The liquid-crystal model could be applied to consider the influence of various physical parameters of the shell on the wall shear stress. Currently, there are very few mathematical models that have been developed to understand sonoporation via acoustic microstreaming [31], [32]. Such a model could consider how the thickness, density and Leslie viscosities of the shell influence the magnitude of the wall shear stress.

This PhD modelled the influence that various material parameters had on the collapse time, the natural frequency and relaxation time of shelled microbubbles. Chapter 2 considered how varying the shear modulus, the Poisson ratio and the thickness of the shell influenced the collapse time. Chapter 3 focussed on modelling the rupture of the shell of a typical UCA shelled microbubble. Chapter 4 considered the shell of the shelled microbubble as a mesophase exhibiting both liquid and solid characteristics. Hopefully such models will aid soft matter scientists' understanding of UCA localised drug delivery and gene therapy.

Appendix A

Justifying the Rayleigh-Plesset equation

Assuming that the fluid flow in the surrounding fluid and in the shell is in the radial direction only, then the velocity, $\mathbf{v}$, of the flow can be related to a fluid potential, ϕ, via $\mathbf{v} = \nabla\phi$. Applying the conservation of mass to an incompressible shell in an incompressible liquid medium gives ([65],p138-139), $\nabla \cdot \mathbf{v} = 0$, and so $\nabla \cdot \nabla\phi = \nabla^2\phi = 0$. Converting this into spherical polars for a radially symmetric flow gives

$$\frac{1}{r^2}\frac{\partial}{\partial r}\left(r^2\frac{\partial\phi}{\partial r}\right) = 0,$$

which is solved giving

$$\frac{\partial\phi}{\partial r} = \frac{A(t)}{r^2},$$
$$\phi = \frac{-A(t)}{r} + B(t).$$

Defining the potential such that $\phi \to 0$ as $r \to \infty$ results in $B(t) = 0$ and so $\phi = -A(t)/r$. The equation $\phi = -A(t)/r$ is a fluid potential ([65], p138-139)which can be either positive or negative and can be written as

$$\phi = \frac{C(t)}{r}, \tag{A.1}$$

where $C(t)$ can be either positive or negative. Using this equation along with the definition of the velocity, $\mathbf{v} = \nabla\phi$, results in

$$\nabla\phi = \frac{-C(t)}{r^2} e_r.$$

At this point let us assume that the inner and outer radii of the shelled microbubble, R, are a function of time alone such that $R \equiv R(t)$ [83]. Defining the velocity of the shelled microbubble as $\dot{R}$ at $r = R$ leads to

$$\nabla\phi|_{r=R} = \frac{-C(t)}{R^2} e_r = \dot{R} e_r,$$

which on rearranging gives $C(t) = -R^2\dot{R}$. From equation (A.1) then, the fluid potential, ϕ, and the radial velocity component of the bubble, v, are given by

$$\phi = \frac{-R^2\dot{R}}{r}, \tag{A.2}$$

and

$$v = \frac{\partial\phi}{\partial r} = \frac{R^2\dot{R}}{r^2}. \tag{A.3}$$

Assuming that the influence of gravity is negligible due to the small density contrast between the contrast agent and the surrounding fluid, the momentum balance

law is given as [83]

$$\rho\frac{\partial \mathbf{v}}{\partial t} + \rho\left(\mathbf{v}\cdot\nabla\right)\mathbf{v} = \nabla\cdot\sigma, \tag{A.4}$$

where ρ denotes the fluid density and σ represents the Cauchy stress. The following derivation focusses on the radial direction of the perturbed, spherical, liquid-crystal shelled microbubble. Equation (A.4) gives

$$\left(\rho\frac{\partial v}{\partial t} + \rho v\frac{\partial v}{\partial r}\right)e_r = \nabla\cdot\sigma, \tag{A.5}$$

or alternatively

$$\left(\frac{\partial v}{\partial t} + \frac{1}{2}\frac{\partial v^2}{\partial r}\right)e_r = \frac{1}{\rho}\left(\nabla\cdot\sigma\right). \tag{A.6}$$

Using equation (A.3), this gives

$$\left(\frac{\partial}{\partial t}\left(\frac{\partial \phi}{\partial r}\right) + \frac{1}{2}\frac{\partial}{\partial r}\left(\left(\frac{\partial \phi}{\partial r}\right)^2\right)\right)e_r = \frac{1}{\rho}\left(\nabla\cdot\sigma\right), \tag{A.7}$$

and if we assume

$$\frac{\partial}{\partial t}\left(\frac{\partial \phi}{\partial r}\right) = \frac{\partial}{\partial r}\left(\frac{\partial \phi}{\partial t}\right),$$

then equation (A.7) can be rewritten as

$$\left(\frac{\partial}{\partial r}\left(\frac{\partial \phi}{\partial t}\right) + \frac{1}{2}\frac{\partial}{\partial r}\left(\left(\frac{\partial \phi}{\partial r}\right)^2\right)\right)e_r = \frac{1}{\rho}\left(\nabla\cdot\sigma\right), \tag{A.8}$$

which can be rearranged to give

$$\left(\frac{\partial}{\partial r}\left(\frac{\partial \phi}{\partial t} + \frac{1}{2}\left(\frac{\partial \phi}{\partial r}\right)^2\right)\right)e_r = \frac{1}{\rho}\left(\nabla\cdot\sigma\right). \tag{A.9}$$

This can be integrated across $r \in [R, \infty)$ to give

$$\int_R^\infty \frac{\partial}{\partial r}\left(\frac{\partial \phi}{\partial t} + \frac{1}{2}\left(\frac{\partial \phi}{\partial r}\right)^2\right) e_r dr = \frac{1}{\rho}\int_R^\infty \nabla \cdot \sigma dr. \tag{A.10}$$

Using equation (A.2) gives

$$\frac{\partial \phi}{\partial t} = -\frac{R^2 \ddot{R}}{r} - \frac{2R\dot{R}^2}{r}, \tag{A.11}$$

and substituting this and equation (A.3) into equation (A.10) gives

$$\int_R^\infty \frac{\partial}{\partial r}\left(\frac{-R^2\ddot{R} - 2R\dot{R}^2}{r} + \frac{R^4\dot{R}^2}{2r^4}\right) e_r dr = \frac{1}{\rho}\int_R^\infty \nabla \cdot \sigma dr. \tag{A.12}$$

Evaluating the integral in (A.12) leads to

$$\left(R\ddot{R} + \frac{3}{2}\dot{R}^2\right) e_r = \frac{1}{\rho}\int_R^\infty \nabla \cdot \sigma dr. \tag{A.13}$$

Polytropic gas and the role of surface tension

The gas encapsulated by the shelled microbubble is assumed to be adiabatic and is modelled using a polytropic equation $P_g V_o^\kappa = pV^\kappa$ where κ denotes the polytropic index which is a dimensionless parameter [45,50], V_o is the equilibrium volume of the gas filled shelled microbubble at a gas pressure of P_g and p is the pressure of the gas during the expansion/contraction phases. Assuming that the shelled microbubble is a sphere with a volume given by $V = (4/3)\pi R^3$ where R denotes the time varying radius of the shelled microbubble, then

$$P_g\left(\frac{4}{3}\pi R_o^3\right)^\kappa = p\left(\frac{4}{3}\pi R^3\right)^\kappa, \tag{A.14}$$

which gives

$$p = P_g \left(\frac{R_o}{R} \right)^{3\kappa}, \tag{A.15}$$

where R_o is the initial (equilibrium) shelled microbubble radius when the total pressure inside the shelled microbubble (p) is equal to the initial gas pressure inside the shelled microbubble (P_g).

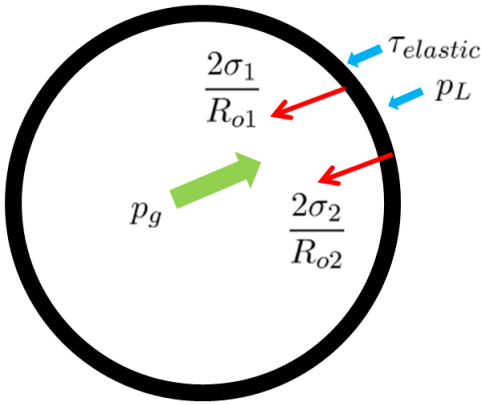

Figure A.1: Illustration of the gas pressure, surface tensions and the stress associated with the elastic energy density acting on a thin shelled microbubble.

Figure A.1 illustrates the pressure balance acting on an isolated shelled microbubble surrounded by a Newtonian fluid with an inwardly acting pressure given by p_L and a gas pressure acting outwards represented by P_g. There is also a stress associated with the elastic energy density of the liquid crystal denoted by τ_{elastic}. There are two surface tensions in Figure A.1 where γ_1 represents the interfacial surface tension between the inner shell and the encapsulated gas layer and γ_2 denotes the surface tension between the outer shell of the shelled microbubble and the surrounding Newtonian fluid [51,52]. Shelled microbubbles are assumed to have a finite, ultra thin thickness with an initial thickness given by the difference between their unperturbed inner and outer radii $R_{o2} - R_{o1}$. The surface tension terms are used to determine their respective pressure terms via the Young-Laplace formula

([84],p230-234). Note that this model assumes that the surface tensions γ_1 and γ_2 are constant and do not vary with the area density as the shelled microbubble expands and contracts.

Justifying the pressure terms for the surface tensions

The energy (work done W) associated with the surface tension of the shelled microbubble is given by

$$W = \int\int \gamma ds = \gamma \int_0^{\pi} \int_0^{2\pi} R^2 \sin\theta d\theta d\phi = 2\pi\gamma R^2 \left(\cos\theta\right)_0^{\pi} = 4\pi\gamma R^2.$$

Using the definition of work done from thermodynamics and rewriting the partial derivative using the chain rule results in

$$p = \frac{\partial W}{\partial V} = \frac{\partial W}{\partial R}\frac{\partial R}{\partial V}.$$

Applying these definitions to the case of a spherical shelled microbubble leads to

$$\frac{\partial V}{\partial R} = 4\pi R^2,$$

and

$$\frac{\partial W}{\partial R} = 8\pi\gamma R,$$

which gives

$$p = \frac{8\pi\gamma R}{4\pi R^2} = \frac{2\gamma}{R}. \tag{A.16}$$

This is the well known Young-Laplace equation describing the pressure contribution of the surface tension of a spherical object such as a shelled microbubble [84].

Balancing the pressures acting in Figure A.1 where $p_L = P_o$ gives

$$P_g = P_o + \frac{2\gamma_1}{R_{o1}} + \frac{2\gamma_2}{R_{o2}} + 4K_1 \left(\frac{1}{R_{o1}^2} - \frac{1}{R_{o2}^2} \right), \tag{A.17}$$

where P_o represents the surrounding ambient liquid pressure and $4K_1 \left(1/R_{o1}^2 - 1/R_{o2}^2\right)$ is the stress associated with the elastic energy density of the liquid crystal and is given by equation (4.34).

Bibliography

[1] P. Narayan and M. A. Wheatley. Preparation and characterization of hollow microcapsules for use as ultrasound contrast agents. *Polymer Engineering and Science*, 39:2242–2255, 1999.

[2] M. Bazan Peregrino, B. Rifai, R. C. Carlisle, J. Choi, C. D. Arvanitis, L. W. Seymour, and C. C. Coussios. Cavitation-enhanced delivery of a replicating oncolytic adenovirus to tumors using focused ultrasound. *Journal of Controlled Release*, 169:40–47, 2013.

[3] D. Gourevich, A. Volovick, O. Dogadkin, L. Wang, H. Mulvana, Y. Medan, A. Melzer, and S. Cochran. In vitro investigation of the individual contributions of ultrasound-induced stable and inertial cavitation in targeted drug delivery. *Ultrasound in Medicine & Biology*, 41:1853–1864, 2015.

[4] J.M. Escoffre, C. Mannaris, B. Geers, A. Novell, I. Lentacker, M. Averkion, and A. Bouakaz. Doxirubicin liposome-loaded microbubbles for contrast imaging and ultrasound triggered drug delivery. *IEEE Transactions on Ultrasonics, Ferroelectrics and Frequency Control*, 60:78–87, 2013.

[5] Ching-Hsiang Fan, Chien-Yu Ting, Hao-Li Liu, Chiung-Yin Huang, Han-Yi Hsieh, Tzu-Chen Yen, Kuo-Chen Wei, and Chih-Kuang Yeh. Antiangiogenic-

targeting drug-loaded microbubbles combined with focused ultrasound for glioma treatment. *Biomaterials*, 34:2142–2155, 2013.

[6] F. Yan, L. Li, Z. Deng, Q. Jin, J. Chen, W. Yang, C. K. Yeh, J. Wu, R. Shandas, X. Liu, and H. Zheng. Paclitaxel-liposome-microbubble complexes as ultrasound-triggered therapeutic drug delivery carriers. *Journal of Controlled Release*, 166:246–255, 2013.

[7] C. Niu, Z. Wang, G. Lu, T. M. Krupka, Y. Sun, Y. You, W. Song, H. Ran, P. Li, and Y. Zheng. Doxorubicin loaded superparamagnetic PLGA-iron oxide multifunctional microbubbles for dual-mode US/MR imaging and therapy of metastasis in lymph nodes. *Biomaterials*, 34:2307–2317, 2013.

[8] A. Delalande, C. Leduc, P. Midoux, M. Postema, and C. Pichon. Efficient gene delivery by sonoporation is associated with microbubble entry into cells and the clathrin-dependent endocytosis pathway. *Ultrasound in Medicine & Biology*, 41:1913–1926, 2015.

[9] C. McEwan, J. Owen, E. Stride, C. Fowley, H. Nesbitt, D. Cochrane, C. C. Coussios, M. Borden, N. Nomikou, A. P. McHale, and J. F. Callan. Oxygen carrying microbubbles for enhanced sonodynamic therapy of hypoxic tumours. *Journal of Controlled Release*, 203:51–56, 2015.

[10] E. Stride and N. Saffari. Microbubble ultrasound contrast agents: a review. *Proceedings of the Institution of Mechanical Engineers Part H*, 217:429–447, 2003.

[11] D. Cosgrove. Ultrasound contrast agents: An overview. *European Journal of Radiology*, 60:324–330, 2006.

[12] E. Stride and C. C. Coussios. Cavitation and contrast: The use of bubbles in ultrasound imaging and therapy. *Proceedings of the Institute of Mechanical Engineers Part H*, 224:171–191, 2010.

[13] J. McLaughlan, N. Ingram, P.R. Smith, S. Harput, P.L. Coletta, S. Evans, and S. Freear. Increasing the sonoporation efficiency of targeted polydisperse microbubble populations using chirp excitation. *IEEE Transactions on Ultrasonics, Ferroelectrics and Frequency Control*, 60:2511–2520, 2013.

[14] O. Falou, A.J. Sojahrood, J.C. Kumaradas, and M.C. Kolios. Modelling the effect of shell thickness on high frequency ultrasound scattering from ultrasound contrast agents. *Canadian Acoustics*, 38:38–39, 2010.

[15] J. Tu, J. Guan, Y. Qiu, and T.J. Matula. Estimating the shell parameters of SonoVue microbubbles using light scattering. *Journal Acoustical Society of America*, 126:2954–2962, 2009.

[16] M.J.K. Blomley, J.C. Cooke, E.C. Unger, M.J. Monaghan, and D.O. Cosgrove. Microbubble contrast agents: a new era in ultrasound. *British Medical Journal*, 322:1222–1225, 2001.

[17] I. Lentacker, S. C. De Smedt, and N. N. Sanders. Drug loaded microbubble design for ultrasound triggered delivery. *Soft Matter*, 5:2161–2170, 2009.

[18] H. Dewitte, K. Vanderperren, H. Haers, E. Stock, L. Duchateau, M. Hesta, J. H. Saunders, S. C. De Smedt, and I. Lentacker. Theranostic mRNA-loaded microbubbles in the lymphatics of dogs: Implications for drug delivery. *Theranostics*, 5:97–109, 2015.

[19] P.A. Dijkmans, L.J.M. Juffermans, R.J.P. Musters, A.Van Wamel, F.J. ten Cate, W. van Gilst, C.A. Visser, N. de Jong, and O. Kamp. Microbubbles and

ultrasound: from diagnosis to therapy. *European Journal of Echocardiography*, 5:245–256, 2004.

[20] M. Cochran, T. Bustamante, J. Eisenbrey, and M. Wheatley. In vitro characterization of docetaxel loaded microbubbles for ultrasound triggered drug delivery. *Pharmaceutical Engineering*, 32:1–10, 2012.

[21] J. McLaughlan, P. Smith, N. Ingram, L. Coletta, S. Evans, and S. Freear. Chirp excitation of polydisperse microbubble populations for increasing sonoporation efficiency. *IEEE International Symposium Proceedings of Ultrasonics*, Dresden, Germany:2298–2301, 2012.

[22] J. M. Burns, P. A. Prentice, A. Cuschieri, and P. A. Campbell. Modelling the microscopic mechanisms of sonoporation. *Nano Science and Technology Institute-Nanotech*, 2:333–336, 2006.

[23] M. M. Forbes and W. D. O'Brien. Development of a theoretical model describing sonoporation activity of cells exposed to ultrasound in the presence of contrast agents. *Journal Acoustical Society of America*, 131:2723–2729, 2012.

[24] C. Crake, M. de S. Victor, J. Owen, C. Coviello, J. Collin, C. C. Coussios, and E. Stride. Passive acoustic mapping of magnetic microbubbles for cavitation enhancement and localization. *Institute of Physics-Physics in Medicine and Biology*, 60:785–806, 2015.

[25] S. Bhatnagar, H. Schiffter, and C. C. Coussios. Exploitation of acoustic cavitation-induced microstreaming to enhance molecular transport. *Journal of Pharmaceutical Sciences*, 103:1903–1912, 2014.

[26] Z. Fan, R. E. Kumon, and C. X. Deng. Mechanisms of microbubble-facilitated sonoporation for drug and gene delivery. *Therapeutic Delivery*, 5:467–486, 2014.

[27] J. Park, Z. Fan, and C. X. Deng. Effects of shear stress cultivation on cell membrane disruption and intracellular calcium concentration in sonoporation of endothelial cells. *Journal of Biomechanics*, 44:164–169, 2011.

[28] G. A. Sotiriou, F. Starsich, A. Dasargyri, M. C. Wurnig, F. Krumeich, A. Boss, Jean-Christophe Leroux, and S. E. Pratsinis. Photothermal killing of cancer cells by the controlled plasmonic coupling of Silica-coated Au/Fe_2O_3 nanoaggregates. *Advanced Functional Materials*, 24:2818–2827, 2014.

[29] J. McLaughlan, S. Harput, D. Cowell, and S. Freear. Molecular-targeted nanorods for the localised destruction of cancer cells. *IEEE International Ultrasonics Symposium Proceedings ULTSYM*, pages 1061–1064, 2014.

[30] S. Ye, G. Marston, J. McLaughlan, D. O. Sigle, N. Ingram, S. Freear, J. J. Baumberg, R. J. Bushby, A. F. Markham, K. Critchley, P. L. Coletta, and S. D. Evans. Engineering gold nanotubes with controlled length and near-infrared absorption for theranostic applications. *Advanced Functional Materials*, 25:2117–2127, 2015.

[31] A.A. Doinikov and A. Bouakaz. Theoretical investigation of shear stress generated by a contrast microbubble on the cell membrane as a mechanism for sonoporation. *Journal Acoustical Society of America*, 128:11–19, 2010.

[32] A.A. Doinikov, L. Aired, and A. Bouakaz. Dynamics of a contrast agent microbubble attached to an elastic wall. *IEEE Transactions on Medical Imaging*, 31:654–662, 2012.

[33] J. Wu. Shear stress in cells generated by ultrasound. *Progress in Biophysics and Molecular Biology*, 93:363–373, 2007.

[34] P. Prentice, A. Cuschieri, K. Dholakia, M. Prausnitz, and P. Campbell. Membrane disruption by optically controlled microbubble cavitation. *Nature Physics*, 1:107–110, 2005.

[35] K. Kooiman, M. Foppen-Harteveld, A.F.W. van der Steen, and N. de Jong. Sonoporation of endothelial cells by vibrating targeted microbubbles. *Journal of Controlled Release*, 154:35–41, 2011.

[36] Lord Rayleigh. On the pressure developed in a liquid during the collapse of a spherical bubble. *Philosophical Magazine, Series 6*, 34:94–98, 1917.

[37] M.S. Plesset. The dynamics of cavitation bubbles. *ASME Journal of Applied Mechanics*, 16:277–282, 1949.

[38] L. Hoff. *Acoustic Characterization of Contrast Agents for Medical Ultrasound Imaging*. Kluwer Academic Publishers, Netherlands, 2001.

[39] A.A. Doinikov and A. Bouakaz. Review of shell models for contrast agent microbubbles. *IEEE Transactions on Ultrasonics, Ferroelectrics and Frequency Control*, 58:981–993, 2011.

[40] C. Herring. Theory of the pulsations of the gas bubble produced by an underwater explosion. *Office of Scientific Research and Development, OSRD*, 1941.

[41] L. Trilling. Collapse and rebound of a gas bubble. *Journal of Applied Physics*, 23:14–17, 1952.

[42] J.B. Keller and I.I. Kolodner. Damping of underwater explosion bubble oscillations. *Journal of Applied Physics*, 27:1152–1161, 1956.

[43] J.B. Keller and M. Miksis. Bubble oscillations of large amplitude. *Journal Acoustical Society of America*, 68:628–633, 1980.

[44] P. Marmottant, S.Van der Meer, M. Emmer, M. Versluis, N. de Jong, S. Hilgenfeldt, and D. Lohse. A model for large amplitude oscillations of coated bubbles accounting for buckling and rupture. *Journal Acoustical Society of America*, 118:3499–3505, 2005.

[45] S. Paul, A. Katiyar, K. Sarkar, D. Chatterjee, W.T. Shi, and F. Forsberg. Material characterization of the encapsulation of an ultrasound contrast microbubble and its subharmonic response: Strain-softening interfacial elasticity model. *Journal Acoustical Society of America*, 127:3846–3857, 2010.

[46] N. de Jong, L. Hoff, T. Skotland, and N. Bom. Absorption and scatter of encapsulated gas filled microspheres: Theoretical consideration and some measurements. *Ultrasonics*, 30:95–103, 1992.

[47] N. de Jong and L. Hoff. Ultrasound scattering of Albunex microspheres. *Ultrasonics*, 31:175–181, 1993.

[48] N. de Jong, R. Cornet, and C.T. Lancèe. Higher harmonics of vibrating gas-filled microspheres. Part one: Simulations. *Ultrasonics*, 32:447–453, 1994.

[49] N. de Jong, R. Cornet, and C.T. Lancèe. Higher harmonics of vibrating gas-filled microspheres. Part two: Measurements. *Ultrasonics*, 32:455–459, 1994.

[50] C.C. Church. The effects of an elastic solid surface layer on the radial pulsations of gas bubbles. *Journal Acoustical Society of America*, 97:1510–1521, 1995.

[51] A.A. Doinikov and P.A. Dayton. Maxwell rheological model for lipid-shelled ultrasound microbubble contrast agents. *Journal Acoustical Society of America*, 121:3331–3340, 2007.

[52] A.A. Doinikov, J.F. Haac, and P.A. Dayton. Modeling of nonlinear viscous stress in encapsulating shells of lipid-coated contrast agent microbubbles. *Ultrasonics*, 49:269–275, 2009.

[53] V.A. Bogoyavlenskiy. Differential criterion of a bubble collapse in viscous liquids. *Physical Review E*, 60:504–508, 1999.

[54] Y. Gorb and J.R. Walton. Dependence of the frequency spectrum of small amplitude vibrations superimposed on finite deformations of a nonlinear, cylindrical elastic body on residual stress. *International Journal of Engineering Science*, 48:1289–1312, 2010.

[55] Y. C. Fung. *Biomechanics: Motion, Flow, Stress and Growth*. Springer, New York, 1990.

[56] Y. C. Fung. *Biomechanics: Mechanical Properties of Living Tissues*. Springer, New York, 1993.

[57] Y. C. Fung. *Biomechanics*. Springer, New York, 1996.

[58] G.A. Holzapfel. *Nonlinear Solid Mechanics*. Wiley, Wiltshire, 2000.

[59] G. A. Holzapfel and R. W. Ogden. *Biomechanics of Soft Tissue in Cardiovascular Systems*. Springer, New York, 2004.

[60] K.A. Lazopoulos and R.W. Ogden. Spherically symmetric solutions for a spherical shell in finite pseudo-elasticity. *European Journal of Mechanics - A/Solids*, 18:617–632, 1999.

[61] K. Tsiglifis and N.A. Pelekasis. Nonlinear radial oscillations of encapsulated microbubbles subject to ultrasound: The effect of membrane constitutive law. *Journal Acoustical Society of America*, 123:4059–4070, 2008.

[62] K. Efthymiou, K. Tsiglifis, S. Serpetzi, and N. Pelekasis. Static and dynamic analysis of contrast agents-parameter estimates and the effect of the constitutive law. *9th EUROMECH Fluid Mechanics Conference*, Rome, Italy, 2012.

[63] R. Gaudron, M.T. Warnez, and E. Johnsen. Bubble dynamics in a viscoelastic medium with nonlinear elasticity. *Journal of Fluid Mechanics*, 766:54–75, 2015.

[64] H. Wang, T.X. Wu, S. Gauza, J.R. Wu, and S. Wu. A method to estimate the Leslie coefficients of liquid crystals based on MBBA data. *Liquid Crystals*, 33:91–98, 2006.

[65] I.W. Stewart. *The Static and Dynamic Continuum Theory of Liquid Crystals*. Taylor and Francis, London, 2004.

[66] I.W. Stewart. Dynamic theory for smectic A liquid crystals. *Continuum Mechanics and Thermodynamics*, 18:343–360, 2007.

[67] R. De Vita and I.W. Stewart. Energetics of lipid bilayers with applications to deformations induced by inclusions. *Soft Matter*, 9:2056–2068, 2013.

[68] J.C. Daniel, A. Tongen, D.P. Warne, and P.G. Warne. A 3D nonlinear anisotropic spherical inflation model for intracranial saccular aneurysm elastodynamics. *Mathematics and Mechanics of Solids*, 15:279–307, 2010.

[69] R. De Pascalis, I.D. Abrahams, and W.J. Parnell. Predicting the pressure-volume curve of an elastic microsphere composite. *Journal of Mechanics and Physics of Solids*, 61:1106–1123, 2013.

[70] R.W. Ogden. *Nonlinear Elastic Deformations*. Dover, New York, 1997.

[71] K. Gou, S. Joshi, and J.R. Walton. Recovery of material parameters of soft hyperelastic tissue by an inverse spectral technique. *International Journal of Engineering Science*, 56:1–16, 2012.

[72] P.J. Blatz. *On the Thermostatic Behaviour of Elastomers - Polymer Networks, Structure and Mechanical Properties*. Plenum Press, New York, 1971.

[73] D. J. Acheson. *Elementary Fluid Dynamics*. Oxford University Press, New York, 1990.

[74] M. Abramovitz and I. A. Stegun. *Handbook of Mathematical Functions with Formulas, Graphs, and Mathematical Tables*. Dover, New York, 1972.

[75] G. Arfken. *Mathematical Methods for Physicists*. Academic Press, Orlando, 1985.

[76] J.L. Schiff. *The Laplace Transform, Theory and Applications*. Springer-Verlag, New York, 1999.

[77] Wolfram Research Inc. Mathematica. Version 10.0, 2016. Champaign, Illinois.

[78] F. Müller and R. Stannarius. Comparison of the rupture dynamics of smectic bubbles and soap bubbles. *Liquid Crystals*, 36:133–145, 2009.

[79] F.M. Leslie. Continuum theory for nematic liquid crystals. *Continuum Mechanics and Thermodynamics*, 4:167–175, 1992.

[80] C. Brennen. *Cavitation and Bubble Dynamics*. Oxford University Press, New York, 1995.

[81] P. G. De Gennes and T. Proust. *The Physics of Liquid Crystals*. Oxford University Press, New York, 1993.

[82] O. Parodi. Stress tensor for a nematic liquid crystal. *Le Journal De Physique*, 31:581–584, 1970.

[83] H.S. Fogler and J.D. Goddard. Collapse of spherical cavities in viscoelastic fluids. *Physics of Fluids*, 13:1135–1141, 1970.

[84] L.D. Landau and E.M. Lifshitz. *Fluid Mechanics*. Pergamon Press, London, 1959.